Preliminary Study on the Fabrication of Alginate/Hyaluronic Acid Scaffolds for Spinal Cord Injury Repair

A Thesis Submitted to the College of

Graduate Studies and Research

In Partial Fulfillment of the Requirements

For the Degree of Master of Science

In the Department of Biomedical Engineering

University of Saskatchewan

Saskatoon

By

Mindan Wang
August 2012

Permission to Use

In presenting this thesis in partial fulfilment of the requirements for a Postgraduate degree from the University of Saskatchewan, I agree that the Libraries of this University may make it freely available for inspection. I further agree that permission for copying of this thesis in any manner, in whole or in part, for scholarly purposes may be granted by the professor or professors who supervised my thesis work or, in their absence, by the Head of the Department or the Dean of the College in which my thesis work was done. It is understood that any copying or publication or use of this thesis or parts thereof for financial gain shall not be allowed without my written permission. It is also understood that due recognition shall be given to me and to the University of Saskatchewan in any scholarly use which may be made of any material in my thesis.

Requests for permission to copy or to make other use of material in this thesis in whole or part should be addressed to:

Head of the Department of Biomedical Engineering
University of Saskatchewan
Saskatoon, Saskatchewan (S7N 5A9)

ABSTRACT

Traumatic spinal cord leads to devastating and permanent loss of neurological function. Artificial tissue engineering scaffolds show potential in spinal cord repair by providing guidance for regrowing axons. In this study, three-dimensional (3D) alginate/hyaluronic acid scaffolds designed for spinal cord repair were fabricated and characterized. Specifically, covalently and ionically crosslinked alginate/hyaluronic acid composite biomaterial was used for Schwann cell culture and for 3D scaffold fabrication and characterization. Carbodiimide mediated amide formation of composite biomaterial was examined in presence of ionic crosslinking and was found to be dependent on the concentrations of carbodiimide and calcium chloride and on the pH value of the reaction. The double-crosslinked composite hydrogels were biocompatible, allowing for Schwann cell survival and growth. No significant difference in cell number was found on the composite hydrogels with varying concentrations of alginate and hyaluronic acid used in this study. The results also indicated that covalent crosslinking and high concentration of hyaluronic acid were not favorable for Schwann cell growth. Finally, 3D porous scaffolds were successfully fabricated using two systems of the dispensing-based rapid prototyping technique. Effects of the fluid behavior, initial needle height, and concentration of calcium chloride were studied. Uniaxial compression mechanical test showed that the concentration of hyaluronic acid had little effect on the mechanical properties of the hydrogels, and that ionically crosslinked composite hydrogels had a similar viscoelastic compressive behavior as native spinal cord and had Young's moduli favorable for neurite outgrowth. This information provides a basis for continuing *in vitro* and *in vivo* tests of the ability of rapid prototyped alginate/hyaluronic acid hydrogel scaffolds to support regeneration of traumatic spinal cord.

ACKNOWLEDGMENTS

Here I want to extend my most sincere appreciation to my two supervisors, Dr. Daniel Chen and Dr. David Schreyer. Their expertise, encouragement, patience and enthusiasm for knowledge impressed me so much and guided me through all the difficulties and challenges occurring in my research projects. I will always be grateful for their supervision.

Also, I would like to thank my Advisory Committee members, Dr. Ildiko Badea and Dr. Chris Zhang for their kind examination and advices on my research work.

I also want to express my gratitude to Dr. Ian Burgess (Department of Chemistry) and Dr. Catherine Niu (Department of Chemical Engineering) for providing me with valuable comments and research instruments. Such research technicians as Tangyne Berry, Doug Bitner, Ruiling Zhai, Pia Wennek, Rob Piece and Natasha Vetter have provided me with lots of technical support for my experiment, without which I could not have finished my research work.

Special thanks are given to the students in the Tissue Engineering Research Group and other department including Peng Zhai, Minggan Li, Ning Zhu, Ning Cao, Haidong Wang, Zhiming Zhang, Wenbin Zhang, Nahshon Bawolin, Ajay Rajaram, Chenglin Liu, Xiaoyu Tian, Xin Yan, Li Zhou, and Huishu Hou.

I would also like to acknowledge the support of a scholarship from the College of Graduate Studies and Research of the University of Saskatchewan and of research funding from the Canadian Institutes of Health Research (CIHR).

DEDICATED TO MY GRANDPARENTS AND PARENTS

TABLE OF CONTENTS

LIST OF TABLES

LIST OF FIGURES

LIST OF ABBREVIATIONS

2D	Two dimensional
3D	Three dimensional
ADH	Adipic dihydrazide
CAD	Computer-aided design
CNS	Central nervous system
DMEM	Dulbecco's Modified Eagle Medium
DRG	Dorsal root ganglia
EDC	1-Ethyl-3-(3-dimethylaminopropyl) carbodiimide
EDTA	Ethylenediaminetetraacetic acid
FBS	Fetal bovine serum
FTIR	Fourier transform infrared spectroscopy
G	Guluronate
IKVAV	Ile-Lys-Val-Ala-Val
KBr	Potassium bromide
M	Mannuronate
MES	2-(N-morpholino) ethanesulfonic acid hydrate
MTT	3-(4, 5-dimethylthiazol-2-yl)-2, 5-diphenyltetrazolium bromide
PBS	Phosphate buffer solution
PLL	Poly-L-lysine hydrobromide
PNS	Peripheral nervous system
RGD	Arg-Gly-Asp

SCI	Spinal cord injuries
YIGSR	Tyr-Ile-Gly-Ser-Arg

CHAPTER 1 Introduction and Objectives

Thousands of people suffer spinal cord injuries (SCI) due to motor vehicle accidents, falls, violence, and sports injuries, among other causes. About 12,000 new cases of spinal cord injury occur each year in the United States, with the estimated annual number of Americans living with SCI at approximately 259,000 [1]. Damage to the spinal cord has severe clinical consequences due to neuronal cell death at the site of injury, and the disruption of axonal pathways crossing through the site of injury. To date, functional training is the principal clinical therapy used to help rehabilitate individuals after SCI. Other clinical treatments, such as anti-inflammatory drugs, help to prevent secondary injury and to reduce pain and swelling, but do not promote tissue repair. Therefore, therapeutic strategies to restore lost tissue and reestablish axonal connectivity after SCI are still urgently needed.

1.1 Spinal Cord Injuries

1.1.1 Organization of Spinal Cord

The nervous system consists of the central nervous system (CNS; brain and spinal cord) and the peripheral nervous system (PNS; nerves and ganglia outside the CNS). Spinal cord tissue is organized so that gray matter is in its centre, composed of neurons, neuropil (small axon terminals, dendrites, and the synaptic contacts they make with each other) and glial cells. The spinal cord white matter columns surround the gray matter, containing ascending and descending axons that travel long distances to establish contacts between different spinal levels, and with the brain. These white matter axonal pathways also contain glial cells, particularly the oligodendrocytes that provide a covering of insulating myelin to the long axons. Dorsal roots of the peripheral nerves relay sensory information to the posterior horn of the spinal cord gray

matter, while the ventral roots leaving the anterior horn carry the motor information to muscles and visceral organs as shown in Figure 1.1.

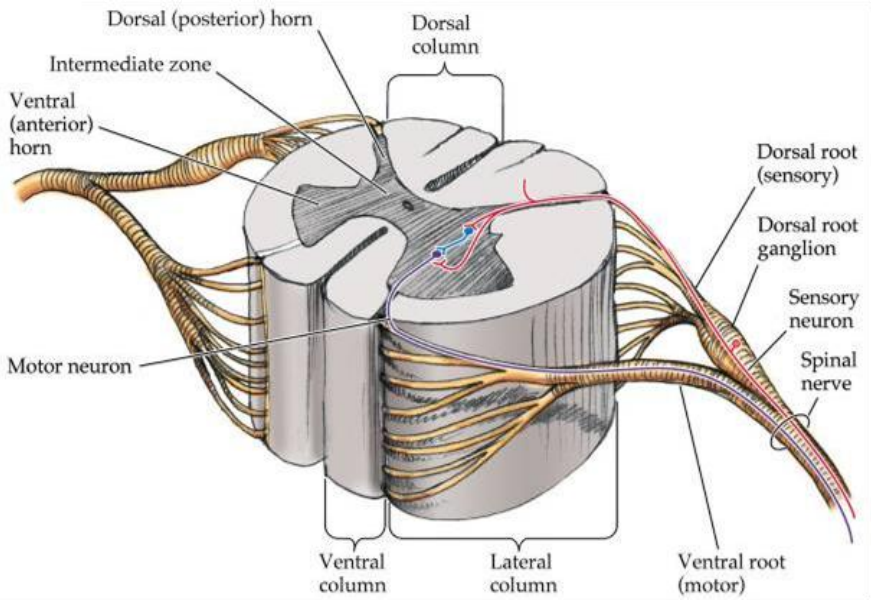

Figure 1.1 Structure of spinal cord and distribution of dorsal and ventral roots [2]. Sensory neurons in the dorsal root ganglion (DRG) receive and relay the sensory information through the dorsal roots of the spinal nerve to the posterior horn of the spinal cord gray matter, and the ventral roots of the spinal nerve leaving the anterior horn carry the motor information to muscles and visceral organs.

Different axon tracts in different locations of spinal cord white matter convey various types of information (Figure 1.2). For example, the fasciculus cuneatus and fasciculus gracilis carry ascending touch information, the anterolateral system carries ascending pain and temperature information, and the spinocerebellar tracts provide ascending sensory feedback about body movement. Meanwhile, the corticospinal tracts, the rubrospinal tract, and the vestibulospinal tracts carry descending information that controls muscle movement. The current emphasis of tissue engineering for SCI repair is to promote re-growth of these essential tracts after injury, which should in turn lead to dramatic restoration of sensory and motor function.

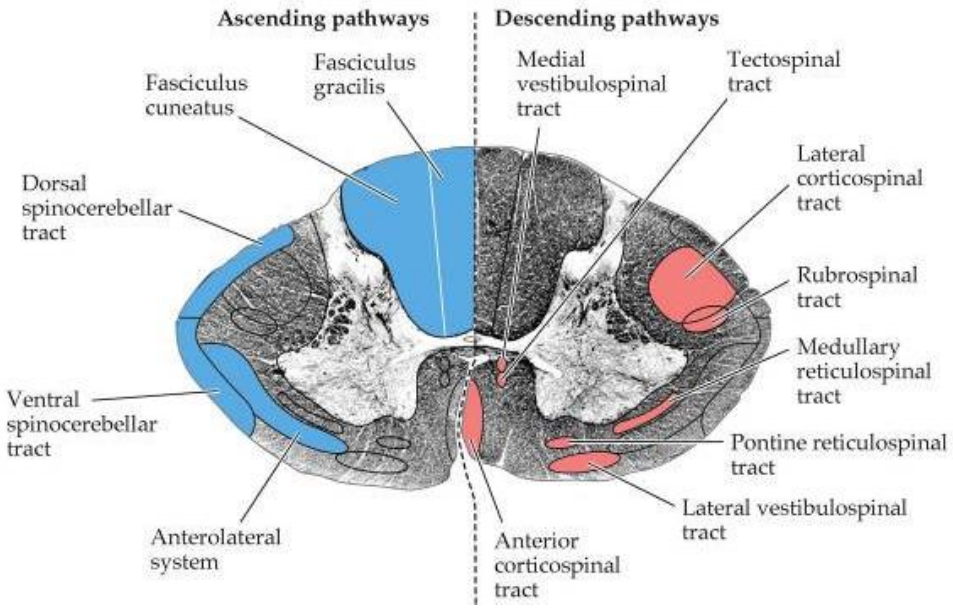

Figure 1.2 Cross-sectional diagram of the spinal cord showing the distribution of the major ascending and descending pathways essential for neurological functions [2].

1.1.2 Spinal Cord Injury

Many factors impede the re-growth of ascending and descending axons that carry signals between the different levels of the spinal cord and the brain, and thereby prevent functional recovery after SCI. The failure of regenerative axonal growth is in large part attributable to a CNS environment that is inhibitory for axonal growth. Factors contributing to growth inhibition in the spinal cord include poor clearance of damaged tissue caused by slow Wallerian degeneration, scarring caused by astrocytes, the presence of myelin-associated axonal growth inhibitors produced by oligodendrocytes and lack of intrinsic regenerative capability [3-8]. The current focus of tissue engineering research is to develop strategies to overcome the unfavorable nature of the scarring, enhance intrinsic axonal regeneration ability, increase the number of damaged ascending and descending axons that regenerate, guide the regenerating axons back to their appropriate target regions, and encourage the remyelination of these regenerating axons [7,

9-12]. In the past few years, considerable progress has been made in the development of bioengineered tissue scaffolds for the promotion of spinal cord repair.

1.1.3 Therapeutic Strategies for Spinal Cord Repair

The goal of tissue engineering for SCI is to create functional tissue repair in a controlled environment that promotes and directs axonal re-growth and penetration into the host spinal cord. Signals such as diffusible factors, extracellular matrix (ECM) proteins, cell-cell interaction, and mechanical stress can be utilized to create a favorable environment for axonal outgrowth, as cells continually sense and respond to these signals [13]. Nerve guidance scaffolds can provide mechanical support for axonal re-growth and serve as a local delivery system for growth factors, and living cells by allowing cell attachment, migration, and differentiation [14]. Thus, bioengineered tissue constructs have shown potential for the repair of the injured spinal cord. Such strategies as electrical stimulation [15-17], incorporation of bioactive molecules and living cells [17-22], delayed transplantation of scaffolds [23-26] and overcoming the hostile environment [27-30] have been demonstrated to promote axonal regeneration after SCI.

Schwann cells, the major glial cell type of the PNS, have been investigated for restoring injured spinal cord since 1981, when transplantation of purified Schwann cells was first carried out [31]. Schwann cells show particular promise as they can be harvested from patients for an autologous transplant. Not only do they provide remyelination of regrowing axons when transplanted into injured spinal cord [22], but the infiltration and remyelination by endogenous Schwann cells from the peripheral nerves into the spinal cord lesion site has been observed, suggesting that host Schwann cells might contribute to the recovery of injured spinal cord [25]. Transplantation of Schwann cells can reduce the size of spinal cysts as well as secrete various

trophic factors and cell adhesion molecules, leading to a more permissive environment for axonal growth and neural survival [32]. Trophic factors that Schwann cells produce include nerve growth factor, brain derived neurotrophic factor, ciliary neurotrophic factor, neurotrophin-3, conserved dopamine neurotrophic factor and fibroblast growth factor [33, 34]. In addition, they express axon guidance cell adhesion molecules on their surfaces, such as laminin. Schwann cell culture on/within the scaffolds is also extensively employed in preliminary studies to study such properties as biocompatibility and effects on cell behavior before the neural cell culture and *in vivo* transplantation. As a result, Schwann cells are used in this study to evaluate the biocompatibility and substrate-cell interaction of the biomaterial.

Despite the beneficial outcome provided by Schwann cell transplantation, decreasing cell numbers after transplantation pose a problem and some studies show insufficient axonal regeneration of brainstem spinal axons using Schwann cells alone; axons moreover, do not leave the Schwann cell graft to reenter the distal host spinal cord. Thus, strategies combining scaffolds with bioactive molecules or other supportive cells are usually used [35, 36]. Both olfactory ensheathing cells and Schwann cells have been widely used to promote axonal re-growth and functional recovery for SCI, yet it is still under investigation which is more beneficial [37, 38]. Studies of regenerating adult rat spinal cord with moderate contusion lesions at the thoracic level demonstrate that Schwann cells lead to more hindlimb locomotor recovery than olfactory ensheathing cells despite their relatively low integration with astrocytes [39]. Whether this also holds for non-human primates or other injury models remains to be determined. The low integration and migration of transplanted Schwann cells with the astrocytes is considered to be related in part to the high level of heparan sulfate proteoglycans, which mediate astrocytosis by facilitating the activity of the fibroblast growth factor family of growth factors [40]. However, by

forcing the transplanted Schwann cells to over-express the polysialylated neural cell adhesion molecule, their integration and migration in the spinal cord were improved, resulting in better axonal regeneration, remyelination and functional restoration [22, 41].

1.2 Biomaterials

Implantation of substrates such as cellular grafts can promote re-growth of axons after SCI. However, the growth of axons is highly random and does not extend past the graft site to re-enter host tissue [42]. Artificial tissue scaffolds are designed to provide mechanical support for axonal re-growth and to potentially serve as a local delivery system for growth-promoting factors, growth-inhibitor neutralizing agents, or other therapeutic drugs, as well as a carrier for supportive cells that might facilitate repair. Biomaterials selected for construction of tissue scaffolds should meet the following criteria: biocompatibility with the host tissue to avoid adverse immune reactions; an adjustable rate of degradation; and degradation products that are non-toxic [9]. Specific to the needs of spinal cord repair, scaffold biomaterials with mechanical properties (specifically the elastic modulus) matched to that of the spinal cord at the lesion site has the ability to reduce astrocytic reaction and fibroblastic gliosis, and allow for cell adhesion and axonal re-growth.

1.2.1 Natural Biomaterials from ECM

Both natural and synthetic biomaterials have been modified to fabricate tissue scaffolds for SCI repair and are reviewed in detail in [43, 44]. Natural biomaterials used as scaffold construct materials for spinal cord repair include hyaluronic acid, alginate, collagen, agarose, chitosan, matrigel, fibrin, and fibronectin hydrogels. These hydrogels mimic the ECM of soft

tissue, being highly hydrated, soft and allowing for the exchange of nutrients and metabolic waste with surrounding tissues. On the other hand, the options for use of available synthetic biomaterials for SCI repair are quite limited due to the fact that the synthetic materials are mostly hard and therefore not suitable for the repair of soft tissues. Thus, hydrogels prepared from natural biomaterials are the focus of bioengineered scaffolds for SCI repair and discussed in detail in the following.

Matrigel, fibrin, fibronectin, collagen and hyaluronic acid are components of native ECM and have been widely investigated for tissue engineering application due to their ability in regulating cell behavior. The ECM constituents provide anchorage and mechanical buffering, trigger intercellular communication and segregate different tissues [45].

Matrigel is an ECM extracted from the Engelbreth Holm Swarm sarcoma and contains laminin, fibronectin and proteoglycans. It has ability to stimulate proliferation and adhesion of Schwann cells, bone marrow stromal cells and olfactory ensheathing cells as well as neurite outgrowth of DRG neurons [46]. However, its origin from mouse tumor cells limits its application in human spinal cord.

Fibrin is a protein formed by enzymatic crosslinking of fibrinogen and thrombin upon mixing at physiological temperature and pH. It has been used as a delivery system for neurotrophic factors, chondroitinase ABC and different supportive cells, which result in increased axonal sprouting, decreased level of inhibitory molecules and significant behavioral recovery [47-51]. Unfortunately, the *in vivo* residence time of fibrin is not sufficient for SCI repair and needs to be prolonged.

Fibronectin is a glycoprotein present outside cells and on the cell surface. It has neuroprotective effect on SCI and permits oriented axonal regeneration with infiltration of

macrophages, Schwann cells, oligodendrocytes and their precursors, and astrocytes. But the forms of fibronectin biomaterials are limited to the fibronectin mats or cables [52-54].

Collagen can promote neural cell attachment and growth while on the other hand collagen is one component of the glial scar, which was suggested to impose a physical and chemical barrier for axonal regeneration after SCI [55-57]. In addition, though collagen is a major component of many tissue types in the body, native CNS tissue contains relatively little collagen. It is argued that the presence of biomaterial scaffolds consisted of un-naturally high concentration of collagen might impose undesirable side effects [58]. On the contrary, the native ECM of CNS contains high amounts of linear polysaccharides and glycosaminoglycans such as hyaluronic acid, chondroitin sulfate and heparin sulfate [59]. Chondroitin sulfate and heparin sulfate are also components of the glial scar and therefore are problematic to be used as natural biomaterials for the construct of scaffolds for SCI repair. Based on the discussion above about different natural biomaterials originated from ECM as well as the beneficial features provided by hyaluronic acid for spinal cord repair (discussed in section 1.3), hyaluronic acid was chosen as one natural biomaterial for the construct of 3D scaffolds for SCI repair.

1.2.2 Other Natural Biomaterials

Other natural biomaterials used for tissue engineering application include chitosan, agarose and alginate. Chitosan is a glycosaminoglycan carbohydrate polymer derived from chemical deacetylation of chitin, the major structural polysaccharide found in crustacean and insect exoskeleton. It has excellent ability for cell adhesion, survival and proliferation. Myelinated and unmyelinated axons as well as blood vessels were found after transplantation of extramedullary chitosan channel in a full transection SCI animal model [60]. On the other hand,

there are studies indicating that chitosan can trigger inflammation with the severity dependent on the degree of deacetylation [61]. Implanted as scaffolds in brain, chitosan biomaterials are ingested by macrophages as part of a foreign body response [62]. This limits the application of chitosan scaffolds in SCI repair.

Agarose is a linear polysaccharide derived from seaweed. It is an alternating copolymer of 1, 4-linked 3, 6-anhydro-α-L-galactose and 1, 3-linked β-D-galactose. Agarose is thermoresponsive, and can gel at temperatures ranging from 17-40 °C depending on the degree of hydroxyethyl substitution on its side chains. Agarose nerve guidance scaffolds with uniaxial linear channels prepared by a freeze-dry process or templating were shown to orient and provide guidance to local spinal cord axons after SCI [63-65]. But the non-degradability property of agarose scaffolds seems to be disadvantageous for SCI repair. Scaffolds with a matching *in vivo* biodegradation profile with new tissue formation are desirable for tissue regeneration.

Alginate is preferable to these natural biomaterials in terms of its biorestorability, biocompatibility and facilitation of scaffold fabrication by instant gelation with multivalent cations under mild conditions. Detailed properties of alginate hydrogels and its potential as a biomaterial for the construct of scaffolds for SCI repair are discussed in section 1.3.

1.3 Hyaluronic Acid and Alginate Hydrogels for SCI Repair

1.3.1 Hyaluronic Acid and Covalent Modification

Hyaluronic acid, widely found in almost all extracellular tissue spaces, is an extremely long, negatively charged, heavily hydrated glycosaminoglycan. It is comprised of repeating disaccharide units of β-1, 4-D-glucuronic acid and β-1, 3-N-acetyl-D-glucosamine, as shown in Figure 1.3. Its hydroxyl groups and carboxyl groups can be targeted for chemical modification.

Hyaluronic acid demonstrates excellent biological properties, being biocompatible, biodegradable and immunoneutral. Hyaluronic acid is widely investigated for its potential for construction of tissue scaffolds. It promotes regeneration of the traumatized peripheral nerve [66-68], in part because of its involvement in such complex cell signaling events as migration, attachment, angiogenesis and neuronal sprouting [69]. In addition, it shows potential for SCI repair as it is shown to inhibit scar formation by inhibiting lymphocyte migration, proliferation, and chemotaxis; granulocyte phagocytosis and degranulation; and macrophage motility.

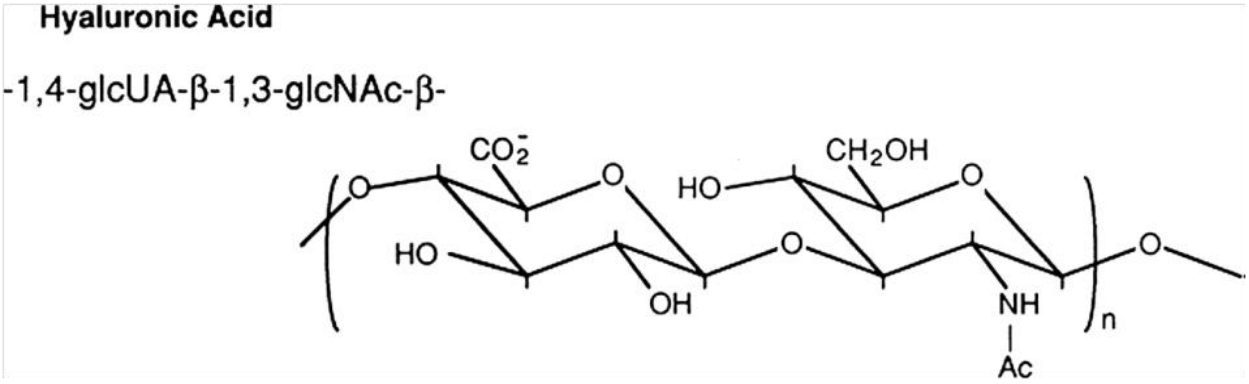

Figure 1.3 Chemical structure of hyaluronic acid consisting of repeating disaccharide units of β-1, 4-D-glucuronic acid and β-1, 3-N-acetyl-D-glucosamine.

The abundance of hyaluronic acid in brain and spinal cord also demonstrates its significance in CNS development, which inspired researchers to investigate the possibility of controlling neuronal progenitor cell differentiation through fabrication of hyaluronic acid hydrogels with tunable mechanical properties [70-72]. Several studies have been conducted to investigate the promise of crosslinked hyaluronic acid hydrogels on neurite outgrowth and recovery from SCI. Recent studies examining brain injury in rats show improved cell infiltration and angiogenesis in hyaluronic acid hydrogel scaffolds engineered to incorporate laminin peptides [73], or covalently crosslinked with poly-D-lysine, a widely used adhesive coating material in the preparation of neuron cultures [74]. Such polymer combinations may also have

promise for the treatment of SCI. But its short residence time *in vivo* and weak mechanical properties turn out to limit the application of hyaluronic acid in the construction of 3D scaffolds for spinal cord restoration.

Numerous methods have been developed to chemically modify hyaluronic acid to control its mechanical properties and promote release of tethered bioactive agents, such as neutralizing antibody against Nogo receptor-66 to block the activity of myelin-associated neurite growth inhibitors in injured rat brain and spinal cord [75, 76]. The application of crosslinked thiolated hyaluronic acid-poly (ethylene glycol)-diacrylate scaffolds resulted in extensive neurite outgrowth *in vitro*, yet neither axonal regeneration nor behavioral recovery after spinal cord transection was observed [77]. Possible explanations for the lack of functional recovery include the incapacity for the crosslinked hyaluronic acid scaffolds to provide mechanical support for axonal growth beyond 8 days and the persistence of a strong inflammatory response. It is unlikely that hyaluronic acid scaffolds alone can lead to the behavioral restoration without additional strategies, for instance, the inclusion of living cells or growth factors. Still, cells do not readily adhere to hyaluronic acid suggesting that modifications to its surface properties may improve the efficacy of a hyaluronic acid scaffold.

In vivo residence of hyaluronic acid can be enhanced by covalent chemical modification. The formation of amide bonds with adipic dihydrazide (ADH) mediated by 1-ethyl-3-(3-dimethylaminopropyl) carbodiimide (EDC) has been demonstrated to enhance the mechanical strength and to control the *in vivo* biodegradation of crosslinked hyaluronic acid constructs [78]. A schematic diagram of chemical crosslinking of hyaluronic acid is shown in Figure 1.4.

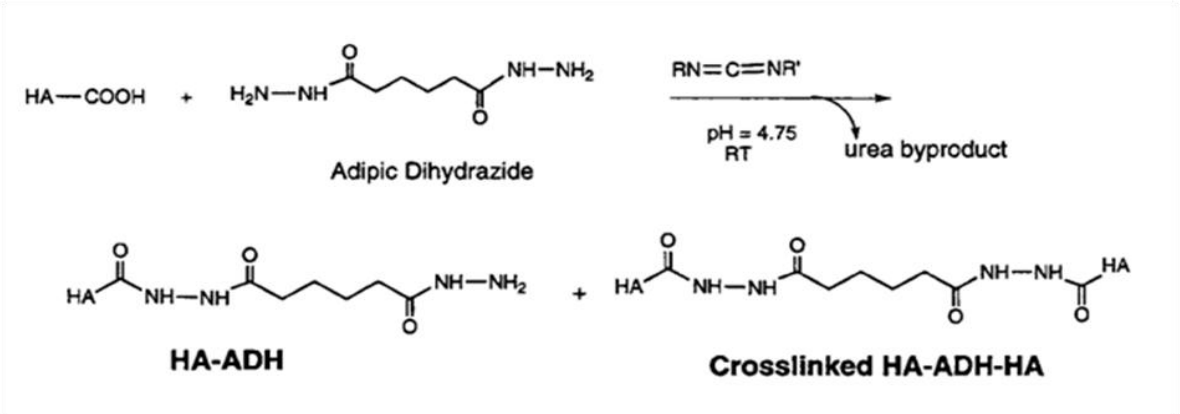

Figure 1.4 Crosslinking of hyaluronic acid using EDC as the crosslinker [78]. Carboxyl groups of the hyaluronic acid can react with the amine groups of the ADH at an acid condition with the presence of EDC to give hyaluronic acid-ADH linked by the amide bonds. With the bifunctional ADH, the crosslinked hyaluronic acid-ADH-hyaluronic acid will be formed.

The carboxyl groups of the hyaluronic acid will react with the amine groups of ADH to form the amide bonds under the mediation of EDC at an acid condition. Since the ADH is bifunctional, intermolecular and intramolecular crosslinking of hyaluronic acid through the amide bonds will take place, which overcomes the insufficient mechanical strength of hyaluronic acid scaffolds. In this reaction, EDC is transferred into urea, which is non-toxic to the native tissue.

The comprehensive mechanism of the amide formation mediated by EDC in aqueous system is illustrated in Figure 1.5, which is quite different and complex from the case in the organic system. EDC can react with the ionized carboxyl group to form nucleophilic compound 3 (O-acylisourea), which will then react with ionized carboxyl group and produce carboxylic anhydride 8 in the case of the cyclizable carboxyl group, which will form the corresponding amide 7 and urea derivative 2 when amine is present. For the non-cyclizable carboxyl group, compound 4 will react with a water molecule or a unionized amine to give carboxylate 6 or amide 7, respectively. The reaction with water will be prevailing. And if the carbodiimide is

added in excess, the carbodiimide would be able to react with compound 4 to form N-acylurea 5 as a byproduct [79].

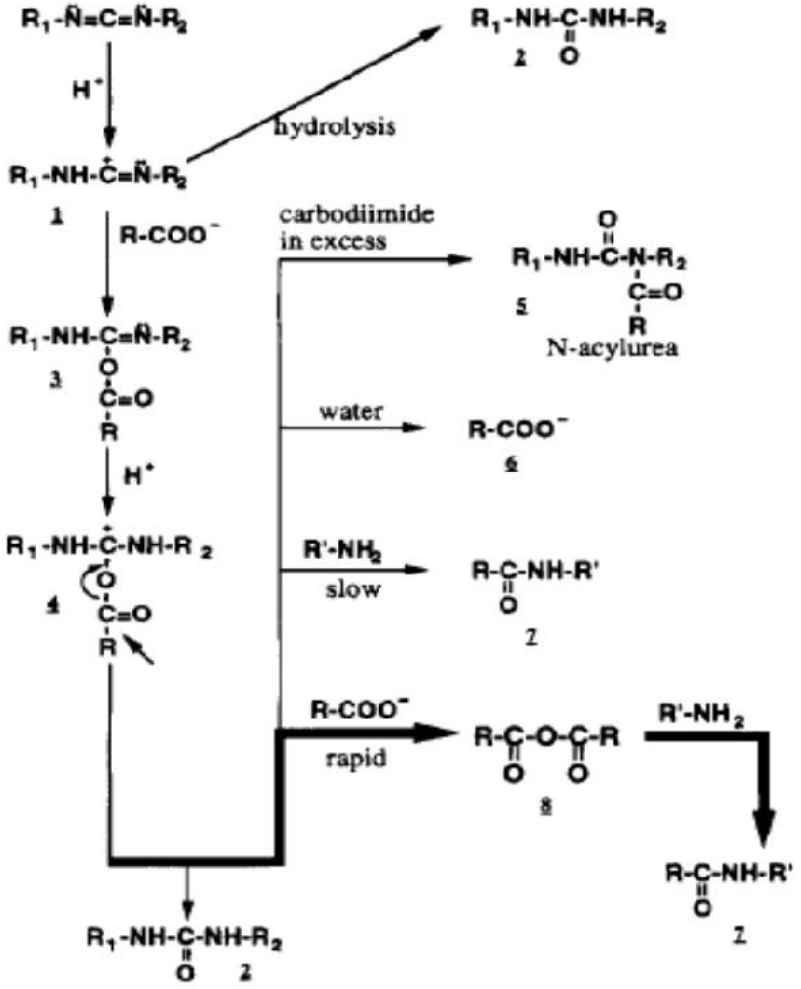

Figure 1.5 Schematic diagram of the mechanism of amide formation mediated by carbodiimide in aqueous media [79]. Carbodiimide 1 can react with an ionized carboxyl group to form compound 3 (O-acylisourea)and because of the reprotonation at the site of Schiff base, compound 3 can change into a carbocation 4, which will react with various bases in the aqueous system to yield different products.

Previously, we found that 3D porous scaffolds cannot be produced using this chemistry, probably due to the non-instant crosslinking of the hyaluronic acid with the EDC in the aqueous

system. The extruded strands swell and collapse before extensive crosslinking takes place. As an alternative, it is possible that the inclusion of alginate, which can gel within seconds with divalent calcium cation (Ca^{2+}), could provide the necessary mechanical support for the dispensed strands. Entrapped by the crosslinked alginate, hyaluronic acid will then be crosslinked and this may further enhance the mechanical strength of the fabricated scaffolds, and result in 3D porous scaffolds with a biodegradation rate suitable for use in SCI repair. There are not many investigations regarding use of the composite biomaterial of alginate/hyaluronic acid for the application of tissue engineering. Thus, this study may also provide insights into the potential of this composite biomaterial for the other tissue engineering applications.

1.3.2 Alginate and Ionic Crosslinking

Alginate is a water-soluble polysaccharide extracted from brown seaweed, consisting of a varying proportion of 1, 4-linked β-D-mannuronate (M) and 1, 4-linked α-L-guluronate (G) blocks (Figure 1.6), depending on the origin. Due to its biocompatibility and bioresorption properties, alginate has been widely used in tissue engineering to encapsulate and implant various growth factors or cell types into lesion sites to enhance the rate of tissue regeneration [80, 81]. In addition, several strategies have been proposed to control the degradation rate of alginate hydrogels, such as incorporating poly (lactide-*co*-glycolide) microspheres loaded with alginate lyase [82]. Non-structured alginate-based substrates transplanted into the mammalian CNS cause no allergic or inflammatory reactions but promote only limited axonal regeneration [83]. Freeze-dried alginate sponge can guide axonal re-growth in transected rat spinal cord, with the formation of functional synapses identified by intracellular electrophysiological recording [84]. Furthermore, alginate-based highly anisotropic capillary hydrogels, when assessed in both

axonal outgrowth assays *in vitro* and adult rat spinal cord lesions *in vivo*, elicit highly oriented linear axonal re-growth and appropriate target neuron reinnervation [85].

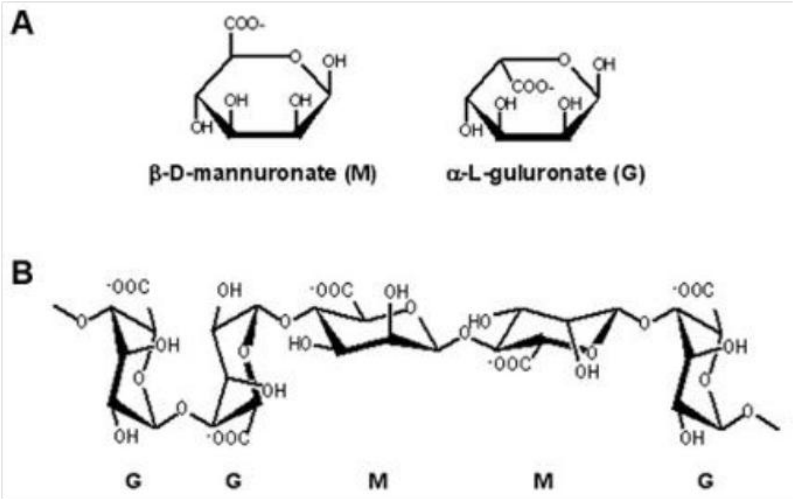

Figure 1.6 Schematic diagrams of the (A) mannuronate (M), guluronate (G) monomers of alginate sodium and (B) an example of the alginate polymer consisting of repeating GGMMG.

Application of alginate in the fabrication of 3D scaffolds using the solid freeform fabrication technique has been demonstrated, either serving as the scaffold biomaterial itself or as supporting additive for other biomaterials. Its instant gelation with divalent cations enables the inclusion of living cells during the dispensing process (Figure 1.7), eliminating the potential toxicity of other crosslinking reactants while allowing for the fabrication of the 3D constructs. However, there is no further study using alginate scaffolds with interconnected pore networks for either *in vitro* or *in vivo* test for SCI repair. Use of calcium crosslinked alginate as a matrix has been shown to permit the viability and growth of Schwann cells, and the neurite outgrowth of chick embryo DRG neurons was promoted by 170% when Schwann cells were suspended in the gel [86]. However, alginate lacks the ability to trigger the cellular and molecular signaling within the mammalian system, making the composite biomaterials of alginate and hyaluronic acid promising for construction of bioengineered scaffolds for SCI repair.

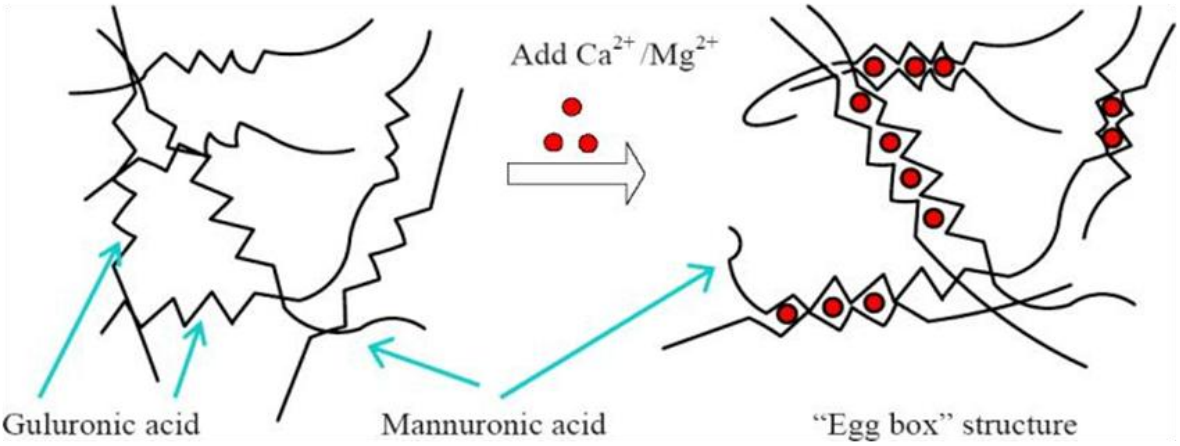

Figure 1.7 Gel formation of alginate with divalent calcium cations to form "egg box" structure [86]. Carboxyl groups in the guluronic acid monomers of the alginate bind to the divalent ions to form the "egg box" structure, resulting in the alginate hydrogels.

1.4 Scaffold Fabrication

1.4.1 Design of Scaffolds

Several requirements should be met when designing scaffolds for SCI repair, including mechanical properties similar to native spinal cord, favorable surface chemistry, sufficient pore size, porosity, pore interconnectivity and surface area for cell loading and cell-surface interaction as well as axonal re-growth and nutrient transport, and a biodegradation profile that produces adequate residence time [65, 87, 88]. However, because the use of artificial scaffolds for the repair of SCI is in its infancy, what constitutes an optimal scaffold remains to be defined. Parameters such as morphology, architecture, mechanical properties, surface properties, biodegradation rate, composition of biological components, and the variations of these factors with time have a substantial effect on the outcome [89, 90]. Systematic consideration of all of these factors will maximize the outcome for a particular application.

1.4.1.1 Surface Chemistry

Surface chemistry of the biomaterials including charges, functional chemical groups and ECM proteins/peptides needs to be taken into account as it influences the interaction of the scaffold with macromolecules and cells. Particular cell types adhere to polymers with different surface charges. For example, the number of mesenchymal stem cells cultured on a positively charged hydrogel is elevated compared to hydrogels with a negative or no charge. This is attributed to absorption of serum macromolecules onto the positively quaternary ammonium groups [23, 91].

In addition to the surface charge of biomaterials, chemical functional groups present on the surface of biomaterial also affect cell behavior through the interaction of receptors on cell membranes with specific ECM proteins absorbed by different chemical groups [92, 93]. Recent studies on the response of neural stem cells to materials with different chemical groups in a serum-free culture system indicate the chemical groups themselves can impose effects on cell behavior without the involvement of ECM proteins [94]. Detailed mechanisms of scaffold surface chemistry with respect to cell responses are not well understood.

Presence of ECM proteins/peptides on the biomaterial scaffolds also influence on cellular activities such as cell migration, axonal guidance, synaptogenesis, cell survival, differentiation, and myelination [95]. Incorporation of ECM proteins or peptides derived from them, either by coating, covalent crosslinking, or blending, may enhance cell adhesion, differentiation, migration and axonal outgrowth [96-100]. Collagen, fibronectin, and laminin are the most widely investigated ECM proteins for biomodification of scaffolds to achieve better axonal regeneration [99, 101-103]. Limitations of modification with whole ECM proteins include batch variation and the risk of disease transmission [104]. Thus, synthetically prepared amino acid sequences from the domains of ECM proteins responsible for cell-substrate interactions are used as alternatives.

Arg-Gly-Asp (RGD), Tyr-Ile-Gly-Ser-Arg (YIGSR), and Ile-Lys-Val-Ala-Val (IKVAV) are the three most commonly used cell adhesion peptides in tissue engineering to promote the biocompatibility and interaction of scaffolds with cells [97, 98]. However, which functionalization technique and protein/peptide species and concentration are most efficient for each different scaffold application is still unknown.

1.4.1.2 Mechanical Properties and Biodegradation Rate

Mechanical properties of the scaffolds need to be taken into consideration when designing scaffolds for SCI repair. The elastic modulus, one key parameter for the mechanical properties of scaffolds, has a great influence on the cell response, depending on the cell type and the range of modulus presented. Soft substrates promote axonal growth but suppress the growth of astrocytes [105]. Besides, proliferation of stem cells can be modulated through the control of the mechanical properties of the scaffolds. For example, hyaluronic acid hydrogels with mechanical properties comparable to those of neonatal brain are found to direct the differentiation of neural progenitor cells into neurons. On the contrary, neural progenitor cells within stiffer hydrogels, with mechanical properties comparable to those of adult brain, differentiate into mostly astrocytes [72]. In general, scaffolds with material elastic modulus matching that of the native growth environment are preferable for cell growth, differentiation and migration across the tissue-implant boundary [106]. The values of the elastic modulus of native spinal cord tissue are reported to be within the range of ~3 KPa to 300 KPa [107, 108]. Due to the effects of mechanical properties of scaffolds on cell behavior, it is important to tune the mechanical properties of scaffolds for a particular application.

In addition to the suitable initial mechanical properties, the mechanical properties of scaffolds are also supposed to match the growth of new tissue to support cell proliferation and

neurite extension. Thus, scaffolds with biodegradation profile matching the new tissue formation are desirable. Basically, the two main degradation mechanisms of scaffolds *in vivo* include uniform bulk degradation due to hydrolysis and proteolytic degradation of natural materials by protease enzymes in the ECM or cells [109].

Several strategies can be applied to control the mechanical properties and biodegradation of scaffolds. Firstly, chemical/enzymatic and physical crosslinking of the natural biomaterials offer an option to control the mechanical properties and degradation profile of the hydrogel scaffolds. Other methods include varying material composition and delivery of particular protease enzymes for the biomaterials [82]. In addition, mechanical properties and biodegradation rate of the scaffolds are correlated with the internal microstructure of scaffolds such as pore size, porosity, and interconnectivity. Fabrication techniques of rapid prototyping are capable to produce controllable and reproducible microstructure of the scaffolds, and therefore provide effective control over the mechanical properties and biodegradation rate of scaffolds. However, with the complexity of the *in vivo* environment, how to monitor and control over the properties of scaffolds *in vivo* is an issue that needs to be further addressed.

1.4.1.3 Macro-Architecture and Micro-Architecture

To date, macro-scale architectures investigated for SCI repair include hydrogels, sponges, single- and multi-channeled guidance tubes, and nanofiber scaffolds. Among these, multi-channeled scaffolds have drawn much attention among researchers as the hollow cylindrical channels can guide regenerating axons while the polymer matrix provides local, sustained release of therapeutic agents [44]. Compared to a single lumen tube, they provide more surface area, allowing for more cell attachment and local release of incorporated growth factors. In the PNS, multi-channeled tissue repair scaffolds resembling the structure of multiple basal lamina tubes

increased the accuracy of motor axonal regeneration in a 1-cm gap in a rat sciatic nerve model compared to single channel conduits [110]. In SCI repair, longitudinal tubes in the scaffolds can be fabricated through templating or adapted freeze-drying techniques. Introduction of uniaxial channels supported linear, organized axonal re-growth and blood vessel infiltration than scaffolds with random porous structure [63, 111]. However, axon migration was found to be independent of the conduit diameters.

Anatomically inspired open-path designs for SCI facilitate axonal regeneration through the lesion site and limit secondary injury progression. In comparison, implants of cylinder, tube, and single-channeled scaffolds result in a doubling of defect length due to secondary damage, and lead to large scar and cyst formation with no neural tissue re-growth [112]. These indicate that the macrostructure of the scaffolds itself is enough to affect the axonal regeneration after SCI.

Implants with anatomical guidance channels positioned for major ascending and descending axon tracts as well as branch structure of the guidance scaffolds may be beneficial for the regeneration of traumatic spinal cord, particularly in combination with therapeutic strategies involving living cells and bioactive molecules [113]. This necessitates the development of advanced fabrication techniques capable to produce sophisticated macro-structure of the scaffolds. Conventional fabrication techniques are unable to do so.

Microstructure of the implanted scaffolds, particularly the porosity, pore interconnectivity, pore size, and orientation of pores, is also important when designing scaffolds for SCI repair due to its impact on mechanical properties, surface to volume ratios, and cell behavior. High porosity and interconnectivity of the pores are essential in ensuring spatially uniform cell distribution, cell survival, proliferation and migration *in vitro* [88]. These features of

scaffolds can extensively affect on the diffusion of physiological nutrients and gases to the removal of metabolic waste and by-products from cells that have penetrated the scaffold. In general, high porosity and pore interconnectivity are preferable. However, high porosity of scaffolds compromises the mechanical strength and thus the proper porosity of scaffolds should be made with considerate care.

Pore size of the scaffolds should not be too small as pore occlusion by cells will inhibit cellular penetration and matrix elaboration within the scaffolds [88]. Meanwhile, it should be small enough to physically align and restrict the direction of axonal growth [114-116]. It is reported that axonal ingrowth into capillary alginate hydrogels was promoted with increasing capillary diameter from 18 μm to 55 μm. In another study, micropatterned grooves with widths of about 30 μm were found to be the most effective at promoting oriented neurite growth [117].

Micropatterning, microgrooves, photolithography, soft lithography, self-assembling and electrospinning are usually used to produce micro- and nano-scale topography, which best mimic the native ECM and thus provide a suitable environment for cell adhesion, migration, proliferation and differentiation. Electrospinning has drawn particular attention due to its capacity to fabricate scaffolds with linear fibers within nano- to micro-scale range. Electrospun nanofibers with linear orientation result in the highly aligned neurite extension of DRG neurons parallel to the fibers [118, 119]. In addition to the guidance of neurite outgrowth, gene expression of β-Tubulin in Schwann cells is upregulated; proliferation and differentiation of mutlipotent cells can be affected [120-122]. Unfortunately, as toxic chemical solvents or high temperatures are required to dissolve most synthetic polymers before electrospinning, the incorporation of cells and/or bioactive molecules when fabricating scaffolds using this technique

is an issue that requires further investigation. And electrospinning of scaffolds consisted of natural biomaterials have not been achieved so far and the shape of scaffolds is limited.

With the emergence of computer-aided design (CAD), scaffolds with controllable, reproducible and bio-mimetic micro-architecture can be fabricated with the rapid prototyping techniques, facilitating the application of different therapeutic strategies for various ascending and descending tracts [44]. Newer technologies give researchers greater capacity to control macro-structure, micro-structure, and biological properties during tissue scaffolds design and production, and this is important to support continued progress. The following section focuses on selected currently available fabrication techniques potentially applicable to spinal cord repair, with emphasis on rapid prototyping techniques.

1.4.2 Fabrication of Scaffolds

Enhancing the biological properties of scaffolds during the fabrication process is a primary goal of tissue engineering. Fabricating artificial scaffolds that are subsequently seeded with living cells in bioreactors and one-step fabrication of scaffolds using a mixed solution of biomaterial and living cells are both methods that belong to the biofabrication domain. Adding cells to scaffolds after they are fabricated imposes limits on the ability to control cellular distribution. Advantages of incorporating cells into the production process include the ability to produce an even spatial distribution of the living cells [123], or even to construct defined cellular arrays. Sustaining the viability of living cells during the fabrication process is essential, and emphasizes the importance of sterile and gentle fabrication procedures. While several techniques have been widely used to fabricate scaffolds with required surface morphology and internal architectures for SCI repair, techniques allowing the inclusion of living cells and bioactive

molecules during the process are quite scarce. Different techniques used for scaffold fabrication and their merits and demerits are summarized in Table 1.1.

Table 1.1 Different Scaffold Fabrication Techniques for SCI Repair

Fabrication Methods	Merits	Demerits	Reference
Freeze drying	No toxic chemicals needed Highly porous structures High pore interconnectivity Control of porosity	Random distribution of pores Incapable of fabricating intricate microstructure Limit to small pore sizes	[64]
Gas foaming	Free of organic solvents and high temperature Controllable porosity and pore size	High pressure involved Compact architecture for cells Lack of interconnectivity	[124]
Salt leaching/ Phase separation	Allows incorporation of bioactive agents	Residual solvents	[125]
Mold casting	Simple, cheap Requires no chemical agents	Incapable of fabricating intricate microstructure	[60]
Electrospinning	Produces long and continuous fibers Control over fiber orientation Versatile for many polymers	Use of high-voltage apparatus Difficult to control fiber assembly Limited to viscous polymer solutions	[99]
Heat compression	Free of organic solvents	High temperature	[126]

Scaffold fabrication techniques can be divided into three groups: conventional methods, textile technologies and solid freeform fabrication. Conventional fabrication techniques are described in detail by Sachlos and Czernuszka [127], and include such methods as solvent-casting, particulate-leaching, gas foaming, phase separation, melt molding, solution casting, and freeze-drying. These methods involve the use of toxic organic solvents and porogens, and lack the ability to precisely control the pore size, pore geometry, and spatial distribution of pores within the scaffolds. As these parameters play important roles in the material properties and functionality of the scaffolds, the utility of such conventional techniques is limited. Furthermore, whether the amorphous, irregular microstructure of conventionally fabricated scaffolds hinders longitudinal axonal regeneration remains to be determined.

1.4.3 Dispensing-Based Rapid Prototyping Technique

Rapid prototyping, also known as solid freeform fabrication, has recently attracted increasing attention. Rapid prototyping can be used to fabricate scaffolds with controllable and reproducible microstructure, thanks to computer-aided fabrication processes that provide control over the physical properties (pore size, porosity, interconnectivity, and mechanical strength) of a scaffold as required for a particular application. Rapid prototyping using natural biopolymers is conducive to the simultaneous inclusion of cells and biomolecules. It is reported that rapid prototyped scaffolds provide better cell seeding in the scaffold interior, lower oxygen gradients, and better cell aggregation compared to conventional fabrication techniques, and can more successfully promote tissue regeneration [89, 128].

Dispensing processes are most commonly used in rapid prototyping techniques and are termed as the dispensing-based rapid prototyping systems (Figure 1.8). Biomaterials are deposited in a predefined dispensing path to form the 3D scaffolds. These dispensing-based rapid prototyping systems, such as the 3D Bioplotter, are capable to fabricate hydrogel scaffolds and integrate supporting cells and bioactive molecules during the fabrication process without the involvement of toxic chemicals or high temperatures. However, few studies are carried out on the fabrication and *in vivo* characterization of rapid prototyped scaffolds for SCI repair. One work worth mentioning describes the fabrication of a new bi-phasic tubular scaffold by 3D bioplotting for SCI regeneration [129]. The favorable outcome of the preliminary *in vivo* test in a hemisection SCI model demonstrates the potential of the dispensing-based rapid prototyping technique to fabricate scaffolds with controllable microstructure, mechanical strength and biological patterns for enhanced promotion of axonal regeneration.

Despite of the advantages offered by this fabrication technique, it has so far proven difficult to precisely control the architecture of the scaffolds by varying such parameters as fluid behavior of the dispensing material, flow rate, dispensing speed, and dispensing nozzle shape, diameter and length. Different models have been developed to evaluate the flow rate with regard to the Newtonian or non-Newtonian fluid behaviors of different dispensing approaches [130-133]. Modeling of scaffold porosity, pore size, and mechanical cell damage has also been carried out to offer an alternative to trial and error processes [134]. These models will greatly facilitate scaffold biofabrication, making it possible to optimize the geometry and process parameters, minimize cell damage during the biofabrication process, and maximize both mechanical and biological properties. Shortcomings of dispensing-based rapid prototyping fabrication include challenges regarding sterilization, cell damage that may occur during the fabrication process, and the inability to fabricate scaffolds from biomaterials that require a lengthy cross-linking process.

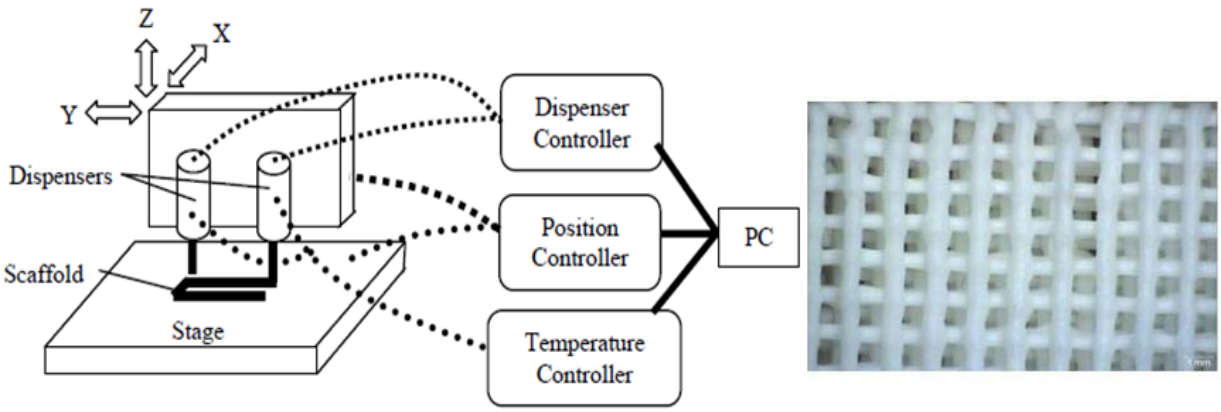

(a) (b)

Figure 1.8 (a) Schematic of a dispensing-based rapid prototyping system composed of two dispensers mounted on a three-axis positioning system, a stage to support the scaffolds fabricated, a personal computer and three controllers interfaced with the personal computer for the control of position, dispenser and temperature; and (b) top view of a multilayer orthogonal scaffold fabricated using the dispensing-based rapid prototyping method [133].

1.5 Objectives

In this research, crosslinked alginate/hyaluronic acid 3D scaffolds will be fabricated and characterized in terms of physical, biological and mechanical properties. The central hypothesis is that 3D scaffolds can be fabricated from crosslinked alginate/hyaluronic acid hydrogels and the composite hydrogels are permissive for Schwann cell viability and growth. If this hypothesis is supported, the alginate/hyaluronic acid composite material could be used in the future as the biomaterial to construct 3D scaffolds for SCI repair. To prove this, the following specific research objectives are to be achieved in this research:

(1) To synthesize and chemically characterize double-crosslinked alginate/hyaluronic acid composite biomaterial;

(2) To examine the biocompatibility of the crosslinked alginate/hyaluronic acid hydrogels for Schwann cell viability and growth;

(3) To design and fabricate 3D porous scaffolds with well-controlled microstructure by dispensing-based rapid prototyping techniques;

(4) To study the effect of concentration of hyaluronic acid on the mechanical properties of the ionically-crosslinked composite hydrogels.

Overall, the present study will shed light on the application of alginate/hyaluronic acid hydrogel as a scaffold material that could serve as a platform for SCI repair.

1.6 Organization of the Dissertation

This dissertation is composed of five chapters in total, and each experimental chapter is divided into four main parts: introduction, materials and methods, results and discussions, and conclusions.

Chapter 1 presents a brief introduction and literature review on the bioengineered scaffolds for spinal cord repair. Specifically, it presents the recent development of bioengineered scaffolds for SCI repair, from the points of view of SCI, current therapeutic strategies, scaffold materials, and fabrication techniques.

Chapter 2 presents the synthesis of double-crosslinked alginate/hyaluronic acid composite hydrogels and their characterization by means of Fourier transform infrared spectroscopy (FTIR). Covalent crosslinking of the composite material was applied and the chemistry was confirmed using FTIR spectroscopy.

Chapter 3 discusses the biocompatibility of alginate/hyaluronic acid hydrogels for Schwann cell viability and growth. Schwann cell cultures were established on double-crosslinked alginate/hyaluronic acid hydrogels with different concentrations of alginate and hyaluronic acid to test the biocompatibility of the substrates. Also, the effect of concentration of hyaluronic acid incorporated and double crosslinking of alginate/hyaluronic acid biomaterial on Schwann cell number in comparison with just ionic crosslinking was studied to find proper substrates for the Schwann cell culture.

Chapter 4 focuses on the fabrication of 3D porous scaffolds by the dispensing-based rapid prototyping technique. The effects of operating parameters, concentration of crosslinker solution and amount of hyaluronic acid incorporated on the formation of multilayer scaffolds were investigated. The mechanical properties of cylindrical ionically-crosslinked alginate/hyaluronic acid scaffolds were also studied by uniaxial compression test.

Chapter 5 presents the main conclusions and discussion of this research, followed by comments for future work.

CHAPTER 2 Syntheses and FTIR Measurements of Composite Hydrogels

2.1 Introduction

Hyaluronic acid has a great potential for constructing tissue scaffolds due to its excellent biological properties to trigger cellular and molecular signaling within the mammalian system. Unfortunately, hyaluronic acid has weak mechanical properties and cannot be used alone to fabricate 3D porous structures with the dispensing-based rapid prototyping system. In contrast, instant gel formation of alginate with calcium chloride ($CaCl_2$) results in hydrogels with mechanical strength that can be handled and tailored to match the application of SCI repair. Thus, composite biomaterial of alginate and hyaluronic acid will facilitate the fabrication of 3D scaffolds using the dispensing-based rapid prototyping system meanwhile maintaining the biological properties of hyaluronic acid. Additionally, covalent crosslinking of alginate/hyaluronic acid with ADH mediated by EDC might prolong the *in vivo* residence time and enhance the mechanical properties of alginate scaffolds. FTIR spectra were used to confirm the amide formation of alginate/hyaluronic acid composite material in the presence of $CaCl_2$ and EDC.

2.2 Materials and Methods

Low viscosity sodium alginate, molecular weight range 12,000~80,000 Da, mannuronic acid 61% and guluronic acid 39% was purchased from Sigma Aldrich Canada. Calcium chloride $CaCl_2$ (Sigma, St. Louis, MO) was used as the crosslinker for sodium alginate. Hyaluronic acid sodium salt (MW 26-27 MDa) was bought from Shandong Freda Biopharm Co., Ltd. (Freda, Jinan, Shandong, China). ADH, 2-(N-morpholino) ethanesulfonic acid hydrate (MES buffer)

with useful pH range of 5.5-6.7, and EDC were all purchased from Sigma Aldrich Canada. Dialysis tubes having a 3500 Dalton molecular weight cut offs were used to dialyze the excess reagents. Potassium bromide (KBr) of the FTIR grade, ≥ 99% trace metals basis (Sigma Aldrich, Canada) was used for the FTIR spectrometers.

2.2.1 Sample Preparation for FTIR

2.2.1.1 Covalent Crosslinking of Hyaluronic Acid

Three samples were used to examine the covalent modification of hyaluronic acid with ADH by EDC at an acid condition. They were hyaluronic acid reacted with EDC alone (HA_4_EDC_stir), hyaluronic acid reacted with ADH and EDC (HA_ADH_4_EDC_stir) and unreacted hyaluronic acid (HA), which served as the negative control. In detail, 0.75% (wt %) of hyaluronic acid was prepared by dissolving hyaluronic acid powder in double distilled water and stirred overnight. The pH value of the hyaluronic acid solution was adjusted by adding drop by drop of 10 mM HCl until it reached a value of 4. This pH value supports good covalent modification as discussed in Chapter 1. For sample HA_ADH_4_EDC_stir, both hyaluronic acid and ADH (w/w, 1:5) were dissolved in double distilled water and the pH value of mixture was also adjusted to 4 by HCl (HA_ADH_4). One mL of the mixtures from each experimental sample was then reacted with 1 mL of 50 mM EDC solution by stirring for hours. The hydrogels were then transferred to two presoaked dialysis tubes and dialyzed for 2 days with three water changes. After dialysis, the hydrogels were then transferred into clean plastic tubes and dried overnight in a Speed Vac before the FTIR measurement.

Table 2.1 Conditions Used to Prepare Different Samples for Crosslinking of Hyaluronic Acid

Sample Abbrebiation	Hyaluronic Acid (wt %)	ADH (wt %)	PH Value	EDC (mM)	Stirring or Immersion	Dialysis and Dried
HA_4_EDC_stir	0.75%, H_20	_	4	50	Stirring	Yes
HA_ADH_4_EDC_stir	0.75%, H_20	3.75%	4	50	Stirring	Yes
HA	Power	_	_	_	_	_

2.2.1.2 Covalent Crosslinking of Alginate

As the alginate precipitates at pH values lower than 3.5, depending on the molecular weight [135], the pH value of the alginate solution cannot be adjusted through adding HCl as was done for hyaluronic acid. To control pH we used MES buffer with the effective pH range of 5.5-6.7 as it doesn't have the carboxyl groups present to disturb the chemistry of the covalent crosslinking. Thus, the alginate was dissolved in 50 mM MES buffer with a pH value of 5.5 to prepare 3% alginate solution (3% alginate_MES_5.5). A mixture of 0.5 mL H_2O and 0.5 mL 3% alginate_MES_5.5 was then stirred with ADH (1.875%, wt %) to get the alginate_ADH mixtures (1.5% alginate_MES_5.5_ADH). One mL of 1.5% alginate_MES_5.5_ADH reacted with 1 mL of 30 mM $CaCl_2$ solution was then used as the negative control (1.5% alginate_MES_5.5_ADH_30mM $CaCl_2$_dispense), while the experimental samples include 1.5% alginate_MES_5.5_ADH immersed within 1 mL of 100 mM EDC solution for 24 hrs (1.5% alginate_MES_5.5_ADH_100mM EDC_dispense) and 1.5% alginate_MES_5.5_ADH gelated with 1 mL of 30 mM $CaCl_2$ solution first before further immersion in 1 mL of 100 mM EDC for 24 hrs (1.5% alginate_MES_5.5_ADH_30mM $CaCl_2$(first)_100mM EDC_dispense). Through this, we can identify whether the alginate can be covalently modified with ADH by EDC and also if alginate can be further covalently crosslinked after ionic crosslinking. After chemical reaction, the hydrogels were dialyzed and dried as described in section 2.2.1.1.

Table 2.2 Conditions Used to Prepare Different Samples for Crosslinking of Alginate

Sample Abbreviation	Alginate (wt %)	ADH (wt %)	$CaCl_2$ (mM)	EDC (mM)	Stirring or Immersion	Dialysis and Dried
1.5% Alginate_MES_5.5_ADH_30mM $CaCl_2$_dispense	1.5%, MES buffer	1.875%	30	_	Immersion	Yes
1.5% Alginate_MES_5.5_ADH_100mM EDC_dispense	1.5%, MES buffer	1.875%	_	100	Immersion	Yes
1.5% Alginate_MES_5.5_ADH_30mM $CaCl_2$(first)_100mM EDC_dispense	1.5% MES buffer	1.875%	30	100	Immersion	Yes

2.2.1.3 Ionic and Covalent Crosslinking of Alginate/Hyaluronic Acid

For the preparation of alginate/hyaluronic acid mixtures for ionic and covalent crosslinking (double crosslinking), 1.5% alginate, 0.375% hyaluronic acid was used. To achieve this without the use of HCl for adjusting the pH value, 3% alginate_MES_5.5 and 0.75% hyaluronic acid_ADH_4 were mixed at 1:1 volume ratio. This mixture has a final pH value of approximately 5 and the solution is symbolized as alginate_hyaluronic acid_ADH_PH in this work. One mL of alginate_hyaluronic acid_ADH_PH solution reacted with 1 mL of 100 mM EDC by stirring was termed as alginate_HA_ADH_PH_100mM EDC_stir. To examine the effect of addition of ADH, sample of alginate_hyaluronic acid_PH without ADH reacted with 1 mL of 100 mM EDC was also used (alginate_HA_PH_100mM EDC_stir). And the one immersed within 100 mM $CaCl_2$, or 100 mM $CaCl_2$ and 100 mM EDC are labeled respectively as alginate_HA_ADH_PH_100mM $CaCl_2$_dispense and alginate_HA_ADH_PH_100mM $CaCl_2$_100mM EDC_dispense. Dialyzed alginate_hyaluronic acid_ADH_PH was termed as alginate_HA_ADH_PH_dialysis, which theoretically gives only alginate/hyaluronic acid after dialysis as ADH should be removed from the mixture during the dialysis process.

Table 2.3 Conditions Used to Prepare Different Samples for Crosslinking of Alginate/Hyaluronic Acid

Sample Abbreviation	**3% Alginate_MES_5.5 : 0.75% Hyaluronic acid_4 (V/V)**	**ADH (wt %)**	**$CaCl_2$ (mM)**	**EDC (mM)**	**Stirring or Immersion**	**Dialysis and Dried**
Alginate_HA_PH_100mM _EDC_stir	1:1	_	_	100	Stirring	Yes
Alginate_HA_ADH_PH_ 100mM_EDC_stir	1:1	1.875%	_	100	Stirring	Yes
Alginate_HA_ADH_PH_ 100mM $CaCl_2$_dispense	1:1	1.875%	100	_	Immersion	Yes
Alginate_HA_ADH_PH_ 100mM $CaCl_2$_100mM EDC_dispense	1:1	1.875%	100	100	Immersion	Yes
Alginate_HA_ADH_PH_ dialysis	1:1	1.875%	_	_	Stirring	Yes

The effect of concentrations of $CaCl_2$ and EDC as well as the pH value of the alginate/hyaluronic acid hydrogel formation was then investigated. Alginate_hyaluronic acid_ADH_PH mixtures were reacted with 100 mM EDC with various concentrations of $CaCl_2$ (0 mM to 100 mM) and the final products were examined by the FTIR spectra. Also, crosslinker solutions of 50 mM $CaCl_2$ with different concentrations of EDC (0 mM to 100 mM) were used to crosslink alginate_hyaluronic acid_ADH_PH mixtures.

For the experiment aimed to evaluate the effect of pH value on the covalent crosslinking, two methods were used to prepare 1.5% alginate_0.375% hyaluronic acid_ADH mixtures. One is to prepare as the way described above: mixing 3% alginate_MES_5.5 and 0.75% hyaluronic acid_ADH_4 at 1:1 volume ratio. Mixture prepared by this method is symbolized as alginate_HA_ADH_PH. The second method is to prepare MES buffer at pH value of 4. And then

dissolve the alginate, hyaluronic acid and ADH powders in this buffer to obtain mixture of alginate_HA_MES_4_ADH. PH value of the final mixture prepared in the second way was around 5.5, which was higher than that of alginate_HA_ADH_PH. The two mixtures were then immersed within 100 mM EDC solutions for crosslinking.

To further understand the effect of pH value on the covalent crosslinking, similar experiment was done on hyaluronic acid. Briefly, one method was to adjust pH of hyaluronic acid_ADH mixture to 4, while the other method was to adjust pH of the hyaluronic acid solution to 4 first before adding ADH powder. Then the two mixtures were crosslinked by immersing them in 200 mM EDC crosslinker solution. All the crosslinked hydrogels were further dialyzed for 2 days with three times water changes and lyophilized on the Speed Vac, after which FTIR measurements were carried out.

2.2.2 FTIR Measurement

Lyophilized 10 mg samples of each reaction product were mixed with 300 mg dry KBr and pressed into a pellet using a macro KBr die kit. The solid pellet was analyzed using FTIR instrument (Perkin-Elmer, PerkinElmer Life And Analytical Sciences, Inc., USA).

2.3 Results and Discussions

To facilitate the following discussion, peak assignment for different chemical bonds in the organic chemicals is summarized in Table 2.4. As shown in Table 2.4, plain hyaluronic acid has the characteristics for carboxylate anions, which are absorption bands at 1600 cm^{-1} and 1412 cm^{-1} assigned to the asymmetric and symmetric strectching vibrations of carboxylate anions. Though

there are amide bonds in the plain hyaluronic acid, peaks for amide bonds in plain hyaluronic acid are not evident due to the small quantity of amide bonds.

Table 2.4 IR Peak Assignment for Different Chemical Bonds of Alginate/Hyaluronic Acid Crosslinking

Chemicals	**Functional Group**	**Molecular Motion**	**Wavenumber(cm^{-1})**
Alginate/hyaluronic acid (pH=~4)	Carboxylic acid -COOH	C=O stretching dimer	~1710
		C=O stretching monomer	~1735
		O-H bend	1440-1400
		O-H stretch	2500-3300
		C-O-H in-plane bend	~1415
		C-O stretch	1320-1210
	Alkane $-CH_3$	C-H stretch	2950-2800
		CH_3-bend	~1375
	Amide bond -CO-NH- Secondary amide	N-H bend (amide II band)	1530±30
		N-H strecth (>= 2 bands)	3330-3060
		C=O stretch	1630-1695
ADH	Amine $-NH_2$ Primary amine	N-H stretch	3400-3500 (two bands)
		N-H bend (scissoring)	1580-1650
		C-N stretch	1000-1250
	Amide bond CO-NH- Secondary amide	N-H bend (amide II band)	1530±30
		N-H strecth (>= 2 bands)	3330-3060
		C=O stretch	1630-1695
	Alkane $-CH_2$	CH_2 bend (scissing)	~1458
Crosslinked alginate/hyaluronic acid hydrogel	Amide bond CO-NH- Secondary amide	N-H bend (amide II band)	1530±30
		N-H strecth (>= 2 bands)	3330-3060
		C=O stretch	1630-1695
	Ester bond -COO	C=O stretch	1750-1735
		C-C(O)-C stretch	1160-1210
	Carboxylate $-COO^-$	C=O stretch	~1620, ~ 1429

Crosslinking of hyaluronic acid with EDC leads to crosslinked hydrogels with enhanced mechanical strength. Spectrum of the resulted hydrogel shows the peaks at the wavenumber of 1708 cm^{-1} and 1114 cm^{-1}, which are assigned to the C=O stretch and C-C(O)-C stretch of ester bond, respectively. Also, there are characteristic peaks for amide bonds (1660 cm^{-1}, 1550 cm^{-1}

and 1423 cm^{-1}). This is propably due to undesired side reaction of the O-acylisourea to rearrange into the stable N-acylurea. As indicated in Figure 1.5, there is formation of N-acylurea when the carbodiimide is in excess. And since the N-acylurea is of high molecular weight, it cannot be gotten rid of during the dialysis process. However, as observed in Figure 2.1, there is a peak at the wavenumber of 1600 cm^{-1}, which indicates that there are unreacted carboxylate groups with only EDC added.

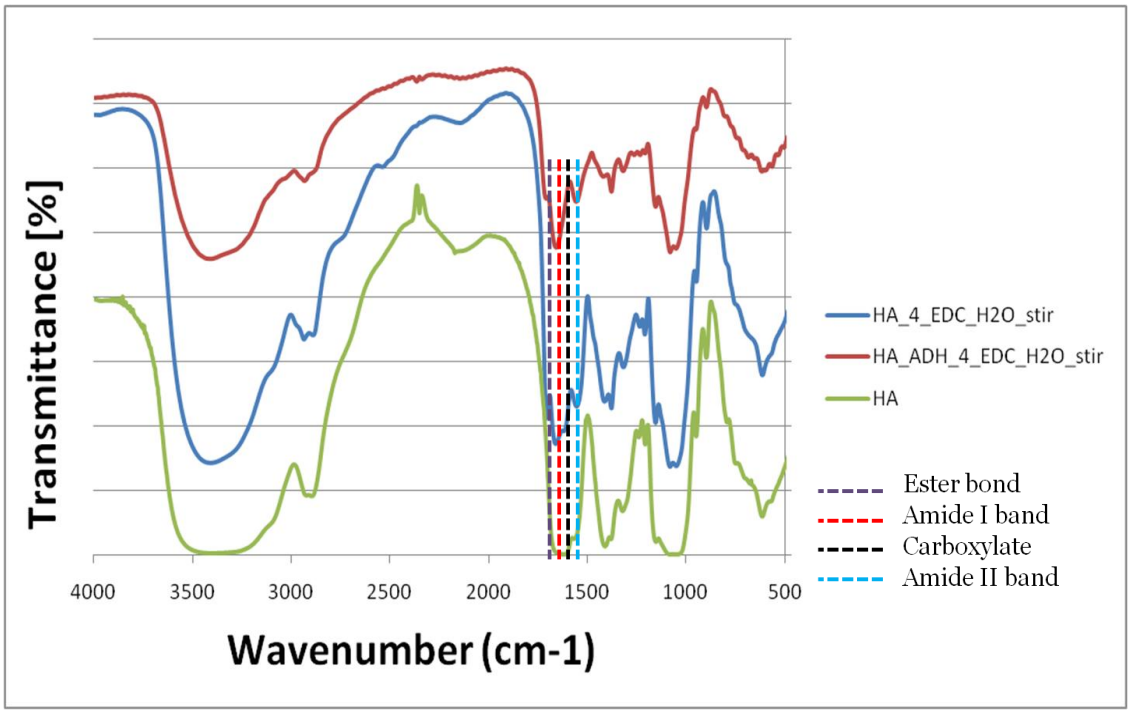

Figure 2.1 FTIR spectra of plain hyaluronic acid, hyaluronic acid stirred with EDC, and hyaluronic acid_ADH mixtures stirred with EDC after dialysis and lyophilization. Reaction of EDC with hyaluronic acid at pH of 4 led to the new characteristic peaks of ester bonds at 1708 cm^{-1}(purple dash line), and amide bonds at 1660 cm^{-1}(red dash line) and 1550 cm^{-1} (blue dash line), with the remaining peak of carboxyl groups at 1600 cm^{-1}(black dash line). Further addition of ADH into the hyaluronic acid, reacted with the presence of EDC, resulted in more amide bonds (red and blue dash line), but fewer ester bonds (purple dash line). And the amide formation was complete with no wave absorption at1600 cm^{-1} , indicating that all the carboxyl groups were transformed into ester bonds and particularly the amide bonds.

Crosslinking of hyaluronic acid_ADH_4 leads to the decrease of the peaks at 1708 cm^{-1}, 1114 cm^{-1}, and 1405 cm^{-1}, and increases the peaks at 1660 cm^{-1} (C=O stretch of secondary amide), 1550 cm^{-1} (N-H bend of amide) and 1423 cm^{-1} (C-N stretch of amide). This indicates the formation of more amide bonds when the ADH is added, which is consistant with the mechanism of EDC mediated crosslinking of carboxyl groups with amine groups. Morphologically, reaction of ADH with hyaluronic acid under the function of EDC resulted in crosslinked hydrogels, with better mechanical strength compared to the one without ADH added. This is attributed to the amine bonds and bifunctional property of ADH, leading to more covalent crosslinking.

Crosslinking of 1.5% alginate with ADH by EDC also leads to the formation of amide bonds as demonstrated in Figure 2.2. MES buffer at pH of 5.5 is used as alginate precipitates at low pH values, making the adjustment of the pH of alginate solution problematic. As noticed, there is still existence of carboxylate anions, which is consistent with the morphology change. The resulted hydrogel is weak at mechanical strength, making it difficult to handle. When compared to the ADH-crosslinked hyaluronic acid, with the same reaction conditions, it seems that alginate was not completely covalently crosslinked. This is probably due to the insufficient amount of ADH or EDC added. And it was found that the coupling efficiency of amine acid to heparin and heparan sulfate is less efficient than that to other glycosoaminoglycan such as hyaluronic acid. It is proposed that the α-L, 1-4 glycosidic bonds between the uronic acid and glucosamine residues of the heparin and heparan sulfate is the main reason [136]. Similarly, it is likely that the structural difference of alginate and hyaluronic acid would lead to the difference in crosslinking extent between alginate and hyaluronic acid with ADH by EDC. Another possibility is that the pH value of 5.5 is not optimal for alginate crosslinking, or there is a part of carboxyl groups in alginate that do not crosslink with ADH by EDC.

It is also found that alginate after ionic crosslinking with $CaCl_2$ can be further crosslinked by ADH to form the amides. This can be explained by the fact that carboxyl groups in the mannuronate blocks, which don't bind to the $CaCl_2$, can still react with ADH to form the amide bonds. But it remains to be determined whether the carboxyl groups in the guluronate blocks could form amide bonds with ADH.

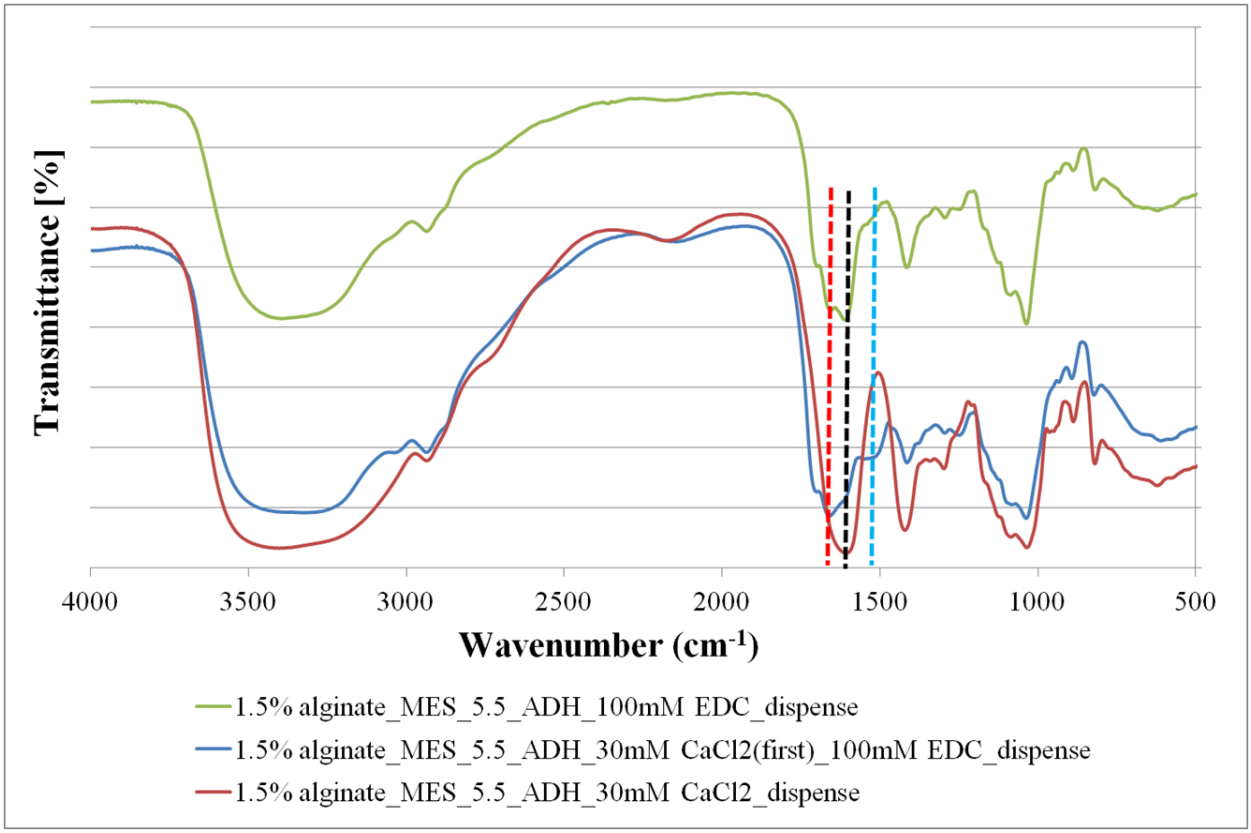

Figure 2.2 FTIR spectra of 1.5% alginate_MES_5.5_ADH crosslinked with $CaCl_2$, EDC or both $CaCl_2$ and EDC. Crosslinking of alginate with $CaCl_2$ didn't change the spectra, while further addition of EDC into the $CaCl_2$ crosslinked alginate led to the characteristic peaks for amide bonds at 1660 cm^{-1}, and 1550 cm^{-1} (red and blue arrows, respectively). Crosslinking of alginate, ADH with EDC also resulted in the amide formation despite that there were carboxyl groups remaining indicated by the black dash line.

Covalent crosslinking of 1.5% alginate/0.375% hyaluronic acid mixture with ADH by EDC was demonstrated in Figure 2.3. Dialyzed mixture of alginate_hyaluronic acid_ADH_PH had the characteristic peaks for carboxylate anions, with no peaks for ADH, which indicates the

efficiency of the dialysis. Ionically crosslinked with $CaCl_2$, the mixture had similar FTIR spectrum profile as that of the non-ionically crosslinked one. Addition of EDC to alginate/hyaluronic acid mixture without ADH led to ester bond formation as well as some amide formation, whereas addition of ADH resulted in more amide bonds and fewer ester bonds. This was consistent with the result of the crosslinking of hyaluronic acid with ADH as described above.

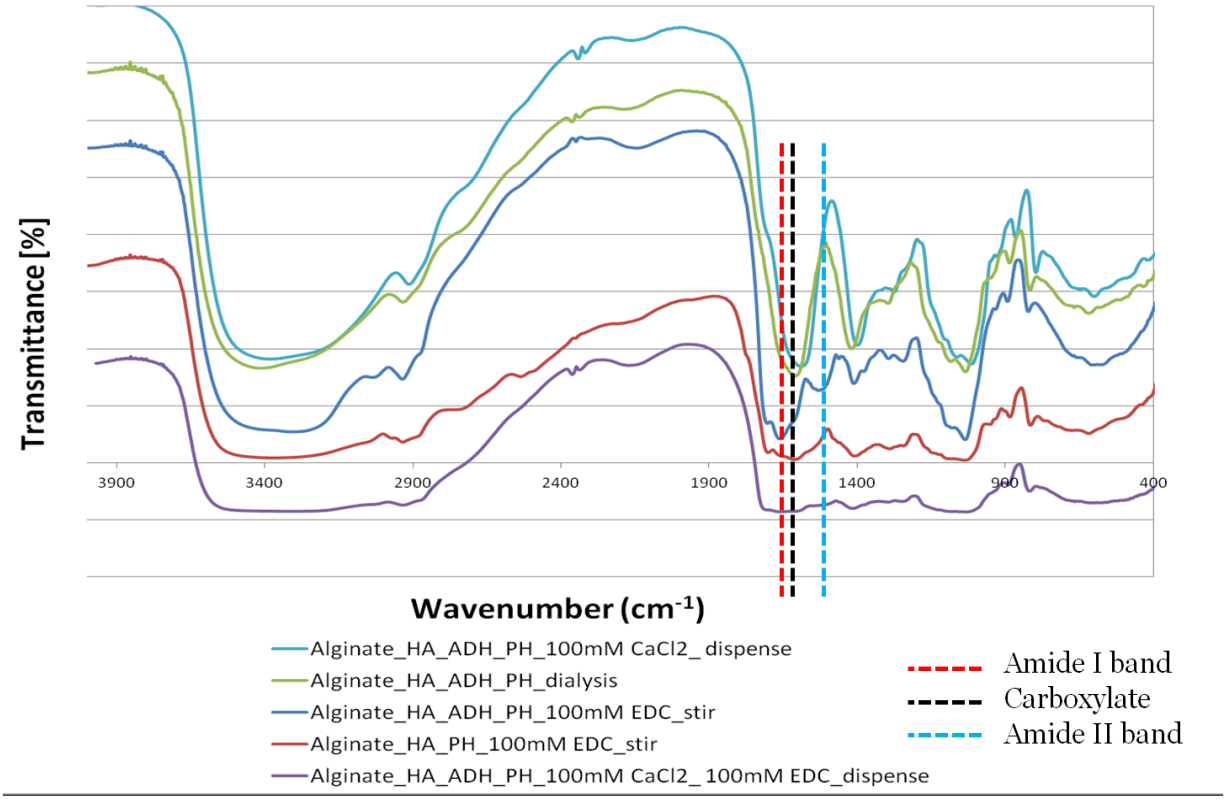

Figure 2.3 FTIR spectra of 1.5% alginate_0.375% hyaluronic acid_ADH_PH mixtures crosslinked with $CaCl_2$, EDC or both $CaCl_2$ and EDC under mixing or dispensing conditions. There was amide formation when EDC was added to the alginate/hyaluronic acid mixture and the reaction efficiency was increased when ADH was further incorporated. Also, the covalent modification was made to the alginate_hyaluronic acid_ADH mixture with the presence of both $CaCl_2$ and EDC. Black dash line indicated the characteristic peak at 1600 cm^{-1} for carboxylate anions, red and blue arrows represent the characteristic peaks at 1660 cm^{-1} and 1550 cm^{-1} for amide bonds.

Also, there was amide formation in the group of alginate_hyaluronic acid_ADH_PH immersed within crosslinker solution of 100 mM $CaCl_2$ and 100 mM EDC. However, peaks in the range of 1400 cm^{-1} to 1750 cm^{-1} are not evident and decent. This was probably due to the presence of the carboxylate anions in the ionically-crosslinked alginate, which might ruffle the spectrum. Also, it is possible that $CaCl_2$ might disturb the amide formation as both ionic and covalent crosslinking are aimed at the carboxyl groups. Primary results indicated that $CaCl_2$ didn't affect on the amide formation of hyaluronic acid with ADH. Thus, it is likely that $CaCl_2$ can influence on the covalent crosslinking through gelation of alginate with $CaCl_2$.

FTIR spectra of alginate_hyaluronic acid_ADH_PH mixtures crosslinked by 100 mM EDC with varying concentrations of $CaCl_2$ were shown in Figure 2.4. Though it is difficult to quantify the amide formation using FTIR spectroscopy measurement, Figure 2.4 demonstrates that amide formation was dependent on the concentration of $CaCl_2$. With less $CaCl_2$ added for ionic crosslinking, there was more amide bond formation concluded from the relative amount of amide II band (blue dash line) and amide I band (red dash line) to the carboxylate anions (black dash line). Ionic crosslinking of alginate with $CaCl_2$ is dependent on the concentration of $CaCl_2$ and gelating time. The more $CaCl_2$ applied and the longer time it is allowed for ionic crosslinking, the fewer carboxylate groups in the alginate are left for amide formation, which takes a longer time. Thus, it is necessary to control the extent of ionic crosslinking so as to permit more covalent modification. And this can be done through limiting the $CaCl_2$ amount and the crosslinking time for ionic modification. On the other hand, ionic crosslinking of alginate in the alginate/hyaluronic acid mixture should be strong enough to provide the structural support for the 3D scaffold during the dispensing process.

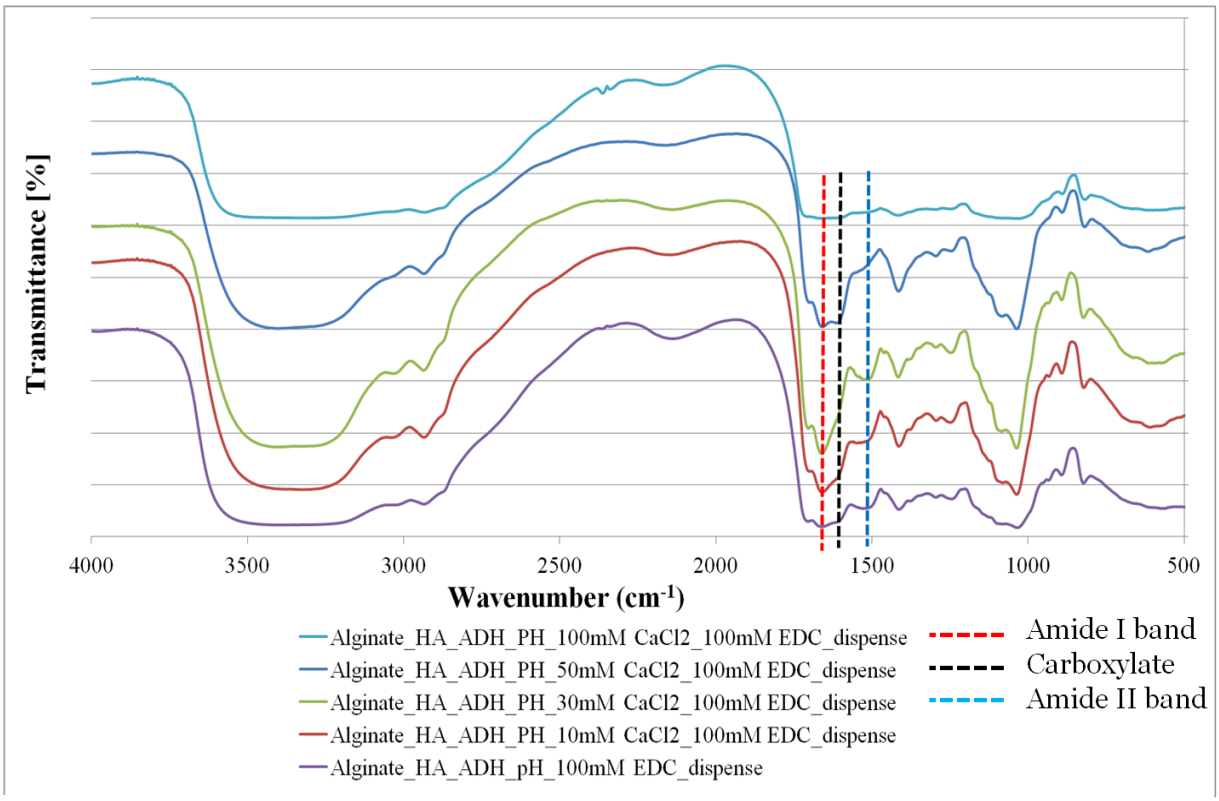

Figure 2.4 Effect of $CaCl_2$ concentrations on the covalent crosslinking of 1.5% alginate_0.375% hyaluronic acid_ADH_PH. With the increase of concentration of $CaCl_2$ solution, there seemed to be fewer amide bonds, as indicated by the characteristic peaks at 1660 cm^{-1} (red dash line), and 1550 cm^{-1} (blue dash line). And higher concentration of $CaCl_2$ masked the FTIR spectrum, with the undistinguishable peaks for different chemical bonds. Black dash line indicated the characteristic peak at 1600 cm^{-1} for carboxylate anions.

Concentration of EDC also affected the amide formation, as shown in Figure 2.5: there was more amide bond formation with higher concentration of EDC. 50 mM EDC was excessive to crosslink the carboxylate groups in the alginate_hyaluronic acid_ADH_PH. As discussed in Chapter 1, excessive EDC leads to more side reaction of N-acylurea formation. However, without homogenization, the covalent crosslinking of alginate/hyaluronic acid was slow and the chance of reagent molecules coming across was quite limited. Thus, higher concentration of EDC is probably needed for more covalent crosslinking of alginate/hyaluronic acid mixture.

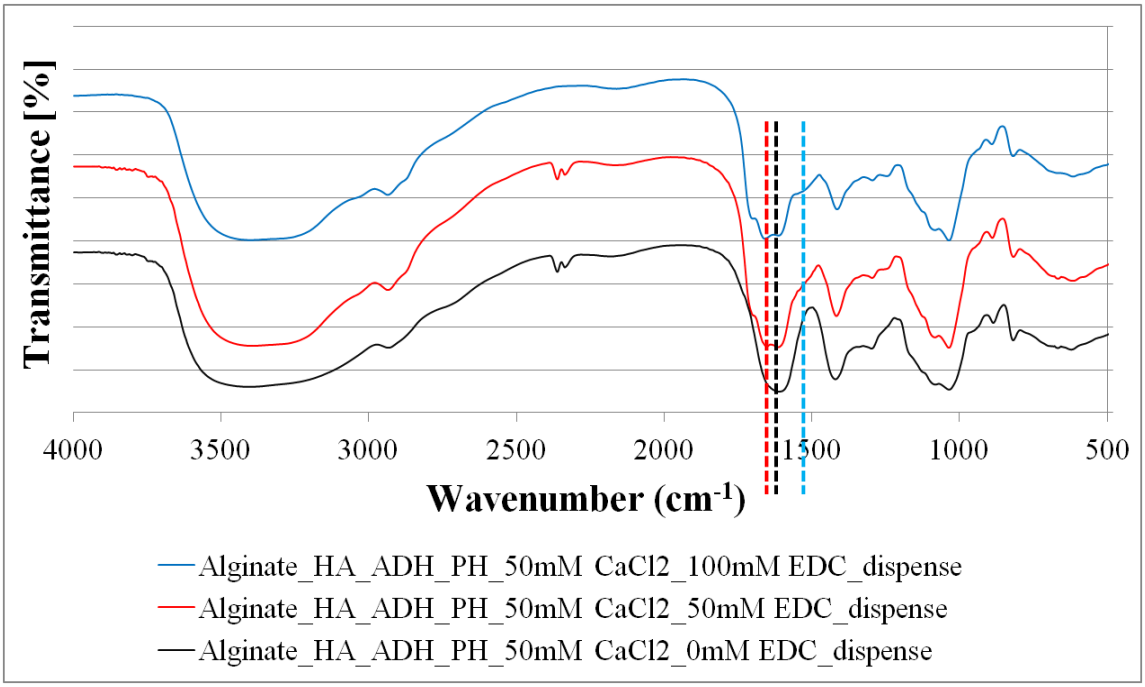

Figure 2.5 Effect of EDC concentrations on the covalent crosslinking of 1.5% alginate_0.375% hyaluronic acid_ADH_PH. There was more amide formation when EDC was added at a higher concentration. Black dash line indicated the characteristic peak at 1600 cm^{-1} for carboxylate anions; red and blue dash lines represented the peaks at 1660 cm^{-1} and 1550 cm^{-1} for amide bonds.

Next, pH value of the reaction was investigated since the respective pH adjustment of alginate and hyaluronic acid solution was troublesome and time-consuming. It would be easier that both alginate and hyaluronic acid can be dissolved in the same buffer, while ensuring the pH value to be high enough to non-precipitate alginate and low enough to allow the chemistry to work. At first attempt, MES buffer at pH of 5.5 was proposed to dissolve both alginate and hyaluronic acid, after which ADH would be added. However, since the MES buffer is effective within the pH range of 5.5 to 6.7 and addition of ADH would increase the pH value. And the primary experimental result shows that mixtures with a lower pH value crosslink sooner. Thus, attempt was tried to prepare MES buffer at pH of 4 initially while addition of ADH makes the final pH value equal 5.5.

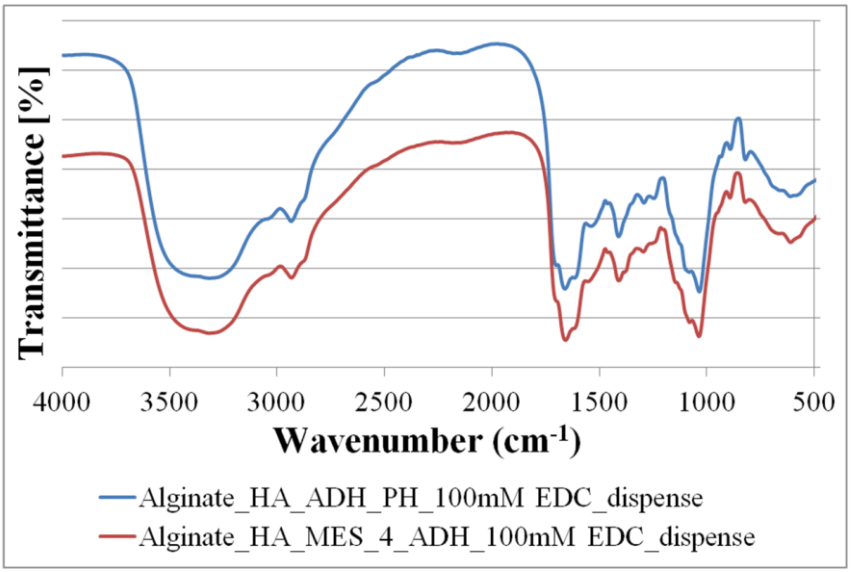

(a)

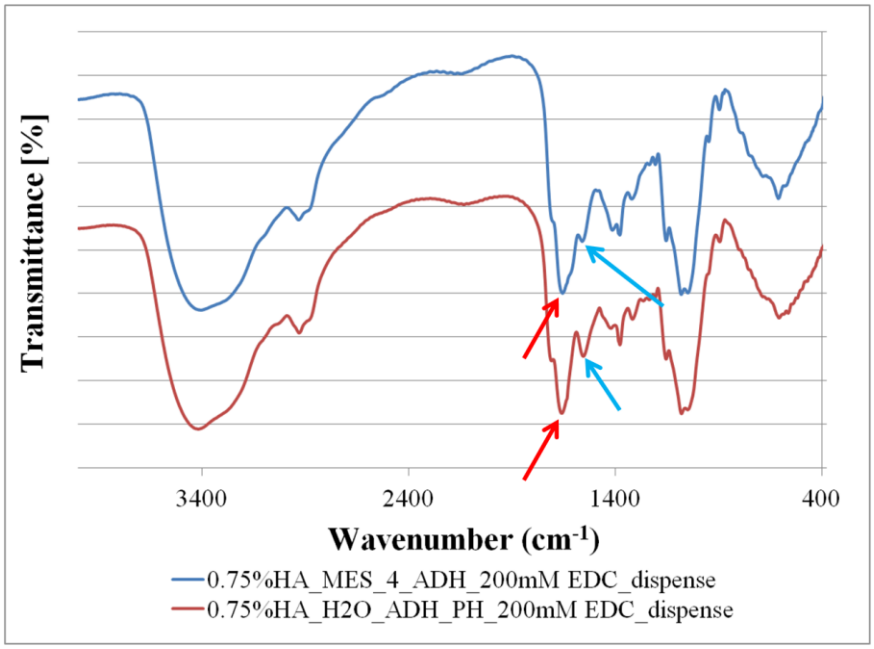

(b)

Figure 2.6 Effect of pH value on the covalent crosslinking of (a) hyaluronic acid, and (b) alginate/hyaluronic acid mixture. (a)More amide bonds were formed for hyaluronic acid at a lower pH as indicated by the relatively more peak absorption at 1533 cm^{-1}; (b)No significant difference of amide formation was observed for alginate/hyaluronic acid mixutures reacted at different pH values.

Comparison of amide formation with different preparation methods of hyaluronic acid hydrogel and alginate/hyaluronic acid hydrogel is shown in Figure 2.6. And we can find that

both methods lead to the formation of amide bonds of hyaluronic acid with ADH, but the crosslinking speed is quicker at pH of 4 and there seems to be more amide bond formation at the lower pH value (Figure 2.6 (a)). As for the alginate/hyaluronic acid mixture, the hydrogel formation is sooner in the group of alginate_hyaluronic acid_ADH_PH group, which has the pH value of 5. The pH value of alginate_hyaluronic acid_MES_4_ADH mixture was around 5.5, and the reaction rate was slower. From the FTIR spectra, we cannot conclude whether there was significant difference of amide formation between these two groups.

The effect of pH value on the EDC-mediated amide formation has been investigated by others, and the result shows that pH value of 5.5 leads to a most efficient conjugation of peptide into the biomaterial [137]. However, with different reaction reagents having different pKa (acid dissociation constant) values, it is possible that the pH value of a particular reaction is unique and this could be achieved by measuring the conjugation efficiency at different pH values. Since the reaction is more favorable under lower pH values, the preparation method of respective pH adjustment of hyaluronic acid_ADH_4 and alginate_MES solution before mixing together was applied for the biocompatibility test in Chapter 3.

2.4 Conclusions

There are covalent crosslinking of alginate/hyaluronic acid mixture with ADH in presence of $CaCl_2$, and the chemical modification is dependent on the concentration of EDC, $CaCl_2$ and pH value of the reaction. Effect of the pH value on the covalent crosslinking efficiency is probably due to the fact that the amide formation requires both ionized carboxyl groups and disassociated protons (as indicated in Figure 1.5), which can be obtained through maintaining the pH within the range of 3.5 to 4.5 [79]. It still remains to be determined whether

the hyaluronic acid in the mixture was covalently crosslinked. The present research shows that alginate, after crosslinking with $CaCl_2$, can further crosslink with ADH by EDC, which might delay the loss of the mechanical strength of alginate *in vivo*. And the incorporation of crosslinked hyaluronic acid may further increase the *in vivo* residence time. For this, *in vivo* biodegradation study of alginate/hyaluronic acid hydrogels may shred a light on this.

CHAPTER 3 Biocompatibility of Alginate/Hyaluronic acid Hydrogels

3.1 Introduction

Covalent crosslinking of alginate/hyaluronic acid mixture with ADH at presence of EDC and $CaCl_2$ were examined, yet it remains to check the biocompatibility of the composite hydrogels for Schwann cells, which are proven to play a key role in both peripheral nerve and spinal cord regeneration. Thus, it is interesting to investigate whether the concentration of alginate and hyaluronic acid have an effect on the Schwann cell viability and growth. Besides, the effects of the covalent modification of the alginate/hyaluronic acid substrates and the concentration of hyaluronic acid incorporated were also studied so as to find the proper composite substrate for Schwann cell culture, which will be promising for SCI repair.

3.2 Materials and Methods

3.2.1 Schwann Cell Culture

In this study, Schwann cells (RSC 96, CRL-2765, passage number from 14 to 22) purchased from ATCC (American Type Culture Collection ATCC, Manassas, VA) were used for the MTT (3-(4, 5-Dimethylthiazol-2-yl)-2, 5-diphenyltetrazolium bromide, a yellow tetrazole) assay to determine the biocompatibility of the composite hydrogels. Schwann cells were cultured in standard Dulbecco's Modified Eagle Medium (DMEM), 10% fetal bovine serum (FBS) (Invitrogen Co, Carlsbad, California, CA, USA), and 1% antibiotics (penicillin/streptomycin/amphotericin-B) on the 10-cm tissue culture dish at 37°C in a 5% CO_2, relatively humidified incubator. Cells were passed at 80-100% confluence using 0.05% Trypsin/ethylenediaminetetraacetic acid (EDTA) (Invitrogen). And cell counting of Nigrosine

dye staining were performed with a hemocytometer. Before cell seeding, the cells were resuspended in fresh medium to the desired cell density.

3.2.2 Substrate Preparation

Low viscosity sodium alginate, molecular weight range 12,000~80,000 Da, mannuronic acid 61% and guluronic acid 39% was purchased from Sigma Aldrich Canada. Calcium chloride (Sigma, St. Louis, MO) was used as the crosslinker for sodium alginate. Hyaluronic acid sodium salt (MW 26-27 MDa) was bought from Shandong Freda Biopharm Co., Ltd. (Freda, Jinan, Shandong, China). ADH, MES buffer with useful pH range of 5.5-6.7, and EDC were all purchased from Sigma Aldrich Canada.

Two dimensional (2D) films of double-crosslinked alginate/hyaluronic acid hydrogel with different volume ratios of 3% alginate_MES_5.5 and 0.75% hyaluronic acid_ADH_4 were formed in 24-well tissue culture plates. Specifically, 100 µL of the alginate_hyaluronic acid_ADH_PH mixture was poured evenly into each well of the plate and 200 µL of 50 mM EDC_50 mM $CaCl_2$ crosslinker solution was applied on the top of the mixture. For the group of 3% alginate, only $CaCl_2$ crosslinking was applied, while for the group of 0.75% hyaluronic acid, merely EDC crosslinker solution was used. The crosslinking process was allowed to proceed for 6 hours or 20 hours at room temperature before rinsed extensively with phosphate buffer solution (PBS) buffer for 5 times, 5 mins per time. The crosslinked substrates were then sterilized with γ-radiation (dose rate: 7.13 Gy per minute) for 20 hours. Substrates made from uncrosslinked alginate or hyaluronic acid as well as crosslinked 20%-80% (V/V) alginate/hyaluronic acid hydrogels coated with 300 µL/well 100 µg/mL poly-l-lysine hydrobromide (PLL) (mol wt 30,000-70,000, Sigma) at 4°C overnight were used as controls.

Schwann cell culture on the 1.5% alginate with different amounts of hyaluronic acid was carried out to investigate the effect of concentration of hyaluronic acid on the Schwann cell viability and growth. Comparison of just ionic crosslinking with both ionic and covalent crosslinking on the cell number was also studied. In detail, mixtures of 1.5% alginate with 0%, 0.375%, 0.50% and 0.75% hyaluronic acid were prepared by dissolving the alginate, hyaluronic acid and ADH (3.75%, wt%) in 100 mM MES buffer at pH value of 4, which resulted in a pH value of 5.5 as mentioned in Chapter 2. 20 µL of the mixtures was then spread evenly in each well of a 96-well tissue culture plate and centrifuged at 4000 rpm/min for 5 mins. The prepared films were then left in air overnight to air dry. After drying, 80 µL of 50 mM $CaCl_2$ was applied in each well on the top of the film for the ionically-crosslinked groups. For the double-crosslinked ones, 80 µL of 50 mM $CaCl_2$_100 mM EDC was applied in each well on the film and crosslinked for 24 hours. Rinsed three times with double distilled water, the films were then immersed in 70% ethanol overnight to sterilize the substrates. After removing the ethanol, the substrates were rinsed twice with double distilled water and one more time with DMEM with 1% antibiotics.

3.2.3 Cell Seeding and MTT Assay

MTT assay is used to assess the cytotoxicity of alginate/hyaluronic acid hydrogels. The reduced insoluble, dark purple formazan of MTT by living cells can be solubilised by dimethyl sulfoxide into a colored solution, whose absorbance will be measured spectrophotometrically [138]. Thus, the cell number is correlated with the absorbance of the formazan reagent.

For the experiment studying the effect of concentration of alginate and hyaluronic acid on Schwann cell survival and growth, Schwann cells were seeded on the prepared 2D substrates at a

density of 100,000 cells/mL and 1 mL of the cell suspension was placed in each well of 24-well tissue culture plates. Cells were incubated in the 5% CO_2, 95% air, 37°C, humidified incubator and motored microscopically every day by Zeiss Axiovert 100 (Zeiss, Germany) supplemented with Retiga EXi Fast 1394 CCD Camera (QImaging, CA). MTT assay was carried out according to the protocol after 2 days' incubation at which the cells were about 95% confluent. Specifically, 5 mg/mL stock solution of MTT (Sigma) was prepared in 10 mM sterile PBS and 120 µL of MTT solution was added to each well. After incubation at 37°C for 3.5 hrs, media were carefully removed without disturbing the cells. 800 µL of dimethyl sulfoxide (Sigma) was added to each well and the plate was agitated on an orbital shaker at 150 rpm for 5 mins. To eliminate the interference of the substrate absorbance of the light, the soluble colored solution was removed to a clean 96-well tissue culture plate and the plate was read by a LISA reader (Spectra Max 340, Molecular Device Inc., CA, USA) at 560 nm with reference filter of 670 nm.

For the experiment studying the effect of covalent crosslinking and concentration of hyaluronic acid incorporated on the cell number of Schwann cells, 1500 cells was placed in each well of the 96-well tissue culture plate and incubated for 2 days, after which the MTT assay was carried out according to the protocol to evaluate the cell number of Schwann cells on the different substrates. The amount of MTT is 5 mg/mL and 20 µL/well. The incubation time is 1 hr.

3.2.4 Statistical Analysis

Measured values are expressed as means ± standard deviation. Levels of significance for comparing mean values of absorbance in the MTT assay were calculated using one-way ANOVA with Turkey post test. All calculations were made using GraphPad Prism 5.0.

3.3 Results and Discussions

Figure 3.1 and Figure 3.2 show the Schwann cell morphology after 2 days' incubation on the 2D double-crossliked alginate/hyaluronic acid hydrogels. The images were taken at same illumination and photography conditions. The results showed that Schwann cells on the alginate/hyaluronic acid hydrogels (Figure 3.1 (c)) and crosslinked hyaluronic acid films (Figure 3.1 (d)) had spherical-shaped morphology, with cells assembling in clusters. In contrast, Schwann cells on the tissue culture plate and PLL-treated tissue culture plate (Figure 3.1 (a) and Figure 3.1 (b), respectively) showed typical spindle-shaped morphology. This indicated that the substrates were even less preferable than the surrounding cells. This can be explained as the non-adhesive properties of alginate and hyaluronic acid. Compared to the 100% hyaluronic acid hydrogel, alginate/hyaluronic acid hydrogels seemed to be more favorable for the Schwann cell attachment. The uncrosslinked alginate was quite favorable for the cell attachment as shown in Figure 3.2 (b), while the uncrosslinked hyaluronic acid film did not permit the attachment of the cells (Figure 3.2 (a)). PLL treatment on the 20%-80% alginate/hyaluronic acid hydrogels, to some extent, enhanced the adhesion of Schwann cells though the attachment was not as good as the tissue culture plate or the uncrosslinked alginate films.

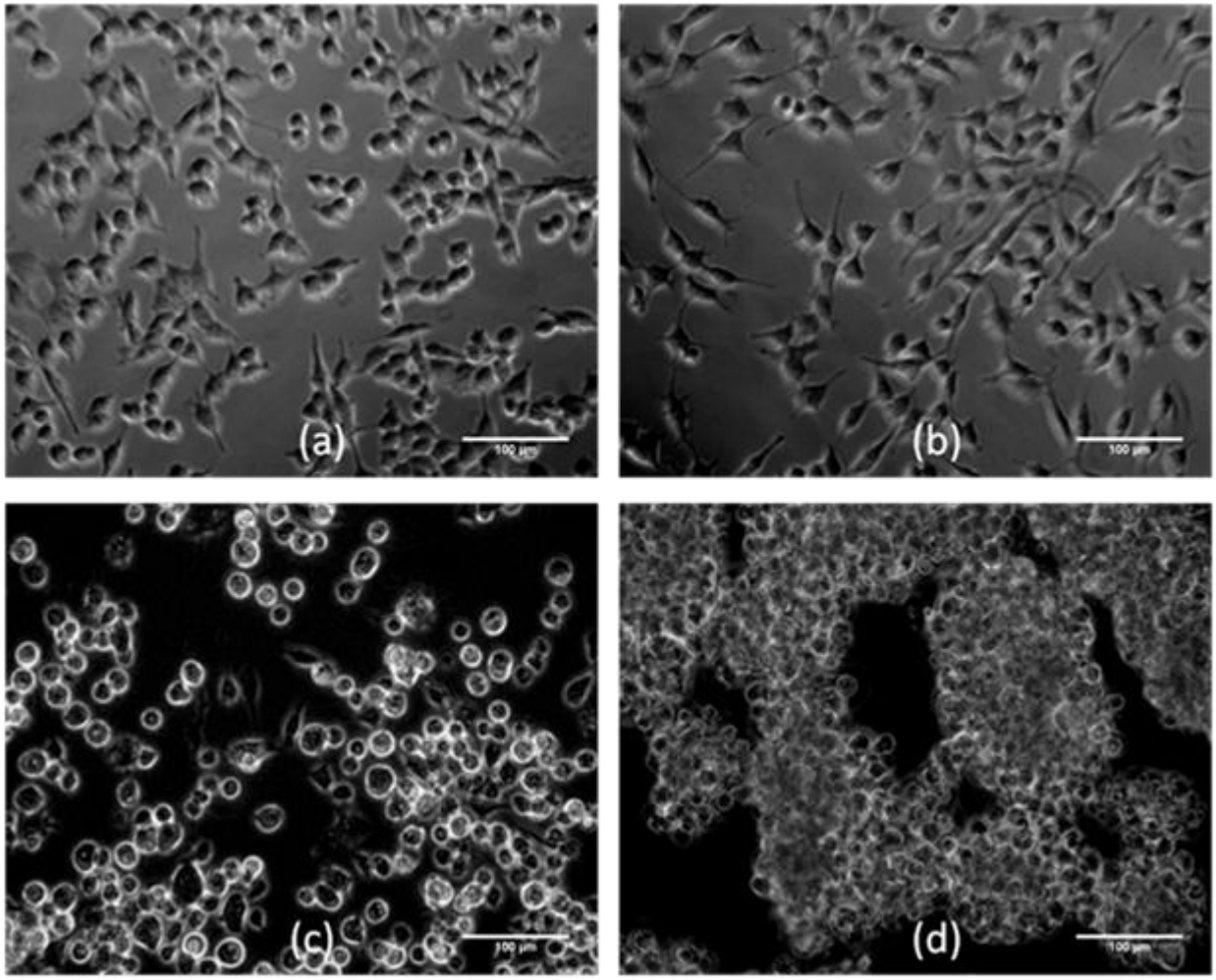

Figure 3.1 Schwann cell morphology after 2 days' culture on (a) tissue culture plate; (b) PLL-coated tissue culture plate; (c) 20%-80% alginate/hyaluronic acid hydrogels; and (d) 100% hyaluronic acid hydrogels. Scale bars: a, b, c, d=100 µm.

Figure 3.3 showed the MTT assay results for the number of Schwann cells after 2 days' incubation on the alginate/hyaluronic acid substrates double-crosslinked for 6 hours (a) or 20 hours (b). There was significant difference between control groups (Schwann cells on tissue culture plate, PLL-treated tissue culture plate, uncrosslinked hyaluronic acid and alginate films) and experimental groups (alginate/hyaluronic acid hydrogels with different concentrations of alginate and hyaluronic acid; and PLL-coated 20%-80% alginate/hyaluronic acid hydrogels), $P < 0.05$.

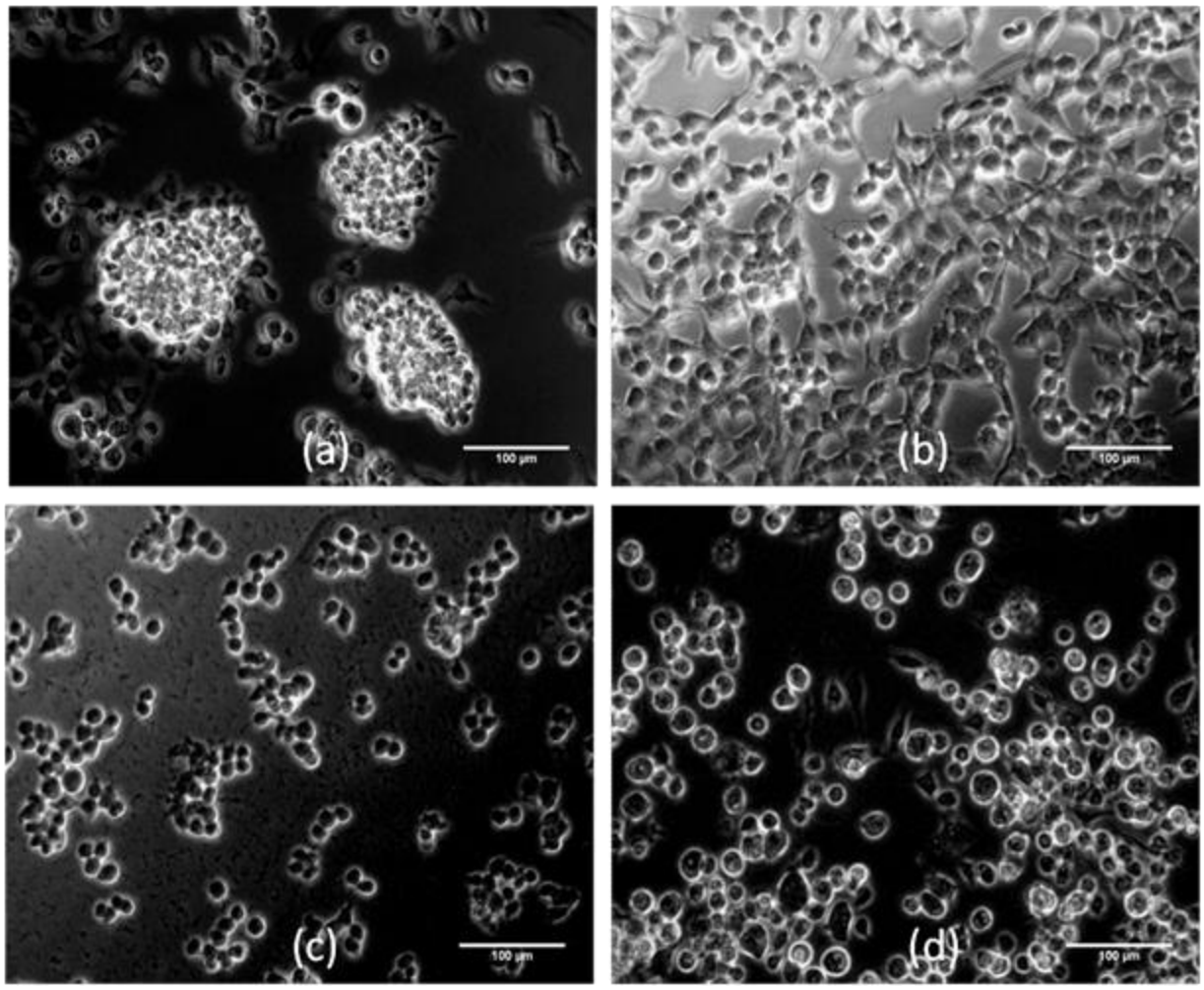

Figure 3.2 Schwann cell morphology after 2 days' culture on (a) uncrosslinked hyaluronic acid films, (b) uncrosslinked alginate films, (c) PLL-coated 20%-80% alginate/hyaluronic acid hydrogels and (d) 20%-80% alginate/hyaluronic acid hydrogels. Scale bars: a, b, c, d=100 µm.

The numbers of Schwann cells on the alginate/hyaluronic acid hydrogels crosslinked for 6 hours with different volume ratios were not significantly different except the group of 100% hyaluronic acid hydrogels with hydrogels at volume ratios of 20%:80%, 50%:50% and 30%:70%. The relatively low number of Schwann cells on the EDC crosslinked hyaluronic acid hydrogels compared to the other groups may be due to the unfavorable adhesion of Schwann cells onto the hyaluronic acid substrate compared to the alginate/hyaluronic acid hydrogels and the barely attached cells were carelessly removed during the MTT assay. The inhibitory effect of

hyaluronic acid with high molecular weight on cell proliferation may also cause the relatively low cell number. Still, from the morphology of the hydrogels prepared, hyaluronic acid hydrogels had a stronger mechanical property in comparison with other alginate/hyaluronic acid hydrogels or alginate hydrogels. This may also lead to the discrepancy of cell number on the hyaluronic acid hydrogels with the composite hydrogels.

(a)

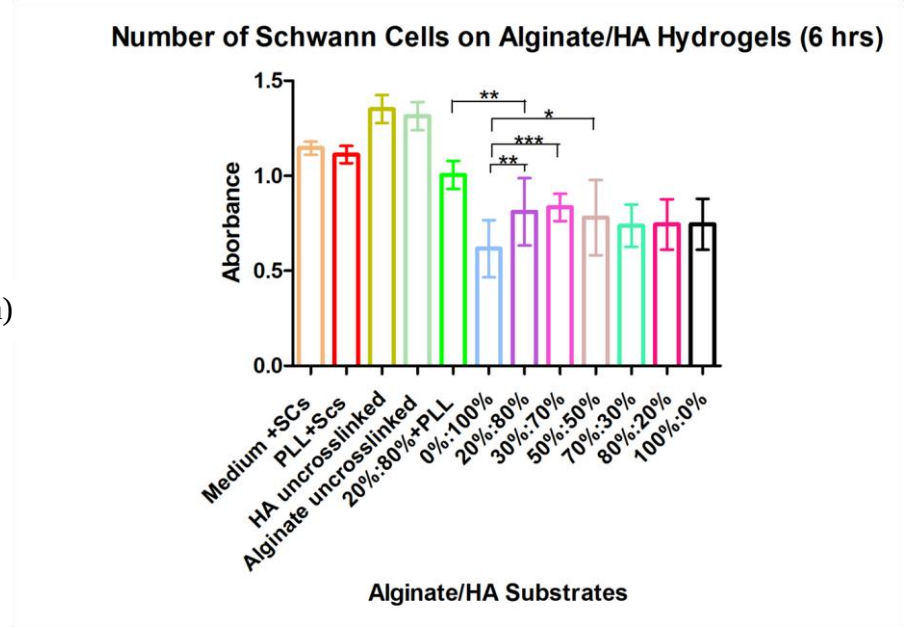

(b)

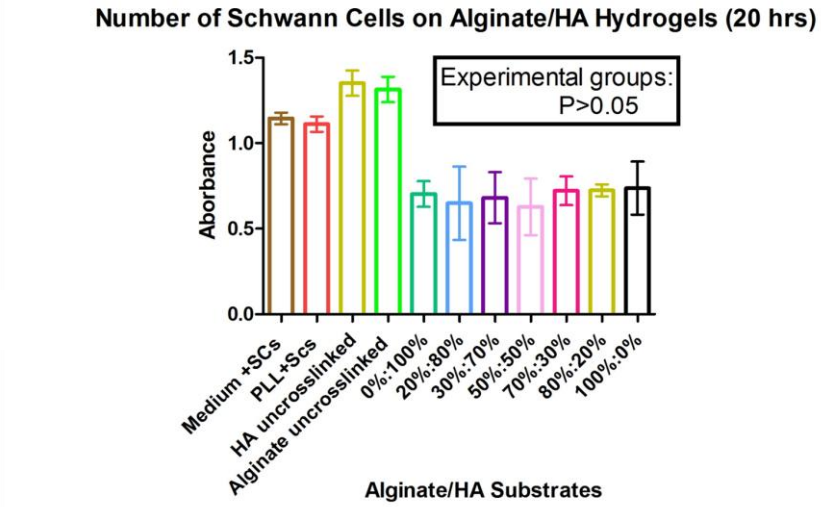

*Figure 3.3 MTT result for the number of Schwann cells on the double-crosslinked alginate/hyaluronic acid hydrogel films with different volume ratios of 3% alginate and 0.75% hyaluronic acid for 6 hours (a) and 20 hours (b). Error bars represent the standard deviation; *p < 0.05, **p < 0.001, ***p < 0.0001*

Compared to the non-PLL-coated 20%-80% alginate/hyaluronic acid hydrogels, the PLL-treated ones had significantly more Schwann cells ($P < 0.001$). For the hydrogels crosslinked for 20 hours, there was no significant difference in the cell number of Schwann cells between different experimental groups, $P > 0.05$. This indicates that the composite hydrogels have a comparable biocompatibility as the individual biomaterial.

Experiment into the effect of covalent crosslinking on the number of Schwann cells was carried out and the result indicated that there was significant difference between the ionically crosslinked alginate/hyaluronic acid hydrogels with their correspondent double-crosslinked ones as shown in Figure 3.4. But there was no significant difference in cell number between the group of 1.5% alginate_0% hyaluronic acid_$CaCl_2$ with that of 1.5% alginate_0% hyaluronic acid_$CaCl_2$, EDC, though there were fewer cells on the latter substrate.

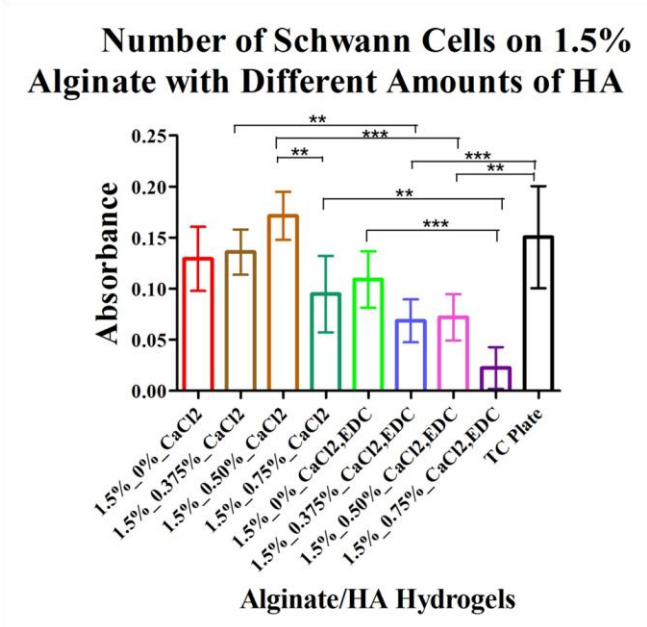

*Figure 3.4 MTT result of Schwann cells after 2 days' culture on the ionically-crosslinked and double-crosslinked alginate/hyaluronic acid hydrogels. Error bars represent the standard deviation; **p < 0.001, ***p < 0.0001.*

For the effect of hyaluronic acid's concentration on the number of Schwann cells on the $CaCl_2$ crosslinked alginate/hyaluronic acid substrates, there was no significant difference in cell number except the group of 1.5% alginate/0.5% hyaluronic acid with that of 1.5% alginate/0.75% hyaluronic acid, with fewer cells in the latter group. This probably is due to the fact that the high molecular weight hyaluronic acid inhibits the cell proliferation [139, 140]. On the other hand, there were no significant differences among other groups with lower concentrations of hyaluronic acid (0%, 0.375%, and 0.5%). This was possibly attributed to the non-covalently incorporated hyaluronic acid, which might escape from the scaffolds into the surrounding environment. In addition, the difference of cell number on these ionically-crosslinked alginate/hyaluronic acid substrates with the group of tissue culture plate was not statistically significant, indicating that the ionically-crosslinked alginate/hyaluronic acid substrates are comparable to the tissue culture plate and thus are quite suitable for Schwann cell culture.

When comparing the ionically-crosslinked 1.5% alginate/0.375% hyaluronic acid, 1.5% alginate/0.5% hyaluronic acid and 1.5% alginate/0.75% hyaluronic acid to their respective double-crosslinked ones, we can find that there were all significant differences. However, no significant difference was found between the groups of ionically-crosslinked 1.5% alginate substrate with the one of double modification. This means that the covalent crosslinking of alginate with ADH by EDC did not affect much on the biocompatibility of the alginate hydrogels. The non-complete covalent crosslinking didn't lead to much physical and mechanical change of the substrates. If these assumptions are applicable to the alginate/hyaluronic acid hydrogels similarly, then the significant differences between the ionically-crosslinked composite hydrogels with their corresponding double-crosslinked ones are attributable to the fact that the incorporated

hyaluronic acid were covalently crosslinked by ADH under the function of EDC, which might affect on the mechanical properties of the substrates and therefore influence on the cell number.

Also, it was found that there were significantly fewer cells on the 1.5% alginate/0.75% hyaluronic acid_$CaCl_2$, EDC substrate in comparison with the 1.5% alginate/0% hyaluronic acid_$CaCl_2$, EDC. This was probably because hyaluronic acid inhibited cell proliferation or the covalent crosslinking of hyaluronic acid resulted in the non-favorable substrate for cell survival and growth.

When comparing the double-crosslinked alginate/hyaluronic acid substrates (1.5%/0.375%, 0.50%, and 0.75%) to the positive control (tissue culture plate), we can conclude that the double-crosslinked composite hydrogels did not permit as much Schwann cell survival and growth as the tissue culture plate. As discussed above, the ionically-crosslinked alginate/hyaluronic acid substrates were comparable to the tissue culture plate in allowing Schwann cell survival and growth. Thus, we can conclude that the ionically-crosslinked alginate/hyaluronic acid substrates are more preferable to the double-crosslinked ones in Schwann cell culture.

3.4 Conclusions

From the MTT assay results for Schwann cell viability and growth, it is observed that both the double-crosslinked and ionically-crosslinked alginate/hyaluronic acid hydrogels allow for the Schwann cell survival and growth, indicating the potential of this composite biomaterial as a matrix for Schwann cells and neurite outgrowth of DRG neurons. There was no significant difference in cell number among the alginate/hyaluronic acid hydrogels with different volume ratios of 3% alginate and 0.75% hyaluronic acid. In terms of the number of Schwann cells,

covalent crosslinking and high concentration of hyaluronic acid seemed to be inhibitory for Schwann cell survival and growth. Thus, hydrogel of ionically-crosslinked 1.5% alginate/0.375% hyaluronic acid or 1.5% alginate/0.5% hyaluronic acid is most suitable for Schwann cell culture.

CHAPTER 4 Fabrication and Mechanical Characterization of Alginate/Hyaluronic Acid Scaffolds

4.1 Introduction

Bioengineered scaffolds with highly interconnected pore networks show promise for SCI repair. Alginate has been used successfully to fabricate scaffolds with reproducible microstructure using the dispensing-based rapid prototyping technique [141]. Unfortunately, the alginate scaffolds show limited interaction with mammalian cells due to the absence of receptors required for binding. Hyaluronic acid, which has been shown to promote robust neurite outgrowth, is incorporated in this study.

In Chapter 3, we have looked into the biocompatibility of the alginate/hyaluronic acid substrates, either ionically crosslinked or double-crosslinked ones. It was found that the ionically-crosslinked alginate/hyaluronic acid hydrogels permitted more survival and growth of Schwann cells. However, in order to fabricate 3D scaffolds, it is necessary to consider the feasibility to produce 3D scaffolds from the composite biomaterial by the dispensing-based rapid prototyping system. Concentration of hyaluronic acid affects on the fluid behavior of the dispensed biomaterial, and therefore influences on the 3D scaffold fabrication process. Thus, the ionically-crosslinked alginate/hyaluronic acid hydrogels with different concentrations of hyaluronic acid were used for the scaffold fabrication. Concentration of ionic crosslinker solution ($CaCl_2$) was also studied to check its effect on the strand profile in terms of strand diameter, linearity, and connectivity between layers.

Mechanical properties of the hydrogels are very important as the implanted scaffold should be strong enough to provide necessary mechanical support while not too hard to damage

the surrounding native tissue. For this, this chapter also presents the mechanical characterization of the 3D alginate/hyaluronic acid hydrogel scaffolds.

4.2 Materials and Methods

Low viscosity sodium alginate, molecular weight range 12,000~80,000 Da, mannuronic acid 61% and guluronic acid 39% was purchased from Sigma Aldrich Canada. Calcium chloride (Sigma, St. Louis, MO) was used as the crosslinker for sodium alginate. Hyaluronic acid sodium salt (MW 26-27MDa) was bought from Shandong Freda Biopharm Co., Ltd. (Freda, Jinan, Shandong, China).

4.2.1 Preparation of Alginate/Hyaluronic Acid Mixture

Stock solution of 6% (w/v) sodium alginate and 2% (w/v) hyaluronic acid were used to prepare four alginate/ hyaluronic acid mixtures with the final alginate concentration of 1.5% and final hyaluronic acid concentrations of 0%, 0.375%, 0.5% and 0.75%. These gel mixtures were proceeded for viscosity measurement, fabrication and mechanical test. $CaCl_2$ solutions of 10 mM, 30 mM, 50 mM, 75 mM, 100 mM and 150 mM were used as the ionic crosslinking media for alginate/hyaluronic acid mixtures. Such concentrations were chosen to validate whether the decrease of crosslinker solution concentration would limit the crosslinking speed and density, which might serve to solve the problem of detachment between different layers during dispensing. Also, as crosslinking extent of the alginate would lead to shrinkage or swelling of the dispensed struts, the variation of $CaCl_2$ concentration might facilitate the fabrication of 3D scaffolds with controllable microstructure.

4.2.2 Viscosity Measurement

The rheological properties of prepared alginate/hyaluronic acid mixtures were measured by a rheometer (Brookfield DV-III+ Programmable rheometer, Brookfield, Middleboro, MA), shown in Figure 4.1.

(a) (b)

Figure 4.1 (a) Wells/Brookfield DV-III+ Cone/Plate rheometer; (b) sample cup spindle for the rheometer.

This rheometer has a cone and plate structure with the shear rate controlled via programming. The rheometer also provides the ability to collect and record the data during the rheological tests. In the present study, a CP 41 spindle was selected for use, which required a sample volume of 2 mL. After zeroing and calibration of the rheometer, the flow behavior of alginate/hyaluronic acid mixtures was measured at varying shear rates via the control of the spindle rotation speed sweeping from 10 RPM to 250 RPM in 30 RPM increments. Only data with the torque value ranging from 10% to 100% was considered to be effective data. All the measurements were done once as the repeatability of the instrument was proven high. Shear

stress-shear rate curves as well as viscosity-shear rate curves were obtained to characterize the flow behavior of different mixtures and the power law was applied to fit the curves:

$$\tau = \tau_0 + K\dot{\gamma}^n \quad \text{(Eq. (4.1))}$$

Where τ is the shear stress, τ_0 is the yield stress, K is the consistency index, $\dot{\gamma}$ is the shear rate (the velocity gradient perpendicular to the plane of shear), and n is the flow behavior index.

4.2.3 Fabrication of Multilayer Scaffolds

4.2.3.1 Scaffold Fabrication by the Adapted Fluid Dispensing System

For the fabrication of 3D hydrogel scaffolds, the dispensing-based rapid prototyping system adapted from a typical commercial fluid dispensing system (C0720M, Asymtek), shown in Figure 4.2, was applied. The pressured air in the pneumatic dispenser drives the fluid flow in the syringe through a small-sized dispensing nozzle. And with the personal computer to control the dispenser, position and temperature, this system enables the construction of 3D scaffolds with reproducible, controllable and complex microstructure. In this study, aqueous mixtures of 1.5% alginate with 0%, 0.375%, 0.50% and 0.75% hyaluronic acid were dispensed layer by layer through 250 μm SmoothFlow nozzle tip into $CaCl_2$ crosslinking solution for gel formation. Unfortunately, with parameters such as air pressure, needle size, nozzle velocity, flow behavior of dispensed biomaterials, as well as the initial nozzle height from the crosslinking solution, it is quite difficult to control the scaffold microstructure. To obviate the time-consuming process of adjusting so many parameters for scaffold fabrication, model of the strut diameter was applied.

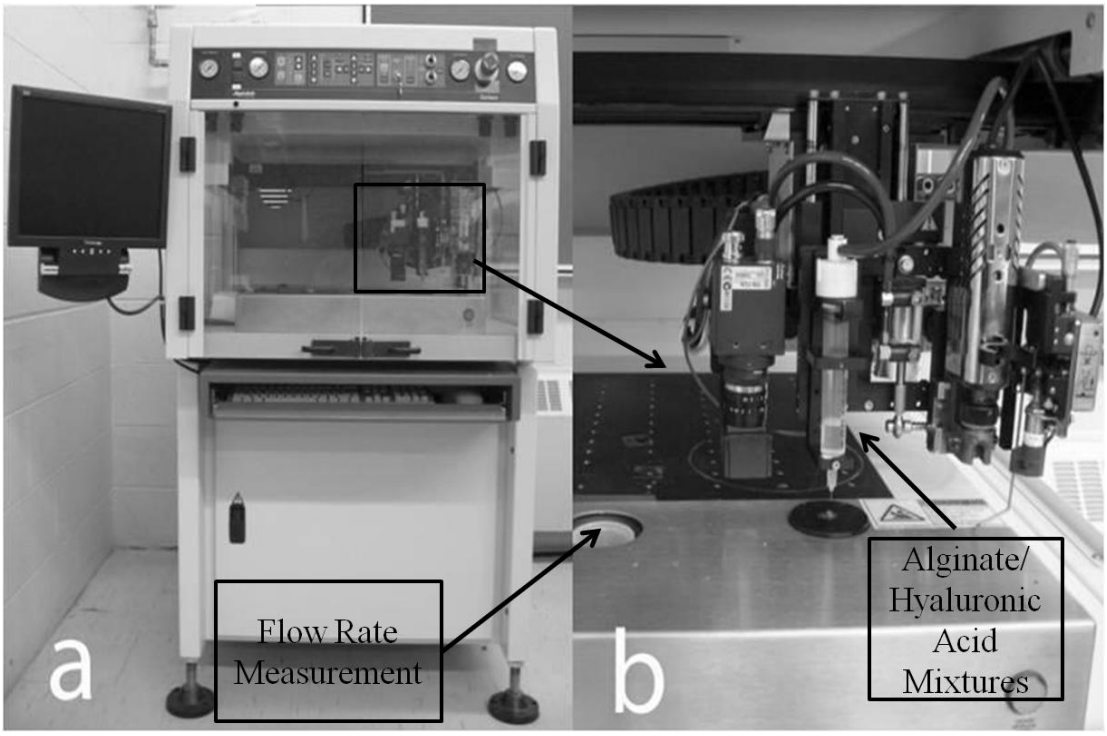

Figure 4.2 Adapted commercial fluid dispensing machine: (a) horizontal view of the whole system; (b) close-up view of the dispensing component.

Diameter of the dispensed struts is dependent on the flow rate, nozzle velocity, swelling rate of the hydrogel strands. Ignorant of the effect of swelling, the relationship between the strut diameter with the flow rate and nozzle velocity can be represented as Eq. (4.2)

$$D=\sqrt{\frac{4Q}{\pi v}} \qquad \text{(Eq. (4.2))}$$

Where Q is the volume flow rate (mL/s) and v is the nozzle deposition velocity.

To obtain deposited struts with diameters equal to the nozzle inner diameter, the velocity of nozzle (defined as nozzle deposition velocity) can be determined in Eq. (4.3)

$$v=\frac{4Q}{\pi D^2} \qquad \text{(Eq. (4.3))}$$

To avoid mechanical vibration of the system caused by high speed nozzle movement, the nozzle deposition velocity was limited to 5 mm/s to 20 mm/s. Thus, with a predefined nozzle deposition velocity and nozzle diameter, flow rate at which the dispensed strut diameter equals to

the nozzle inner diameter can be calculated according to Eq. (4.3). And with the help of the mass flow rate measurement function provided by the dispensing system, air pressure was then adjusted to get the flow rate needed. Table 4.1 summarizes the calculated and experimental flow rate and strut diameter correspondent to different nozzle deposition velocities for 1.5% alginate/0.75% hyaluronic acid.

Table 4.1 Calculated and Experimental Flow Rate, and Strut Diameter Correspondent to Different Nozzle Deposition Velocities for 1.5% Alginate/0.75% Hyaluronic Acid

Nozzle Deposition Velocity (mm/s)	Calculated Volume Flow Rate	Calculated Mass Flow Rate	Experimental Mass Flow Rate	Calculated Strut Diameter
5 mm/s	0.25 µl/s	0.244 mg/s	0.26 mg/s	260.52 µm
10 mm/s	0.50 µl/s	0.488 mg/s	0.52 mg/s	260.65 µm
15 mm/s	0.75 µl/s	0.731 mg/s	0.76 mg/s	257.29 µm
20 mm/s	1.00 µl/s	0.975 mg/s	1.00 mg/s	266.85 µm

To overcome the surface tension of the first layer, the initial level of $CaCl_2$ solution was lowered to just cover the Petri dish surface. For the following layers, the level of $CaCl_2$ solution was increased after each layer by an increment equal to the layer thickness. The amount of the added $CaCl_2$ solution each layer can be calculated as Eq. (4.4)

$$V = \pi r^2 h = \frac{\pi D^2}{4} h \qquad \text{(Eq. (4.4))}$$

Using the glass tissue culture Petri dish (D=100 mm, h=15 mm), the volume of the crosslinking solution added for each layer will be 2 mL for 250 µm nozzle tip. While dispensing,

the initial needle height from the Petri dish bottom was adjusted to obtain the strands that are uniform and straight with the diameter approximate to 250 μm.

$CaCl_2$ concentration affects the crosslinking speed and density of alginate, and thus is important for the attachment of scaffold layers and the control of strand diameter. The concentration of $CaCl_2$ was varied from 10 mM to 150 mM for each mixture to examine its influence on the fabrication of scaffolds, which was characterized in terms of strut diameter, linearity and connectivity between layers.

To quantify the effect of hyaluronic acid's addition and $CaCl_2$ crosslinker concentration on the feasibility and manufacturability of scaffold fabrication, top and front view images of four 4-layer scaffolds from each group were taken microscopically to visually show the strand profile as well as the intersectional part. Average strut diameter was determined by averaging the diameters of 4 randomly chosen struts using the equipped image software. The 4-layer scaffolds (n=5) were then placed in 3 mL of $CaCl_2$ solution for 24 hours to validate the attachment between different layers. The criteria is that scaffolds with straight line of predefined diameter, less fusion but more connection between layers are better.

4.2.3.2 Fabrication of Scaffold by 3D BioplotterTM System

The adapted fluid dispensing system is not sophisticated, leading to the uncontrollable and non-repetitive results. Because of this, the 3D Bioplotter™ system was used instead to check the feasibility of fabricating 3D scaffolds with controllable and repetitive microstructure from composite biomaterial. The 3D-Bioplotter™ (EnvisionTEC, 4th generation) is a proper rapid prototyping tool for the 3D scaffold fabrication with defined inner and outer structure. It handles a very wide range of biomaterials, from soft hydrogels for soft tissue regeneration over melting polymers such as polycaprolactone to hard ceramics and metals. It offers an axis resolution of

0.001 mm and a needle sensor resolution of 0.001 mm, making the dispensing process quite repetitive and controllable. One another advantage of this rapid prototyping system is that it is particularly designed to work in sterile environment in a laminar flowbox, making the fabrication of scaffolds with living cells possible.

The 3D-Bioplotter™ is delivered together with a personal computer workstation which operates and monitors the system. When fabricating, a 3D CAD model was first established and then transferred to the equipped personal computer and processed by the Bioplotter^{TM} Software Package. The 3D Bioplotter^{TM} then receives the preprocessed data and starts building the 3D scaffolds, which is still monitored by the Bioplotter^{TM} software.

The low temperature dispensing cartridge was used in this experiment to load the dispensing materials: composite material of 1.5% alginate/0.375% hyaluronic acid. After calibrating the X, Y, Z position and the needle height, trials were made to find the suitable air pressure and dispensing velocity to obtain desired strand diameter. Once these parameters were determined, the fabrication of 3D scaffolds started. It was found that if the composite biomaterial was dispensed into the $CaCl_2$ solution, the dispensed strands floated on the surface of the solution and the strands were curved. Thus, attempts were tried to dispense 2-layer scaffold onto the Petri dish first, after which very little amount of $CaCl_2$ solution was applied carefully onto the 2-layer scaffold to let the crosslinking take place. After that, excess $CaCl_2$ solution was removed using the Kimwipe without disturbing the integrity of scaffold structure. This was done to avoid the surface tension caused by the material with the $CaCl_2$ solution. Repeat the same procedure every 2 layers before the final scaffold was completed. The fabricated scaffolds were then imaged microscopically to examine the internal and external structures.

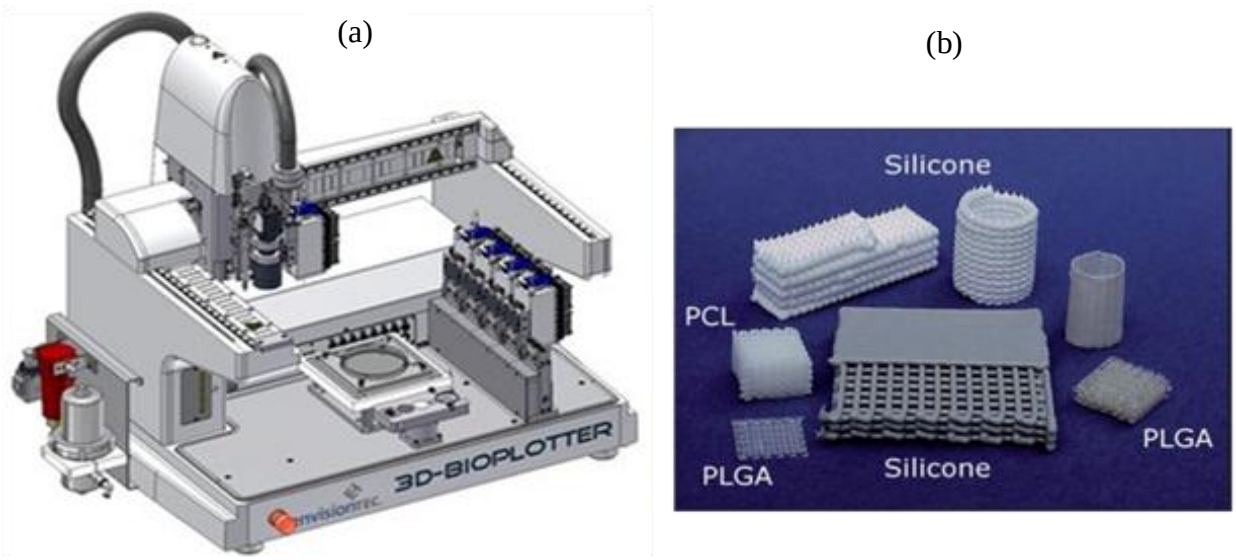

Figure 4.3 (a) 3D Bioplotter™ system and (b) examples of the 3D scaffolds fabricated from different materials using the 3D Bioplotter™ system.

4.2.4 Mechanical Test

In this study, 50 mM $CaCl_2$ was chosen for the crosslinking of the four aqueous alginate/hyaluronic acid mixtures for uniaxial compression test to study the effect of hyaluronic acid's addition on the mechanical property. Alginate/hyaluronic acid mixtures and 100 mM $CaCl_2$ solution were poured into custom-made cylindrical Teflon molds (10 mm diameter × 20 mm length) at a volume ratio of 2:1 to crosslink for 12 hours at room temperature. The hydrogels (n=4) was then removed and placed in large quantity of 50 mM $CaCl_2$ solution for additional 12 hours. The cylindrical hydrogels scaffolds were then cut at both ends to obtain sample size of 10 mm diameter × 10 mm length. Sample sizes of diameter and length were measured in triplet before applying compressive force.

The mechanical tests were all performed on a desktop measurement system, ElectroForce® 3100 test instrument (Bose Corporation, ElectroForce® Systems Group, USA), as shown in Figure 4.4. The instrument can provide high resolution of a minimum 6 mN

controllable peak-to-peak force and minimum 0.0015 mm controllable peak-to-peak displacement. Thus, this instrument is well suited for the tissue mechanics research, micro-indentation of cartilage and other soft tissue, dynamic mechanical analysis of tissues, elastomers and other soft materials. Apply a ramp displacement generated by the WinTest® digital control system at a constant rate of 0.083 mm/s (5 cm/min) on the specimens to provide a compressive force till a 20% strain (2.0 mm) was achieved. Collect the data of load and displacement, from which the stress-strain curves can be obtained. Such mechanical properties as compressive elastic modulus, and tangent modulus were then determined from the stress-strain curves.

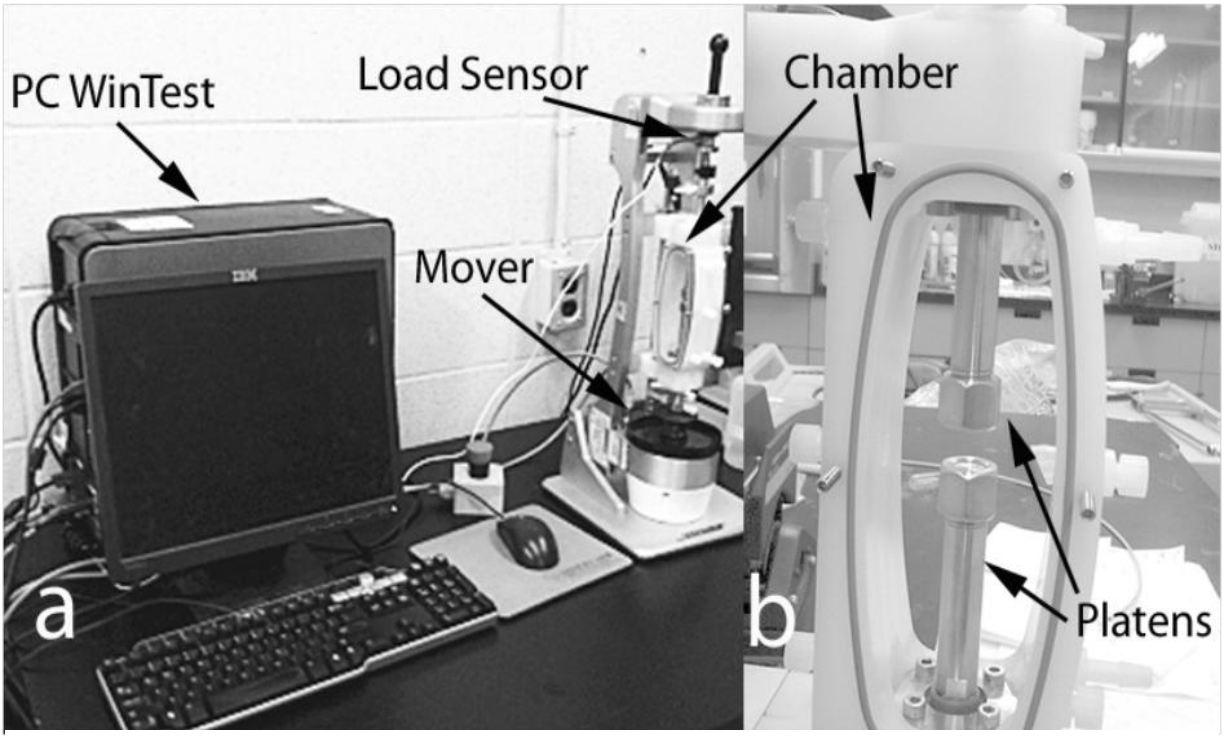

Figure 4.4 The ElectroForce® 3100 test instrument: a) the hardware of the instrument including the WinTest digital control system, load sensor, a mover and a chamber; b) the chamber structure, providing a sterilized and isolated environment as a bioreactor for the sample during the mechanical test.

4.2.5 Statistical Analysis

Measured values are expressed as means ± standard deviation. Levels of significance were calculated using one-way ANOVA with Turkey post test. All calculations were made using GraphPad Prism 5.0.

4.3 Results and Discussions

4.3.1 Flow Behavior

The relationship of shear stress with shear rate for different mixtures of alginate/hyaluronic acid is shown in Figure 4.5. As is shown, 1.5% alginate behaves like Newtonian fluid, where the shear stress is directly proportional to the shear rate. It has a constant viscosity of 41 cp. Mixtures of alginate with hyaluronic acid instead behave like the non-Newtonian fluid, with the flow behavior index being less than one (Table 4.2). The mixtures has the viscosity decreasing with increasing shear rate (shear thinning), which is illustrated in Figure 4.6. Table 4.2 summarizes the different parameters (named flow behavior parameters) for the generalized power law mentioned in section 4.2.2 for each mixture. The flow behavior measurement results showed that the flow behavior parameters, particularly the yield stress and consistency index varied with the concentration of hyaluronic acid. Mixtures with higher concentration of hyaluronic acid had bigger yield stress and higher consistency index, but lower flow index. As yield stress of the biomaterials for the scaffold fabrication needs to be high to maintain the 3D interconnected microstructures, the addition of hyaluronic acid into 1.5% alginate solution makes the mixtures a more feasible biomaterial for 3D scaffold fabrication using the dispensing-based rapid prototyping system [134].

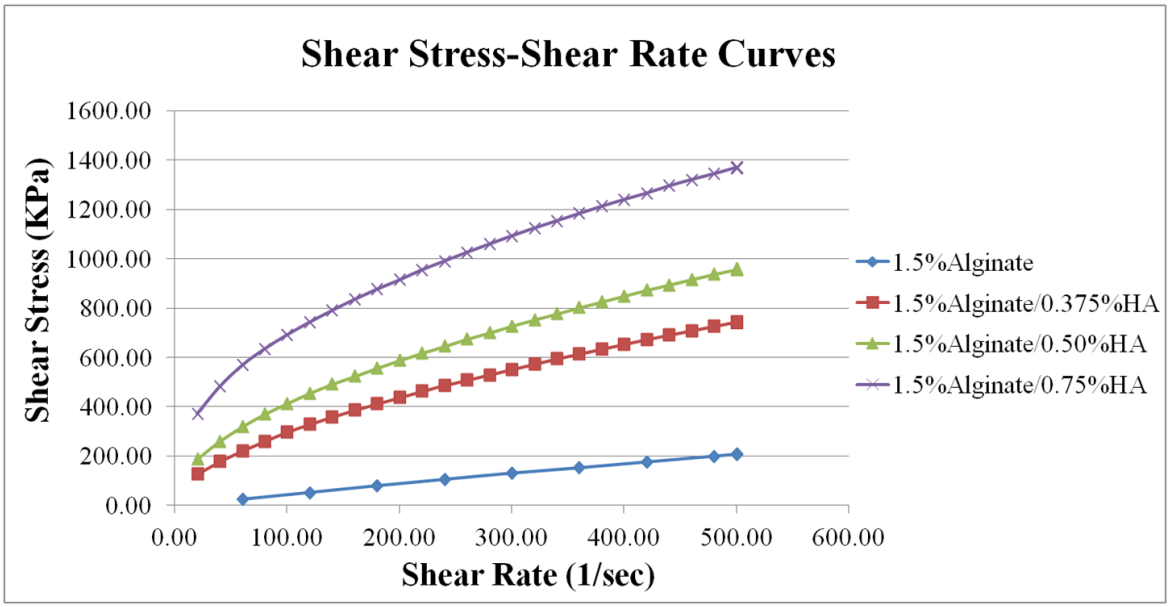

Figure 4.5 Shear stress vs. shear rate curves of alginate/hyaluronic acid mixtures at different shear rates. 1.5% alginate behaved like Newtonian fluid while the alginate/hyaluronic acid mixtures behaved like non-Newtonian fluid. With the increase of the concentration of hyaluronic acid, yield stress of the mixture increased.

Table 4.2 Flow Behavior Parameters for Four Alginate/Hyaluronic Acid Mixtures

Mixtures	τ_0 (D/cm)	K (cp)	n
1.5% Alginate/0% Hyaluronic Acid	-11.38	100.2	0.87
1.5% Alginate/0.375% Hyaluronic Acid	20.30	1719.0	0.60
1.5% Alginate/0.50% Hyaluronic Acid	37.20	2835.0	0.56
1.5% Alginate/0.75% Hyaluronic Acid	113.6	6151.0	0.49

Viscosity-shear rate curves of alginate/hyaluronic acid mixtures in Figure 4.6 showed that the viscosity of mixtures increased with the increased amount of hyaluronic acid at low strain rates, while the difference was not significant at high strain rates.

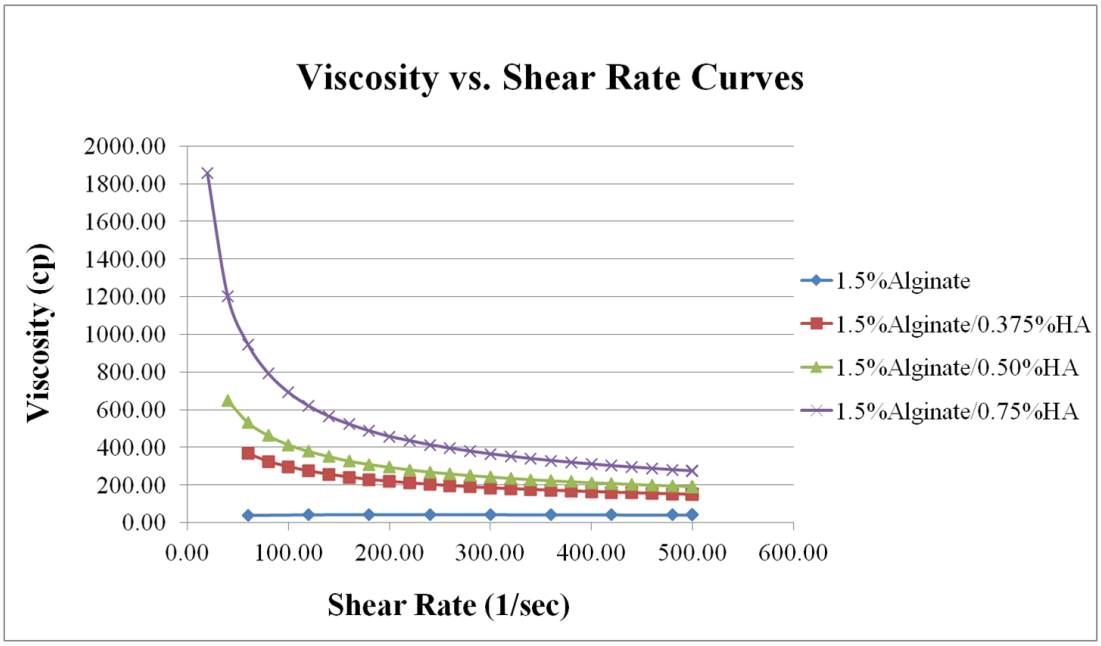

Figure 4.6 Viscosity vs. shear rate curves of alginate/hyaluronic acid mixtures. Alginate/hyaluronic acid mixtures behaved like non-Newtonian fluid, with the viscosity decreasing with increasing shear rate. The viscosity of mixtures increased with the increased amount of hyaluronic acid. 1.5% alginate solution behaved like Newtonian fluid and had a constant viscosity of 41 cp.

4.3.2 Scaffold Fabrication

Scaffold fabrication was carried out based on the model of the strut diameter. Volume flow rate with predefined needle geometry and nozzle disposition velocity was calculated according to Eq. (4.3). The adapted fluid dispensing machine has the function to measure the mass flow rate. Thus, the air pressure can be adjusted to get the required flow rate. Different dispensing velocities were tested to investigate the effectiveness of proposed fabrication technique and to examine the effect of nozzle deposition velocity on the strut structure. From Figure 4.7, we can see the orthogonal pore structure for scaffolds dispensed at velocities of 5 mm/s and 10 mm/s. Strands of the first layer had a larger diameter compared to those of the second layer, probably because of the surface tension and contact angle. Higher velocities of 15

mm/s and 20 mm/s led to the non-linear strand profile of scaffolds. As indicated by the first layers which had uniform and linear strand profile, the dispensing parameters such as dispensing velocity, needle size, and air pressure were suitable for the fabrication process of 1.5% alginate/0.75% hyaluronic acid mixture. Thus, the irregular shaped 2D scaffolds dispensed at 15 mm/s and 20 mm/s may be due to the mechanical vibration of the dispensing system, initial needle height or crosslinker solution level.

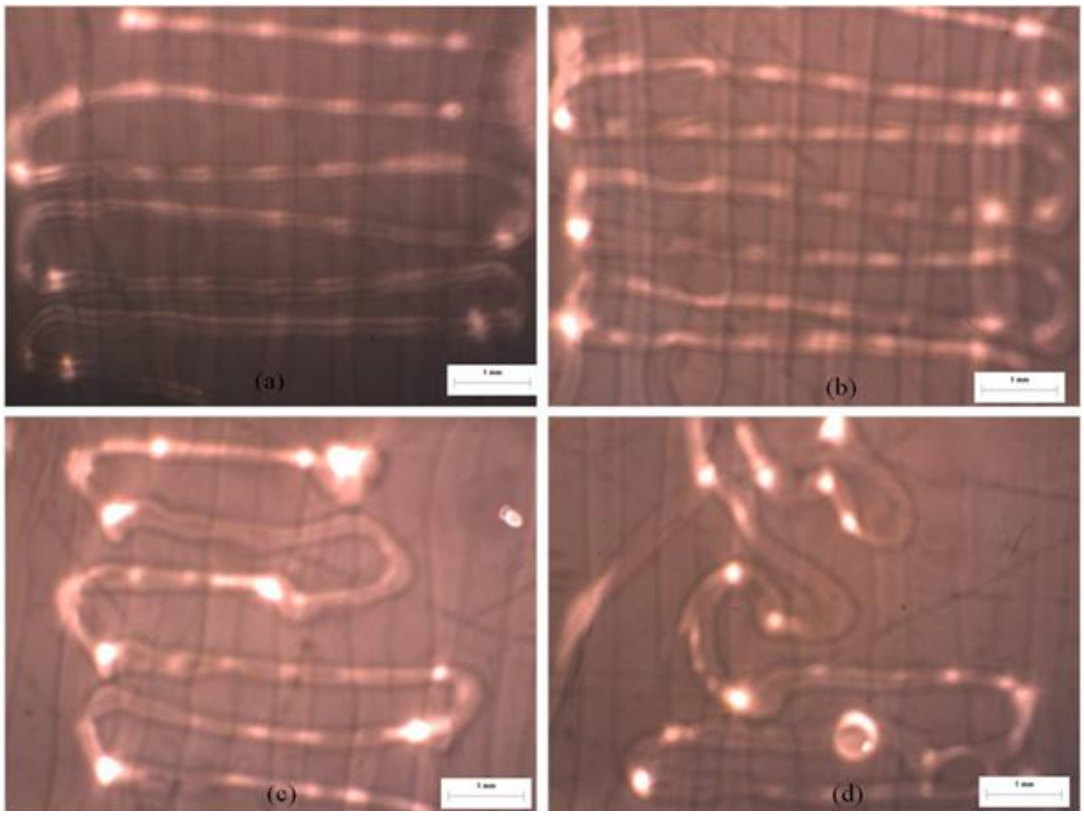

Figure 4.7 Images of 1.5% alginate/0.75% hyaluronic acid scaffolds dispensed at different velocities and correspondent mass flow rates (a) 5 mm/s, 0.26 mg/s (b) 10 mm/s, 0.52 mg/s (c) 15 mm/s, 0.76 mg/s, and (d) 20 mm/s, 1.00 mg/s. Scale bars: a, b, c, d=1 mm.

Effect of initial needle height on the strut diameter and linearity was then investigated and the result shown in Figure 4.8 indicated that strand formation was highly dependent on the initial needle height. For the mixture of 1.5% alginate/0.75% hyaluronic acid and the dispensing parameters of nozzle deposition velocity at 10 mm/s, mass flow rate at 0.52 mg/s, and needle

size of 250 μm, an initial needle height of 0.35 mm results in linear strands (Figure 4.8 (a)) while higher needle heights of 0.40 mm, 0.45 mm, 0.55 mm led to curved strand structures as shown in Figure 4.8 (b), (c), and (d). Figure 4.8 (e) and (f) revealed the even less uniform shape of the dispensed strands with further increase of the initial needle height.

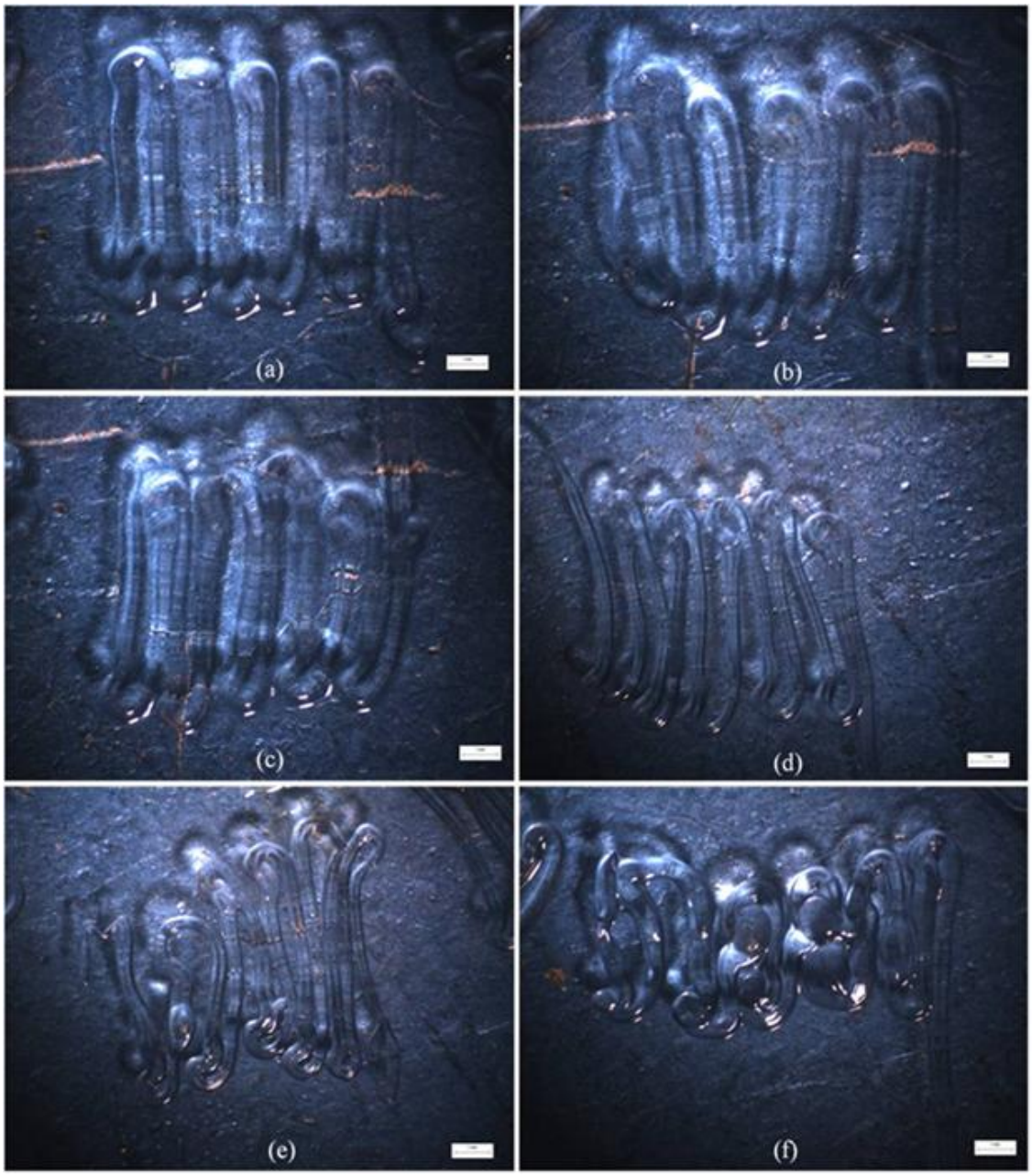

Figure 4.8 Initial needle heights of (a) 0.35 mm, (b) 0.40 mm, (c) 0.45 mm, (d) 0.55 mm, (e) 0.60 mm, and (f) 0.65 mm tested to assess the effect of initial needle height on the strut diameter and linearity. Scale bars: a, b, c, d=1 mm.

Possible explanation for the effect of initial needle height on the strand profile is that the dispensed fluid didn't touch the Petri dish bottom until enough liquid was accumulated for the gravity force to overcome the surface tension. Thus, the actual velocity of deposition was smaller than the calculated value, which was supposed to match the correspondent flow rate. Along with this, the strand had a shorter length and a bigger diameter with a higher initial needle height compared to a lower initial needle height.

Crosslinking of alginate/hyaluronic acid mixtures by $CaCl_2$ is dependent on the $CaCl_2$ concentration, which may in turn affect the strut diameter and attachment between layers. High $CaCl_2$ concentration leads to extensive crosslinking of alginate and shrinkage of strut diameter. On the other hand, gelation speed of the dispensed strut increases with the $CaCl_2$ concentration, which might result in the detachment of different layers. Thus, it is important to study the effect of $CaCl_2$ concentration on the geometrical formation of 3D scaffolds. Figure 4.9 showed the strut diameters of 1.5% alginate/0.375% hyaluronic acid mixture dispensed into $CaCl_2$ solution with different concentrations. As observed, all concentrations led to a bigger strut diameter than 250 μm. This may be due to the swelling of the uncrosslinked hyaluronic acid in the strut after one day. And there was significant difference in strut diameter between 10 mM and the rest concentrations, $P < 0.0001$. Though higher concentration of $CaCl_2$ seemed to result in a smaller strut diameter, the difference was not significant.

In terms of connectivity between layers, 50 mM or 75 mM $CaCl_2$ is preferable for 1.5% alginate/0.375% hyaluronic acid. Five samples of 4-layered scaffolds were fabricated for each concentration and immersed in correspondent $CaCl_2$ solution for one day, after which the integrity of the scaffolds were examined visually. The result showed that concentrations of 10 mM, 50 mM and 75 mM maintained the integrity of the fabricated scaffolds. Group of 100 mM

$CaCl_2$ had two scaffolds falling apart and three intact. And higher concentration of 150 mM had all the scaffolds lose their structure. For the mixture of 1.5% alginate/0.5% hyaluronic acid, 100 mM of $CaCl_2$ was found to be more favorable in terms of strut diameter and connectivity.

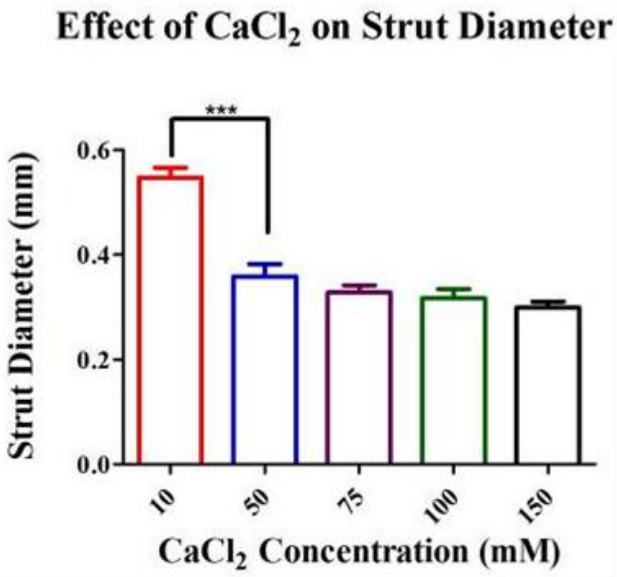

*Figure 4.9 Effect of $CaCl_2$ concentrations on strut diameter of ionically-crosslinked 1.5% alginate/0.375% hyaluronic acid hydrogel scaffolds. Error bars represent the standard deviation; *** $P < 0.0001$.*

Concentration of $CaCl_2$ has an effect on the strut diameter and the connectivity between different layers of the scaffolds. High concentration of $CaCl_2$ leads to more ionic crosslinking of alginate, which would result in the shrinkage of dispensed struts. As for the connectivity, it is likely that the presence of hyaluronic acid would hinder the crosslinking of alginate with $CaCl_2$, thus the problem of detachment between dispensed layers using the same concentration of $CaCl_2$ will become less severe for the mixture with higher concentration of hyaluronic acid compared to the one without or with lower concentration of hyaluronic acid. This, on the other hand, indicates that a higher concentration of $CaCl_2$ might be more suitable for the alginate/hyaluronic acid mixture with higher concentration of hyaluronic acid. This helps to explain why higher concentration of $CaCl_2$ (100 mM) is more appropriate for 1.5% alginate/0.5% hyaluronic acid

while mixture of 1.5% alginate/0.375% hyaluronic acid requires 50 mM or 75 mM of $CaCl_2$ to obtain the desired strut diameter and good attachment of different layers.

Figure 4.10 shows two examples of the multilayer scaffolds fabricated using the adapted fluid dispensing system: (a) four-layer scaffold with the first two layers detached; (b) top view of a 10-layer scaffold. As we can see, while the 4 or 5 layer scaffolds can be fabricated with open pores, scaffolds with more layers is problematic with non-interconnected pores.

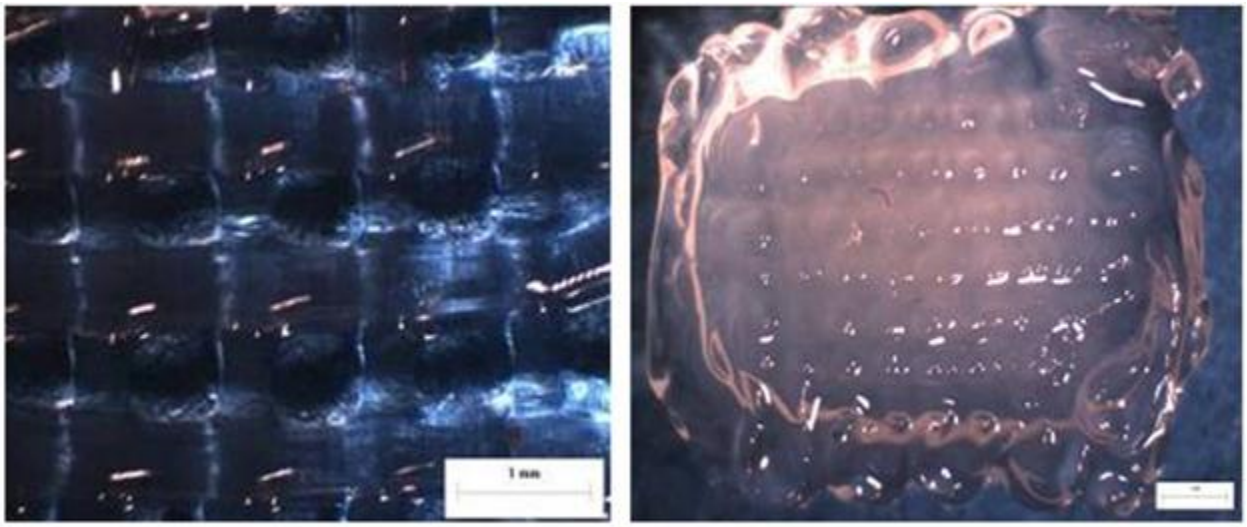

(a) (b)

Figure 4.10 Examples of the multilayer 1.5% alginate/0.375% hyaluronic acid scaffolds fabricated by the adapted fluid dispensing system: (a) four-layer scaffold with the first two layers detached; and (b) top view of a 10-layer scaffold. Scale bars: a, b=1 mm.

Multilayer scaffolds fabricated from the 3D Bioplotter^{TM} system were shown in Figure 4.11. As we can see, the strands were linear and uniform, with interconnected pore structures. This indicated the feasibility of fabricating 3D scaffolds with predefined and reproducible microstructure using the 3D Bioplotter^{TM} system.

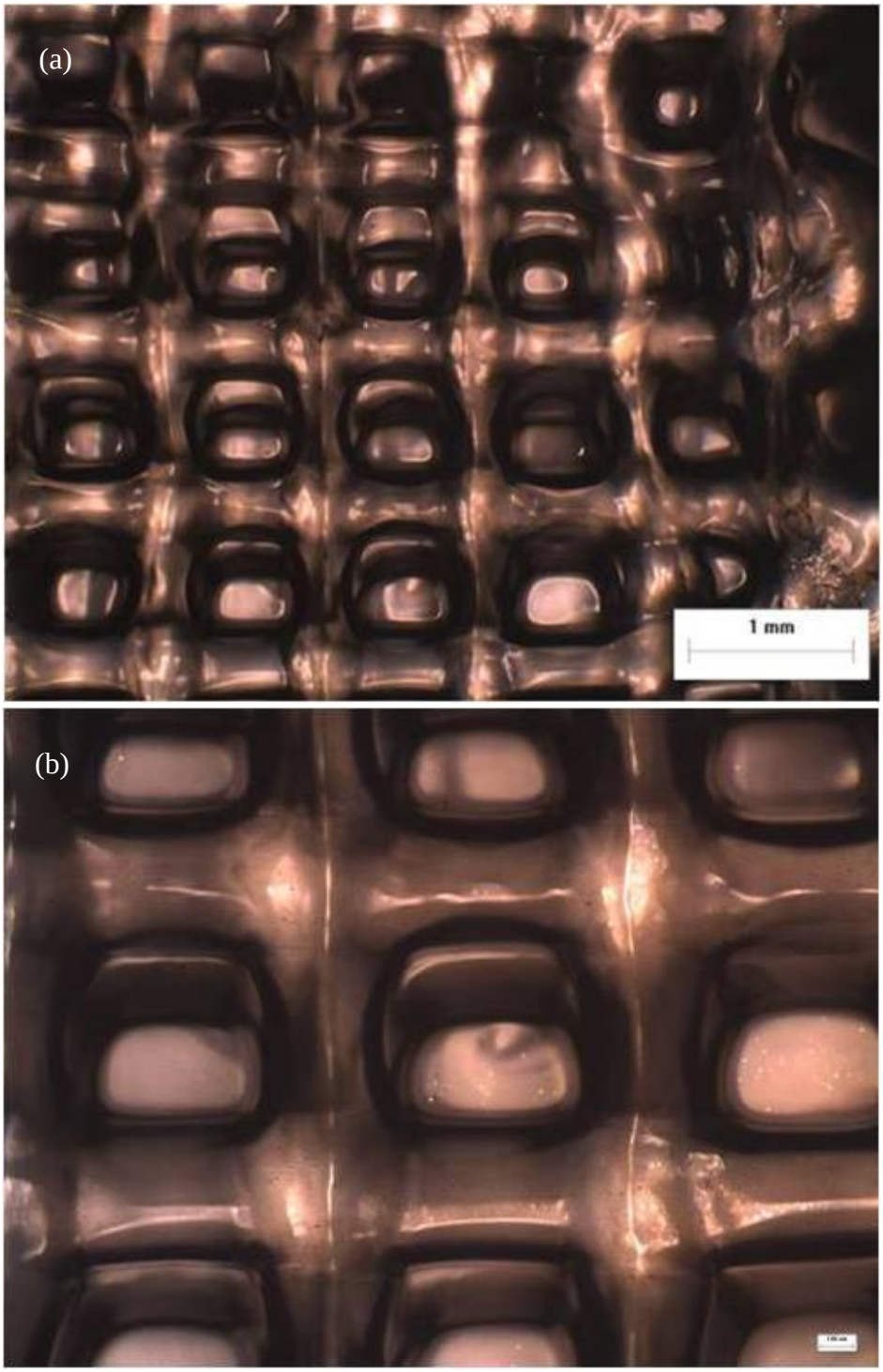

Figure 4.11 An example of the multilayer scaffolds fabricated using the 3D Bioplotter™ system. (a) 3D porous structure of 1.5% alginate/0.375% hyaluronic acid hydrogel scaffolds dispensed by SmoothFlow™ Tapered Tips with the inner diameter of 200 um, image taken at 25× magnification, scale bar=1 mm; (b) the same scaffold imaged at 50× magnification, scale bar=100 µm.

4.3.3 Mechanical Properties

Bioengineered tissue scaffolds provide necessary mechanical support for the native tissue while the scaffold should not be too hard to damage the surrounding tissue. And compression is the most common form of spinal cord trauma. Thus, uniaxial compression test was carried out on the alginate/hyaluronic acid hydrogels to study their mechanical properties. Though the 3D porous scaffolds dispensed by the dispensing-based rapid prototyping system were aimed for the later *in vitro* and *in vivo* study of SCI repair in animal models, measurement on the cylindrical hydrogel samples would facilitate the fabrication process while providing important information about the mechanical properties of the hydrogels. The result indicated that the stress-strain curves of four samples from each group were not very consistent, probably due to the difficulty to accurately transfer the viscous mixtures into the molds, the non-uniform crosslinking density or the uneven surface of the hydrogels. These are the common issues involved with the mechanical test of hydrogels.

Typical stress-strain curves for each group of hydrogels were shown in Figure 4.12. As shown in the figure, 1.5% alginate hydrogels with different amounts of hyaluronic acid added behaved like soft tissue, having stress-strain curves of an exponential shape. An initial linear region existed in each group with hyaluronic acid added. The elastic modulus or Young's modulus for compression, one key parameter of the mechanical properties, is the slope of the linear region of the stress-strain curve. Elastic moduli of the different alginate/HA hydrogels were difficult to obtain as the elastic regions are hard to determine and stress-strain curves of each group varied quite a lot from sample to sample. However, the slope of the stress-strain curve at the strain of 0.03 was calculated for each sample and averaged to get the average elastic modulus for each alginate/HA hydrogel. And no significance was found in the elastic modulus

for compression between different groups, as shown in Figure 4.13. Stress of 1.5% alginate/0% HA hydrogels had a linear relationship with strain, demonstrating as an elastic material. After the point of the proportional limit, the hydrogels had the non-linear profile of the stress-strain curve, indicating the materials underwent plastic deformation. For this non-linear region, tangent modulus, the slope of the stress-strain curve at a certain strain, is used to characterize the mechanical properties of materials stressed beyond the yield point. Calculating the tangent moduli of different hydrogels at the same strain of 0.18, surprisingly, we can find that there was no significant difference in the tangent modulus between different hydrogels, as shown in Figure 4.14.

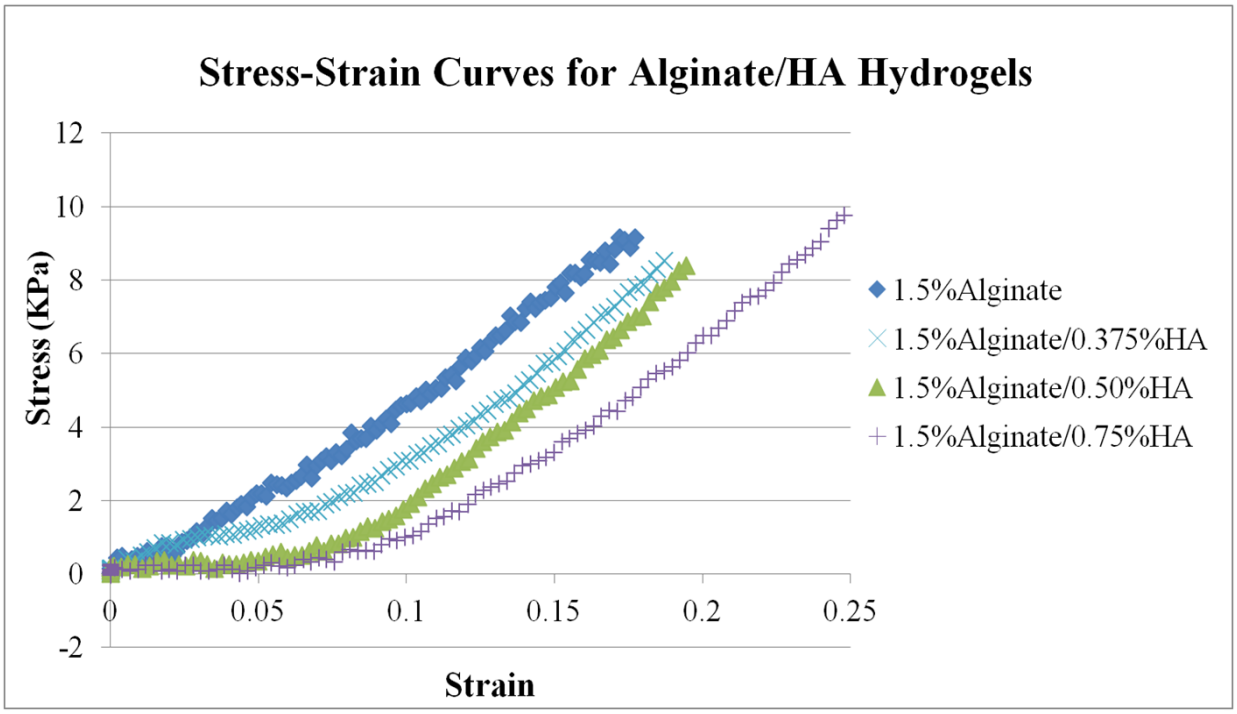

Figure 4.12 Stress-strain curves of cylindrical alginate/hyaluronic acid hydrogels measured at the strain rate of 0.0083/s. One typical stress-strain curve was selected from each group. The alginate/hyaluronic acid hydrogels behaved like soft tissue, having stress-strains of an exponential shape while alginate hydrogels demonstrated as an elastic material with linear strain-strain curves.

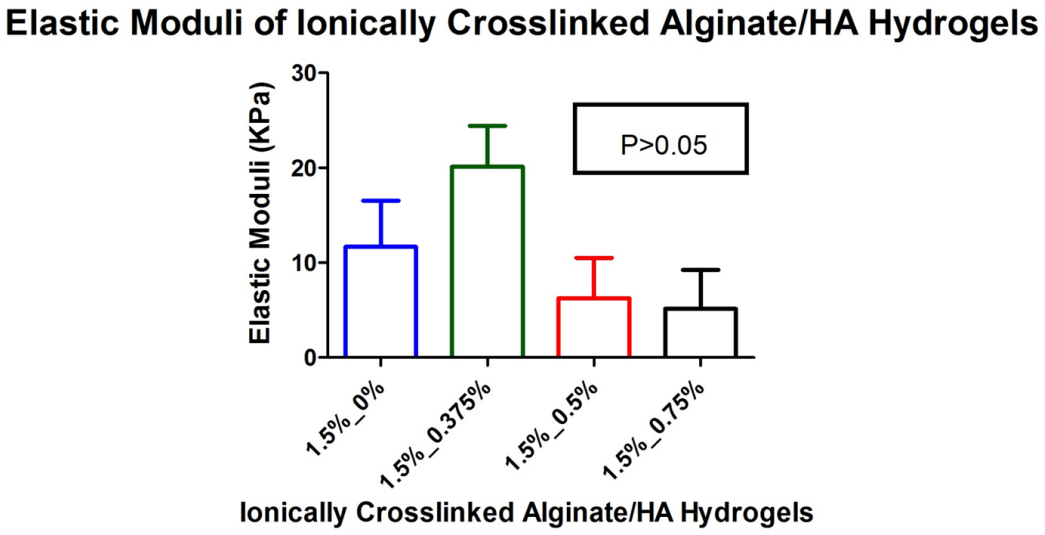

Figure 4.13 Average elastic moduli of ionically-crosslinked hydrogels of 1.5% alginate with 0%, 0.375%, 0.5% and 0.75% hyaluronic acid. Elastic modulus represents the slope of the stress-strain curve at the proportional region. Error bars represent the standard deviation; P > 0.05.

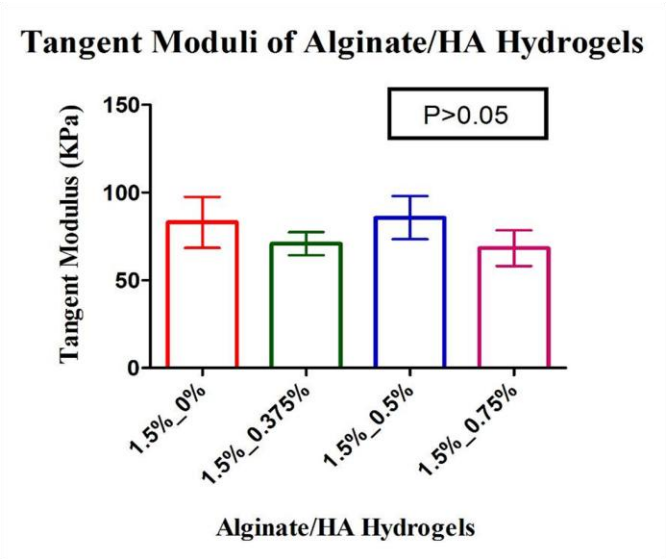

Figure 4.14 Average tangent moduli of four alginate/hyaluronic acid hydrogels at the strain of 0.18. Error bars represent the standard deviation and no significant difference was found between the different hydrogels based on the one-way ANOVA.

Scaffolds' mechanical test showed that the cylindrical hydrogels crosslinked by 50 mM $CaCl_2$ for 24 hours demonstrated a viscoelastic compressive behavior as native spinal cord and

had tangent moduli of 70-80 KPa (measured at the strain rate of 0.0083/s). Also, there was no significant difference in the elastic modulus and tangent modulus between different hydrogels. There are many tension tests on both animal and human spinal cord, but not many compression studies have been done on the spinal cord samples. The reported mechanical properties for the spinal cord tissue are not consistent but usually within the range of 3 KPa to 300 KPa [72, 107, 108, 142]. Stress-strain curves of porcine spinal cord white matter all have an exponential shape at different strain rates [143]. To achieve biomimetic mechanical properties of the spinal cord tissue, the concentration of $CaCl_2$, and gelating time used for ionic crosslinking can be adjusted to meet a particular application.

Also, it was found that elastic modulus of 2 KPa to 5 KPa is likely to be most favorable for neurite extension and neural differentiation of progenitors [144-146]. The elastic moduli of different hydrogels were around 5 KPa to 20 KPa and had no significant difference between different groups. This indicated that the $CaCl_2$-crosslinked hydrogels of 1.5% alginate with different amounts of HA had quite suitable mechanical properties for neurite outgrowth and neural differentiation. And the composite biomaterial with adjustable mechanical properties (by changing the $CaCl_2$ concentration) could be applied to culture the neuron stem cells for cell differentiation and proliferation studies.

4.4 Conclusions

This chapter presents the fabrication of 3D scaffolds of $CaCl_2$ crosslinked 1.5% alginate with different concentrations of hyaluronic acid using the dispensing-based rapid prototyping systems, both the adapted fluid dispensing system and the 3D Bioplotter^{TM}. Flow behavior of the different mixtures was characterized to facilitate the fabrication process. And the results showed

that 3D construct cannot be produced from ionically-crosslinked 1.5% alginate, due to the low yield stress necessary for 3D configuration. And 3D scaffolds can be fabricated from $CaCl_2$ crosslinked 1.5% alginate with 0.375%, 0.5% and 0.75% hyaluronic acid. Due to the unsatisfying resolution and difficulty to adjust the air pressure to exact value of the adapted fluid dispensing system, fabricated scaffolds aren't quite reproducible. This also makes the interpretation of experiment results challenging. Application of more sophisticated rapid prototyping fabrication systems such as 3D Bioplotter™ to repeat this part of work would extensively make this piece of work more worthwhile. And the fabricated 3D scaffolds using the 3D Bioplotter™ system also indicated its superiority in producing scaffolds with controllable and reproducible microstructure over the adapted fluid dispensing machine.

CHAPTER 5 General Discussions

5.1 Summary and Conclusions

In this study, composite biomaterial made from alginate and hyaluronic acid was synthesized and characterized by the FTIR spectrum to confirm the covalent crosslinking in Chapter 2. Alginate's instant gelation with $CaCl_2$ was employed to make use of its ease to construct 3D structure by the dispensing process while incorporation of hyaluronic acid may provide cellular and molecular interaction with native tissue to improve SCI repair outcome. Covalent crosslinking of hyaluronic acid and alginate with ADH mediated by EDC under an acidic condition may postpone the *in vivo* residence time, which is typically several months for SCI repair. The loss of mechanical strength of alginate hydrogels with 15 hours after *in vivo* transplantation could be overcome by the covalently-crosslinked hyaluronic acid and alginate. The FTIR measurements showed that there was covalent modification with the crosslinking protocol described in Chapter 2. The covalent modification was found to be dependent on the concentrations of EDC and $CaCl_2$, as well as the pH value of the reaction.

In Chapter 3, the biocompatibility of the composite hydrogels for Schwann cells, which are proven to play a key role in the spinal cord regeneration, was investigated. For this, substrates double-crosslinked for both 6 hours and 20 hours were examined for Schwann cell viability and growth. The results indicated that cells survived on the double-crosslinked alginate/hyaluronic acid hydrogels, despite that there were not as many cells as the tissue culture plate. Also, there was no significant difference between different substrates prepared from different volume ratios of 3% alginate and 0.75% hyaluronic acid. Treated with PLL coating, the 20%-80% alginate/hyaluronic acid hydrogels showed improved Schwann cell adhesion and had more cells growing compared to the non-treated group. However, cells remained circular without

extended processes, indicating the lack of adhesive property of the hydrogels for Schwann cells. Additionally, covalent crosslinking by EDC mediated amide formation and high concentration of hyaluronic acid seemed to be inhibitory for Schwann cell survival and growth, resulting in fewer cells when compared to the controls. Hydrogels of ionically-crosslinked 1.5% alginate/0.375% hyaluronic acid or 1.5% alginate/0.5% hyaluronic acid may be most suitable for Schwann cell culture.

In Chapter 4, 3D scaffold fabrication by the dispensing-based rapid prototyping systems was investigated. The result indicated the feasibility to fabricate 3D alginate/hyaluronic acid tissue construct with controllable microstructure using the dispensing-based rapid prototyping systems. The influence of flow behavior, initial needle height and $CaCl_2$ concentration for the formality of scaffolds was examined. The result showed that 3D scaffolds can be fabricated from mixtures of 1.5% alginate with hyaluronic acid but not 1.5% alginate alone. The initial height of the dispensing needle tip from the surface of $CaCl_2$ solution imposed a significant effect on the formality of scaffolds. Concentration of $CaCl_2$ solution had an impact on the strand profile with 50 mM or 75 mM preferable for 1.5% alginate/0.375% hyaluronic acid and 100 mM for 1.5% alginate/0.5% hyaluronic acid in terms of strand diameter and attachment between layers.

Scaffolds' mechanical test showed that the cylindrical hydrogels crosslinked by 50 mM $CaCl_2$ for 24 hours demonstrated a viscoelastic compressive behavior as native spinal cord and had tangent moduli of 70-80 KPa (measured at the strain rate of 0.083mm/s). Also, there was no significant difference in the tangent modulus between different hydrogels. Two fabrication methods were tried on the adapted commercial fluid dispensing system and the 3D Bioplotter™ respectively and both methods were successful in fabricating multilayer scaffolds. However, in

terms of the ease to fabricate 3D scaffolds, the method to dispense first two layer patterns onto the tissue culture plate without the presence of $CaCl_2$ is more controllable and repetitive.

5.2 Discussions

This is the first study of synthesis, characterization and fabrication of alginate/hyaluronic acid composite hydrogels for the application of SCI repair. Alginate was incorporated into the hyaluronic acid in this study so as to enhance the feasibility to fabricate 3D scaffold from the composite biomaterial. Fast gelation of alginate with $CaCl_2$ provides the mechanical strength of dispensed strands. Without alginate, hyaluronic acid could not form scaffolds with open pores even if the covalent crosslinking of hyaluronic acid with ADH by EDC was applied. This is because the covalent modification is not quick enough to solidify the dispensed strands.

The concentration of alginate was set at 1.5% as 1.5% alginate was high enough to be crosslinked by $CaCl_2$ to provide sufficient mechanical support in the dispensing process. Higher concentrations of the alginate are unwanted as alginate has been shown to be not favorable for Schwann cell adhesion with cells demonstrating spherical shape. It also inhibits the Schwann cell metabolic activity and neurite outgrowth of the DRG neurons [46]. Addition of fibronectin increased the DRG neurite outgrowth but cannot change the spherical morphology of Schwann cells [46]. Thus, it is unnecessary that the alginate/hyaluronic acid hydrogels will not permit DRG neurite outgrowth even though the morphology of the cultured Schwann cells on the composite biomaterial indicated that the hydrogels were not suitable for Schwann cell attachment. Culture of DRG neurons on or within the alginate/hyaluronic acid composite hydrogels will shred a light on this.

Also *in vivo* transplantation of the alginate/hyaluronic acid hydrogels should be done even when the primary *in vitro* study of the composite biomaterial in promoting neurite outgrowth of DRG neurons is not encouraging. This is due to the fact that cell culture on the 2D scaffold or within 3D scaffold *in vitro* differs from the *in vivo* study with the transplanted scaffolds. The underlying mechanisms are complex and not well understood. It is likely that the composite biomaterial of alginate and hyaluronic acid might result in an advantageous effect in promoting axonal regeneration though the outcome of DRG culture may be quite negative.

Hyaluronic acid is not adhesive for cell attachment both *in vitro* and *in vivo*. The non-adhesive property of hyaluronic acid limits the attachment of Schwann cells and DRG neurons. Thus, it is likely that the composite hydrogels may restrain the neurite outgrowth of DRG neurons *in vitro*. And it is interesting to find out that there was extensive neurite outgrowth of a single DRG neuron in the crosslinked thiol-modified hyaluronic acid-poly (ethylene glycol)-diacrylate though there was no significant improvement of motor evoked potentials, retrograde axonal labeling or behavioral assessment *in vivo* in a complete thoracic spinal cord transection rat model [77].

Application of hyaluronic acid to the SCI lesion site results in significant decrease in scar formation and astrocytic response; it is necessary to maintain the excellent biological benefits provided by the hyaluronic acid when modification of hyaluronic acid is made for better SCI regeneration. Application of soluble high molecular weight hyaluronic acid *in vitro* decreased astrocyte activation and proliferation and the deposition of inhibitory chondroitin sulfate proteoglycans. The implantation of the crosslinked hyaluronic acid hydrogels with the biomimetic mechanical strength in a rat model of spinal dorsal hemisection injury also showed significant decrease of immune cells, chondroitin sulfate proteoglycans production, and astrocyte

response [147]. It was suggested that the interaction of high molecular hyaluronic acid with the CD 44 receptor on cell membrane accounted for the inhibitory effect of hyaluronic acid on scar formation after SCI [148, 149]. Y.T. Wei *et al.* had implanted the freeze-dried hyaluronic acid hydrogels modified with nogo-66 antibody and PLL in a rat model of lateral hemisection of spinal cord and they found that the hydrogels resulted in angiogenesis, reduction of glial scar, and axons growing into the hydrogels [76]. With the encouraging results of these studies, it is likely that the interconnected microstructure offered by the rapid prototyped alginate/hyaluronic acid scaffolds in this study might further increase the possibility of alginate/hyaluronic acid composite hydrogels to promote axonal regeneration.

In this study, the feasibility of alginate/hyaluronic acid composite biomaterial for 3D scaffolds for the applications in SCI repair was studied from the aspects of chemistry, biocompatibility, and feasibility of 3D scaffold fabrication. And the result of chemical characterization showed that there was covalent crosslinking of the alginate/hyaluronic acid composite substrates by EDC with ADH, even in the presence of $CaCl_2$.

EDC mediated amide formation has been widely used in tissue engineering to modify the biomaterial, either to couple one material to another, or to incorporate bio-functional biomolecules such as cell adhesion peptides into the biomaterial [150]. The reaction is highly dependent on the pH value and the optimal pH for the two steps of reaction is different. On one hand, carboxylic acid activation by EDC is most efficient in an acidic environment with pH value of 3.5-4.5 [79]. Meanwhile, amide formation is suggested to be best done at high pH value when the amine is deprotonated. At high pH, EDC can rapidly hydrolyze into the N-acylurea by-product and no amidation may occur. Thus, amines with high pKa are not easily conjugated to the polymer by EDC. Replacing diamines by dihydrazides, such as ADH, which have much

lower pKa values of 2-3, increase the coupling efficiency to up to 56% [151]. However, excessive ADH added will only lead to single functionalization of hyaluronic acid, which doesn't result in the crosslinked hyaluronic acid. In this study, the physical change of the hyaluronic acid or alginate solution into hydrogels with mechanical strength indicated that the covalent crosslinking of the polymers did occur.

The reaction efficiency of EDC mediated amide formation of alginate/hyaluronic acid with ADH was not measured in this study. This could be measured through the radio-labeled ADH. In this way, the amide formation of hyaluronic acid, alginate and alginate/hyaluronic acid with ADH will be quantitatively confirmed. It can also help to determine the carboxylate groups responsible for the covalent modification of alginate. If the alginate in alginate/hyaluronic acid mixture can be further crosslinked with ADH by EDC as the alginate solution itself, this would help to reduce the biodegradation rate of alginate/hyaluronic acid hydrogels *in vitro* and *in vivo* and may affect the mechanical and swelling properties of the hydrogels. As discussed in Chapter 1 about EDC crosslinking, the side reaction of EDC with carboxyl groups to form N-acylurea may affect on the amide formation of carboxyl groups of the polymer with ADH to crosslink the alginate/hyaluronic acid. Thus, measurement of conjugation efficiency will help to determine the proper EDC concentration, ADH amount, $CaCl_2$ concentration and pH value for the covalent crosslinking. Thus, quantitative measurement of the amide formation is essential.

The biocompatibility of alginate/hyaluronic acid hydrogels for viability and growth of Schwann cells was identified in this study. Primary examination of the Schwann cell growth on the double-crosslinked alginate/hyaluronic acid hydrogels on 2^{st}, 3^{nd} and 5^{th} day demonstrated that Schwann cells survived and grew on the substrates, indicating that the hydrogels were permissive for Schwann cell growth. No significant difference was found in the double-

crosslinked alginate/hyaluronic acid hydrogels with various concentrations of alginate and hyaluronic acid. This probably is attributable to the lack of HA's mediation on cell proliferation. Schwann cells express CD44, a major HA binding protein that mediates various cellular processes including cell-cell adhesion, migration and differentiation [152, 153]. However, HA may not affect the Schwann cell survival and proliferation though high molecular weight HA was found to inhibit the proliferation of astrocytes. Findings of Suri S and Schmidt C E also illustrated this when incorporation of HA into collagen did not change the Schwann cell viability and proliferation [154]. Studies need to be carried out to confirm this. One another explanation is that the variance of the HA concentration was not large enough to affect on the cell number of Schwann cells. The maximal concentration of HA was 0.75%, as higher concentrations of HA were too viscous to handle and would be difficult for the fabrication process.

Treatment of PLL coating on the double-crosslinked alginate/hyaluronic acid hydrogels increased the adhesion and cell number of Schwann cells. PLL is positively charged and through the electrostatic interaction between negatively charged ions of the cell membrane of Schwann cells and the culture surface (alginate/hyaluronic acid hydrogels), the adhesion of Schwann cells could be increased. However, here the PLL itself is not sufficient to overcome the non-adhesive property of alginate/hyaluronic acid hydrogels. Studies using hyaluronic acid hydrogels covalently modified by PLL on the hippocampus neuron culture also demonstrated the lack of cell spreading and attachment [76]. Modified with both PLL and Nogo-66 receptor antibody, neurons exhibited multipolar or bipolar morphology [76]. This indicated the necessity to carefully modify the alginate/hyaluronic acid hydrogels so as to promote the adhesion of Schwann cells and neurons as well as the neurite outgrowth both *in vitro* and *in vivo*.

Modification of alginate or hyaluronic acid hydrogels to permit cell adhesion and neurite

outgrowth has been successfully achieved by either incorporating other natural ECM component (e.g., laminin, collagen) or cell adhesive polypeptides (laminin peptides) [96, 100, 150, 155-158]. It remains to be determined what functionalization method, protein/peptide species and concentration are most effective and efficient for the alginate/hyaluronic acid composite hydrogels.

Number of Schwann cells on the ionically crosslinked 1.5% alginate/0.375%, 0.5% and 0.75% hyaluronic acid hydrogels have a significant difference from those of the double-crosslinked ones. The loss of uncrosslinked hyaluronic acid in the ionically crosslinked alginate/hyaluronic acid hydrogels into the culture media may reduce the inhibitory effect of hyaluronic acid on the cell proliferation. EDC was applied as the enzyme to activate the chemical reaction as it is thought to be the "green crosslinker", having better biocompatibility with the product transferred into urea. However, there has been research indicating the toxicity of EDC-mediated amide formation. The acid condition required by the reaction is also an issue. Non-reacted EDC crosslinker may be also toxic to the cells, leading to the low cell number in the double-crosslinked alginate/hyaluronic acid hydrogels.

In addition, mechanical properties of the double-crosslinked hydrogels are likely to differ from the ionically crosslinked ones, leading to decreased cellular activities as studies have indicated that the mechanical properties of substrates can modulate such cellular activities as attachment, differentiation, and proliferation [72, 159-161]. In general, scaffolds with most biomimetic mechanical properties as the ECM environment of particular cells will result in most cell differentiation, and proliferation and migration. For Schwann cells and neurons, soft scaffolds support more cell proliferation. Therefore, the fewer cells growing on the double-crosslinked alginate/hyaluronic acid hydrogels may indicate the stronger mechanical properties

of hydrogels caused by the double crosslinking. Mechanical tests on the double-crosslinked hydrogels and the ionically crosslinked ones as described in Chapter 4 would provide insights into this.

3D scaffold fabrication of 1.5% alginate/0.375%, 0.5% and 0.75% hyaluronic acid hydrogels were successfully achieved and the effect of initial needle height, concentration of $CaCl_2$ and fluid behavior on the formation of 3D scaffolds was evaluated. The method of dispensing alginate/hyaluronic acid mixture into $CaCl_2$ crosslinker solution involved the problem of surface tension, which made the fabrication process hard to control. Surface tension refers to the property of the surface of a liquid that allows it to resist an external force. It causes the floating of the dispensed strands on the surface of the $CaCl_2$ solution, in spite of the higher density of alginate/hyaluronic acid mixtures. The surface tension then causes the liquid surface to contract to the minimal area. The dispensed strands were then contracted by the tension force, leading to the non-uniform strand structure. Also, the stream of alginate/hyaluronic acid mixture tends to adhere to the dispensing needle tip until the point where the gravity overcomes the surface tension to stretch the stream to fall. Mixtures assemble into spherical drops rather than streams. This makes the fabrication of alginate/hyaluronic acid scaffolds difficulty.

The effect of initial needle height on the formation of strands illustrated in Chapter 4 is attributed to the surface tension and can be minimized by setting the distance of the needle tip from the surface of the Petri dish to a value that allows the dispensed strand to form the bridge between the needle tip and the Petri dish surface [162]. Once the effect of surface tension is excluded, the fabrication process could be facilitated by the model of strut diameter and mass flow rate measurement. With predefined nozzle geometry and nozzle deposition velocity, the volume flow rate needed for strand diameter equal to the nozzle diameter can be obtained. The

air pressure required will be then determined through the measurement of mass flow rate.

There was no significant difference in strand diameter at different concentrations of $CaCl_2$ solution except the group of 10 mM $CaCl_2$. Concentration of 50 mM to 150 mM led to extensive ionic gelation of alginate with calcium cations. High concentration of $CaCl_2$ leads to the shrinkage of the dispense strands. However, this effect is probably overcome by the swelling of alginate/hyaluronic acid hydrogels. The detachment of different layers is an issue occurring in the fabrication process when the alginate/hyaluronic acid mixture is dispensed into the $CaCl_2$ solution. To eliminate this problem, the dispensing process should be instant, with little time interval between different layers. Also, the volume of the $CaCl_2$ solution should be controlled to just cover the dispensed layers. Still, the $CaCl_2$ concentration should not be too high. One another method is to incorporate EDTA and/or citric acid to lower the speed of ionic crosslinking. Affected by the competitive sequestering of calcium ions by the EDTA and/or citric acid, the gelation of alginate with $CaCl_2$ could be decreased.

Fabrication of 3D alginate/hyaluronic acid scaffolds by the 3D Bioplotter™ is a little bit different from the way using the adapted commercial fluid dispensing system. With the precise control of air pressure and displacement, fabrication of strands with desired diameter is quite easy, making the mass flow rate measurement useless. Directly dispensing the material onto the Petri dish surface avoids the problem of surface tension caused by the $CaCl_2$ solution. Removal of the excess $CaCl_2$ solution every two layers after crosslinking was also done to eliminate the effect of surface tension. The initial needle height from the Petri dish can be set at a value equal to 80% of the strand diameter and was heightened by the same value layer by layer. 80% instead of 100% of the desired strand diameter was used to ensure the well attachment of different layers. The problem of this method is that there is probably fusion at the contact region of the newly

dispensed layer and the previously dispensed layer as illustrated in Figure 4.11. The newly dispensed strands may yield and spread before the application of crosslinker solution. Mixtures of 1.5% alginate with 0.5% hyaluronic acid or 0.75% hyaluronic acid have larger yield stresses and thus are less likely to yield and spread while solution of 1.5% alginate is not viscous enough to maintain its structure. In term of this, incorporation of hyaluronic acid into 1.5% alginate facilitates the fabrication process.

5.3 Recommendations for Future Work

In this study, the double-crosslinked alginate/hyaluronic acid hydrogels were synthesized and characterized by the FTIR spectrum. The amide formation were examined, but the amount of covalent modification and the responsible carboxyl groups in the composite hydrogels for covalent modification need to be further investigated through the quantitative measurement of amide formation. Characterization of the synthesized composite hydrogels from the aspects of swelling rate measurement, *in vitro* and *in vivo* biodegradation study should be carried out to better understand the properties of the composite material. Effects of crosslinker solutions, ADH concentration and gelation time on the properties of the composite material should also be well studied to tailor the biomaterial for a particular application.

Biocompatibility study of the composite biomaterial, either ionically crosslinked or double-crosslinked ones, was carried in this work using the *in vitro* Schwann cell culture. As discussed in the section of discussions, though the biomaterial allowed for the Schwann cell viability and growth, the substrates were not well suited for cell attachment. Modification of the non-adhesive property of the alginate/hyaluronic acid hydrogels to promote cell attachment and neurite outgrowth needs to be investigated. The reason for the decreased cell number on the

double-crosslinked alginate/hyaluronic acid hydrogels compared to the ionically crosslinked alginate/hyaluronic acid hydrogels is unknown and requires further investigation.

Fabrication of 3D scaffolds from the ionically crosslinked alginate/hyaluronic acid hydrogels was tried and the mechanical properties of the cylindrical hydrogels were evaluated. Work done on the adapted fluid dispensing system should be repeated on the 3D Bioplotter™ system, with its higher resolution provided, to better understand the results. Future work looking into mechanical properties of the double-crosslinked cylindrical hydrogels and the dispensed 3D porous scaffolds as well as the effects of gelation time, crosslinker concentration, strain rate, and microstructure on the mechanical properties of scaffolds needs to be done.

Lastly, *in vitro* and *in vivo* study of the fabricated 3D porous scaffolds using the DRG culture and a rat model of SCI will finally show the promise of this composite biomaterial for axonal regeneration and functional recovery of traumatic spinal cord. Integrated with other therapeutic strategies such as incorporation of bioactive molecules, living cells and electrical stimulation, the rapid prototyped alginate/hyaluronic acid scaffolds may turn out to be a promising option for SCI repair.

LIST OF REFERENCES

1. NSCISC. Spinal cord injury facts and figures at a glance 2011; Available from: www.nscisc.uab.edu/public_content/facts_figures_2009.aspx.
2. Blumenfeld H. Neuroanatomy through clinical cases. Sunderland, Sinauer Associates, 2002.
3. Fawcett JW, Asher RA. The glial scar and central nervous system repair. Brain Res Bull 49(6): 377-91, 1999.
4. George R, Griffin JW. Delayed macrophage responses and myelin clearance during Wallerian degeneration in the central nervous system: the dorsal radiculotomy model. Exp Neurol 129(2): 225-36, 1994.
5. Buss A, Schwab ME. Sequential loss of myelin proteins during Wallerian degeneration in the rat spinal cord. Glia 42(4): 424-32, 2003.
6. Ridet JL, Malhotra SK, Privat A, Gage FH. Reactive astrocytes: cellular and molecular cues to biological function. Trends Neurosci 20(12): 570-7, 1997.
7. Schnell L, Schwab ME. Axonal regeneration in the rat spinal cord produced by an antibody against myelin-associated neurite growth inhibitors. Nature 343(6255): 269-72, 1990.
8. Fawcett JW. Intrinsic neuronal determinants of regeneration. Trends Neurosci 15(1): 5-8, 1992.
9. van Blitterswijk C HJ, Cancedda R, de Bruijn JD, Lindahl A, Sohier J, Williams D. Tissue Engineering. London, Academic Press, 2008.
10. Neumann S, Bradke F, Tessier-Lavigne M, Basbaum AI. Regeneration of sensory axons within the injured spinal cord induced by intraganglionic cAMP elevation. Neuron 34(6): 885-93, 2002.
11. Neumann S, Woolf CJ. Regeneration of dorsal column fibers into and beyond the lesion site following adult spinal cord injury. Neuron 23(1): 83-91, 1999.
12. Imaizumi T, Lankford KL, Waxman SG, Greer CA, Kocsis JD. Transplanted olfactory ensheathing cells remyelinate and enhance axonal conduction in the demyelinated dorsal columns of the rat spinal cord. Journal of Neuroscience 18(16): 6176-6185, 1998.
13. De Laporte L, Shea LD. Matrices and scaffolds for DNA delivery in tissue engineering. Adv Drug Deliv Rev 59(4-5): 292-307, 2007.
14. Chvatal SA, Kim YT, Bratt-Leal AM, Lee H, Bellamkonda RV. Spatial distribution and acute anti-inflammatory effects of Methylprednisolone after sustained local delivery to the contused spinal cord. Biomaterials 29(12): 1967-75, 2008.
15. Lishko VK, Novokhatny VV, Yakubenko VP, Skomorovska-Prokvolit HV, Ugarova TP. Characterization of plasminogen as an adhesive ligand for integrins alpha(M)beta(2) (Mac-1) and alpha(5)beta(1) (VLA-75). Blood 104(3): 719-726, 2004.
16. Zhang M, Yannas IV. Peripheral nerve regeneration. Adv Biochem Eng Biotechnol 94: 67-89, 2005.
17. Lu P, Jones LL, Tuszynski MH. BDNF-expressing marrow stromal cells support extensive axonal growth at sites of spinal cord injury. Exp Neurol 191(2): 344-60, 2005.
18. Kamei N, Tanaka N, Oishi Y, Hamasaki T, Nakanishi K, Sakai N, Ochi M. BDNF, NT-3, and NGF released from transplanted neural progenitor cells promote corticospinal axon growth in organotypic cocultures. Spine (Phila Pa 1976) 32(12): 1272-8, 2007.

19. Grill R, Murai K, Blesch A, Gage FH, Tuszynski MH. Cellular delivery of neurotrophin-3 promotes corticospinal axonal growth and partial functional recovery after spinal cord injury. J Neurosci 17(14): 5560-72, 1997.
20. Chen J, Wu J, Apostolova I, Skup M, Irintchev A, Kugler S, Schachner M. Adeno-associated virus-mediated L1 expression promotes functional recovery after spinal cord injury. Brain 130(Pt 4): 954-69, 2007.
21. Inoue M, Honmou O, Oka S, Houkin K, Hashi K, Kocsis JD. Comparative analysis of remyelinating potential of focal and intravenous administration of autologous bone marrow cells into the rat demyelinated spinal cord. Glia 44(2): 111-8, 2003.
22. Papastefanaki F, Chen J, Lavdas AA, Thomaidou D, Schachner M, Matsas R. Grafts of Schwann cells engineered to express PSA-NCAM promote functional recovery after spinal cord injury. Brain 130(Pt 8): 2159-74, 2007.
23. Lesny P, Pradny M, Jendelova P, Michalek J, Vacik J, Sykova E. Macroporous hydrogels based on 2-hydroxyethyl methacrylate. Part 4: growth of rat bone marrow stromal cells in three-dimensional hydrogels with positive and negative surface charges and in polyelectrolyte complexes. J Mater Sci Mater Med 17(9): 829-33, 2006.
24. Hejcl A, Urdzikova L, Sedy J, Lesny P, Pradny M, Michalek J, Burian M, Hajek M, Zamecnik J, Jendelova P, Sykova E. Acute and delayed implantation of positively charged 2-hydroxyethyl methacrylate scaffolds in spinal cord injury in the rat. J Neurosurg Spine 8(1): 67-73, 2008.
25. Hill CE, Moon LD, Wood PM, Bunge MB. Labeled Schwann cell transplantation: cell loss, host Schwann cell replacement, and strategies to enhance survival. Glia 53(3): 338-43, 2006.
26. Coumans JV, Lin TT, Dai HN, MacArthur L, McAtee M, Nash C, Bregman BS. Axonal regeneration and functional recovery after complete spinal cord transection in rats by delayed treatment with transplants and neurotrophins. J Neurosci 21(23): 9334-44, 2001.
27. Maier IC, Ichiyama RM, Courtine G, Schnell L, Lavrov I, Edgerton VR, Schwab ME. Differential effects of anti-Nogo-A antibody treatment and treadmill training in rats with incomplete spinal cord injury. Brain 132(Pt 6): 1426-40, 2009.
28. Qiu J, Cafferty WB, McMahon SB, Thompson SW. Conditioning injury-induced spinal axon regeneration requires signal transducer and activator of transcription 3 activation. J Neurosci 25(7): 1645-53, 2005.
29. Orive G, Anitua E, Pedraz JL, Emerich DF. Biomaterials for promoting brain protection, repair and regeneration. Nat Rev Neurosci 10(9): 682-92, 2009.
30. Zawko SA, Schmidt CE. Crystal templating dendritic pore networks and fibrillar microstructure into hydrogels. Acta Biomater 6(7): 2415-21, 2010.
31. Duncan ID, Aguayo AJ, Bunge RP, Wood PM. Transplantation of rat Schwann cells grown in tissue culture into the mouse spinal cord. J Neurol Sci 49(2): 241-52, 1981.
32. Oudega M, Xu XM. Schwann cell transplantation for repair of the adult spinal cord. J Neurotrauma 23(3-4): 453-67, 2006.
33. Goto E, Mukozawa M, Mori H, Hara M. A rolled sheet of collagen gel with cultured Schwann cells: model of nerve conduit to enhance neurite growth. J Biosci Bioeng 109(5): 512-8, 2010.
34. Deng LX, Hu J, Liu N, Wang X, Smith GM, Wen X, Xu XM. GDNF modifies reactive astrogliosis allowing robust axonal regeneration through Schwann cell-seeded guidance channels after spinal cord injury. Exp Neurol 229(2): 238-50, 2011.

35. Olson HE, Rooney GE, Gross L, Nesbitt JJ, Galvin KE, Knight A, Chen B, Yaszemski MJ, Windebank AJ. Neural stem cell- and Schwann cell-loaded biodegradable polymer scaffolds support axonal regeneration in the transected spinal cord. Tissue Eng Part A 15(7): 1797-805, 2009.
36. Meijs MF, Timmers L, Pearse DD, Tresco PA, Bates ML, Joosten EA, Bunge MB, Oudega M. Basic fibroblast growth factor promotes neuronal survival but not behavioral recovery in the transected and Schwann cell implanted rat thoracic spinal cord. J Neurotrauma 21(10): 1415-30, 2004.
37. Cao L, Liu L, Chen ZY, Wang LM, Ye JL, Qiu HY, Lu CL, He C. Olfactory ensheathing cells genetically modified to secrete GDNF to promote spinal cord repair. Brain 127(Pt 3): 535-49, 2004.
38. Imaizumi T, Lankford KL, Kocsis JD. Transplantation of olfactory ensheathing cells or Schwann cells restores rapid and secure conduction across the transected spinal cord. Brain Res 854(1-2): 70-8, 2000.
39. Takami T, Oudega M, Bates ML, Wood PM, Kleitman N, Bunge MB. Schwann cell but not olfactory ensheathing glia transplants improve hindlimb locomotor performance in the moderately contused adult rat thoracic spinal cord. J Neurosci 22(15): 6670-81, 2002.
40. Santos-Silva A, Fairless R, Frame MC, Montague P, Smith GM, Toft A, Riddell JS, Barnett SC. FGF/heparin differentially regulates Schwann cell and olfactory ensheathing cell interactions with astrocytes: a role in astrocytosis. J Neurosci 27(27): 7154-67, 2007.
41. Bachelin C, Zujovic V, Buchet D, Mallet J, Baron-Van Evercooren A. Ectopic expression of polysialylated neural cell adhesion molecule in adult macaque Schwann cells promotes their migration and remyelination potential in the central nervous system. Brain 133(Pt 2): 406-20, 2009.
42. Saberi H, Moshayedi P, Aghayan HR, Arjmand B, Hosseini SK, Emami-Razavi SH, Rahimi-Movaghar V, Raza M, Firouzi M. Treatment of chronic thoracic spinal cord injury patients with autologous Schwann cell transplantation: an interim report on safety considerations and possible outcomes. Neurosci Lett 443(1): 46-50, 2008.
43. Tabesh H, Amoabediny G, Nik NS, Heydari M, Yosefifard M, Siadat SO, Mottaghy K. The role of biodegradable engineered scaffolds seeded with Schwann cells for spinal cord regeneration. Neurochem Int 54(2): 73-83, 2009.
44. Friedman JA, Windebank AJ, Moore MJ, Spinner RJ, Currier BL, Yaszemski MJ. Biodegradable polymer grafts for surgical repair of the injured spinal cord. Neurosurgery 51(3): 742-51; discussion 751-2, 2002.
45. Yu LMY, Leipzig ND, Shoichet MS. Promoting neuron adhesion and growth. Materials Today 11(5): 36-43, 2008.
46. Novikova LN, Mosahebi A, Wiberg M, Terenghi G, Kellerth JO, Novikov LN. Alginate hydrogel and matrigel as potential cell carriers for neurotransplantation. Journal of Biomedical Materials Research Part A 77A(2): 242-252, 2006.
47. Hyatt AJT, Wang D, Kwok JC, Fawcett JW, Martin KR. Controlled release of chondroitinase ABC from fibrin gel reduces the level of inhibitory glycosaminoglycan chains in lesioned spinal cord. Journal of Controlled Release 147(1): 24-29, 2010.
48. Itosaka H, Kuroda S, Shichinohe H, Yasuda H, Yano S, Kamei S, Kawamura R, Hida K, Iwasaki Y. Fibrin matrix provides a suitable scaffold for bone marrow stromal cells transplanted into injured spinal cord: A novel material for CNS tissue engineering. Neuropathology 29(3): 248-257, 2009.

49. Johnson PJ, Parker SR, Sakiyama-Elbert SE. Controlled Release of Neurotrophin-3 From Fibrin-Based Tissue Engineering Scaffolds Enhances Neural Fiber Sprouting Following Subacute Spinal Cord Injury. Biotechnology and Bioengineering 104(6): 1207-1214, 2009.
50. Taylor SJ, Rosenzweig ES, McDonald JW, Sakiyama-Elbert SE. Delivery of neurotrophin-3 from fibrin enhances neuronal fiber sprouting after spinal cord injury. Journal of Controlled Release 113(3): 226-235, 2006.
51. Johnson PJ, Tatara A, McCreedy DA, Shiu A, Sakiyama-Elbert SE. Tissue-engineered fibrin scaffolds containing neural progenitors enhance functional recovery in a subacute model of SCI. Soft Matter 6(20): 5127-5137, 2010.
52. Ahmed Z, Underwood S, Brown RA. Nerve guide material made from fibronectin: Assessment of in vitro properties. Tissue Engineering 9(2): 219-231, 2003.
53. King VR, Henseler M, Brown RA, Priestley JV. Mats made from fibronectin support oriented growth of axons in the damaged spinal cord of the adult rat. Exp Neurol 182(2): 383-98, 2003.
54. King VR, Phillips JB, Hunt-Grubbe H, Brown R, Priestley JV. Characterization of non-neuronal elements within fibronectin mats implanted into the damaged adult rat spinal cord. Biomaterials 27(3): 485-96, 2006.
55. Harley BA, Spilker MH, Wu JW, Asano K, Hsu HP, Spector M, Yannas IV. Optimal degradation rate for collagen chambers used for regeneration of peripheral nerves over long gaps. Cells Tissues Organs 176(1-3): 153-65, 2004.
56. Tsai EC, Dalton PD, Shoichet MS, Tator CH. Matrix inclusion within synthetic hydrogel guidance channels improves specific supraspinal and local axonal regeneration after complete spinal cord transection. Biomaterials 27(3): 519-33, 2006.
57. Klapka N, Muller HW. Collagen matrix in spinal cord injury. J Neurotrauma 23(3-4): 422-35, 2006.
58. Khaing ZZ, Schmidt CE. Advances in natural biomaterials for nerve tissue repair. Neurosci Lett 519(2): 103-14, 2012.
59. Novak U, Kaye AH. Extracellular matrix and the brain: components and function. J Clin Neurosci 7(4): 280-90, 2000.
60. Nomura H, Zahir T, Kim H, Katayama Y, Kulbatski I, Morshead CM, Shoichet MS, Tator CH. Extramedullary chitosan channels promote survival of transplanted neural stem and progenitor cells and create a tissue bridge after complete spinal cord transection. Tissue Eng Part A 14(5): 649-65, 2008.
61. Chenite A, Chaput C, Wang D, Combes C, Buschmann MD, Hoemann CD, Leroux JC, Atkinson BL, Binette F, Selmani A. Novel injectable neutral solutions of chitosan form biodegradable gels in situ. Biomaterials 21(21): 2155-61, 2000.
62. Crompton KE, Tomas D, Finkelstein DI, Marr M, Forsythe JS, Horne MK. Inflammatory response on injection of chitosan/GP to the brain. J Mater Sci Mater Med 17(7): 633-9, 2006.
63. Stokols S, Tuszynski MH. Freeze-dried agarose scaffolds with uniaxial channels stimulate and guide linear axonal growth following spinal cord injury. Biomaterials 27(3): 443-51, 2006.
64. Stokols S, Tuszynski MH. The fabrication and characterization of linearly oriented nerve guidance scaffolds for spinal cord injury. Biomaterials 25(27): 5839-46, 2004.

65. Stokols S, Sakamoto J, Breckon C, Holt T, Weiss J, Tuszynski MH. Templated agarose scaffolds support linear axonal regeneration. Tissue Eng 12(10): 2777-87, 2006.
66. Burd DA, Greco RM, Regauer S, Longaker MT, Siebert JW, Garg HG. Hyaluronan and wound healing: a new perspective. Br J Plast Surg 44(8): 579-84, 1991.
67. Ozgenel GY. Effects of hyaluronic acid on peripheral nerve scarring and regeneration in rats. Microsurgery 23(6): 575-81, 2003.
68. Lee HS, Kim JC. Effect of amniotic fluid in corneal sensitivity and nerve regeneration after excimer laser ablation. Cornea 15(5): 517-24, 1996.
69. Peattie RA, Nayate AP, Firpo MA, Shelby J, Fisher RJ, Prestwich GD. Stimulation of in vivo angiogenesis by cytokine-loaded hyaluronic acid hydrogel implants. Biomaterials 25(14): 2789-98, 2004.
70. Oohira A, Matsui F, Matsuda M, Shoji R. Developmental change in the glycosaminoglycan composition of the rat brain. J Neurochem 47(2): 588-93, 1986.
71. Meszar Z, Felszeghy S, Veress G, Matesz K, Szekely G, Modis L. Hyaluronan accumulates around differentiating neurons in spinal cord of chicken embryos. Brain Res Bull 75(2-4): 414-8, 2008.
72. Seidlits SK, Khaing ZZ, Petersen RR, Nickels JD, Vanscoy JE, Shear JB, Schmidt CE. The effects of hyaluronic acid hydrogels with tunable mechanical properties on neural progenitor cell differentiation. Biomaterials 31(14): 3930-40, 2010.
73. Hou S, Xu Q, Tian W, Cui F, Cai Q, Ma J, Lee IS. The repair of brain lesion by implantation of hyaluronic acid hydrogels modified with laminin. J Neurosci Methods 148(1): 60-70, 2005.
74. Tian WM, Hou SP, Ma J, Zhang CL, Xu QY, Lee IS, Li HD, Spector M, Cui FZ. Hyaluronic acid-poly-D-lysine-based three-dimensional hydrogel for traumatic brain injury. Tissue Eng 11(3-4): 513-25, 2005.
75. Tian WM, Zhang CL, Hou SP, Yu X, Cui FZ, Xu QY, Sheng SL, Cui H, Li HD. Hyaluronic acid hydrogel as Nogo-66 receptor antibody delivery system for the repairing of injured rat brain: in vitro. J Control Release 102(1): 13-22, 2005.
76. Wei YT, He Y, Xu CL, Wang Y, Liu BF, Wang XM, Sun XD, Cui FZ, Xu QY. Hyaluronic acid hydrogel modified with nogo-66 receptor antibody and poly-L-lysine to promote axon regrowth after spinal cord injury. J Biomed Mater Res B Appl Biomater 95(1): 110-7, 2010.
77. Horn EM, Beaumont M, Shu XZ, Harvey A, Prestwich GD, Horn KM, Gibson AR, Preul MC, Panitch A. Influence of cross-linked hyaluronic acid hydrogels on neurite outgrowth and recovery from spinal cord injury. J Neurosurg Spine 6(2): 133-40, 2007.
78. Prestwich GD, Marecak DM, Marecek JF, Vercruysse KP, Ziebell MR. Controlled chemical modification of hyaluronic acid: synthesis, applications, and biodegradation of hydrazide derivatives. J Control Release 53(1-3): 93-103, 1998.
79. Nakajima N, Ikada Y. Mechanism of amide formation by carbodiimide for bioconjugation in aqueous media. Bioconjug Chem 6(1): 123-30, 1995.
80. Perets A, Baruch Y, Weisbuch F, Shoshany G, Neufeld G, Cohen S. Enhancing the vascularization of three-dimensional porous alginate scaffolds by incorporating controlled release basic fibroblast growth factor microspheres. J Biomed Mater Res A 65(4): 489-97, 2003.

81. Tobias CA, Dhoot NO, Wheatley MA, Tessler A, Murray M, Fischer I. Grafting of encapsulated BDNF-producing fibroblasts into the injured spinal cord without immune suppression in adult rats. J Neurotrauma 18(3): 287-301, 2001.
82. Ashton RS, Banerjee A, Punyani S, Schaffer DV, Kane RS. Scaffolds based on degradable alginate hydrogels and poly(lactide-co-glycolide) microspheres for stem cell culture. Biomaterials 28(36): 5518-25, 2007.
83. Suzuki K, Suzuki Y, Ohnishi K, Endo K, Tanihara M, Nishimura Y. Regeneration of transected spinal cord in young adult rats using freeze-dried alginate gel. Neuroreport 10(14): 2891-4, 1999.
84. Suzuki Y, Kitaura M, Wu S, Kataoka K, Suzuki K, Endo K, Nishimura Y, Ide C. Electrophysiological and horseradish peroxidase-tracing studies of nerve regeneration through alginate-filled gap in adult rat spinal cord. Neurosci Lett 318(3): 121-4, 2002.
85. Prang P, Muller R, Eljaouhari A, Heckmann K, Kunz W, Weber T, Faber C, Vroemen M, Bogdahn U, Weidner N. The promotion of oriented axonal regrowth in the injured spinal cord by alginate-based anisotropic capillary hydrogels. Biomaterials 27(19): 3560-9, 2006.
86. Mosahebi A, Simon M, Wiberg M, Terenghi G. A novel use of alginate hydrogel as Schwann cell matrix. Tissue Eng 7(5): 525-34, 2001.
87. Murugan R, Ramakrishna S. Design strategies of tissue engineering scaffolds with controlled fiber orientation. Tissue Eng 13(8): 1845-66, 2007.
88. Leong KF, Cheah CM, Chua CK. Solid freeform fabrication of three-dimensional scaffolds for engineering replacement tissues and organs. Biomaterials 24(13): 2363-78, 2003.
89. Hollister SJ. Porous scaffold design for tissue engineering. Nat Mater 4(7): 518-24, 2005.
90. Hutmacher DW, Sittinger M, Risbud MV. Scaffold-based tissue engineering: rationale for computer-aided design and solid free-form fabrication systems. Trends Biotechnol 22(7): 354-62, 2004.
91. Hejcl A, Lesny P, Pradny M, Michalek J, Jendelova P, Stulik J, Sykova E. Biocompatible hydrogels in spinal cord injury repair. Physiol Res 57 Suppl 3: S121-32, 2008.
92. Keselowsky BG, Collard DM, Garcia AJ. Integrin binding specificity regulates biomaterial surface chemistry effects on cell differentiation. Proc Natl Acad Sci U S A 102(17): 5953-7, 2005.
93. Keselowsky BG, Collard DM, Garcia AJ. Surface chemistry modulates focal adhesion composition and signaling through changes in integrin binding. Biomaterials 25(28): 5947-54, 2004.
94. Ren YJ, Zhang H, Huang H, Wang XM, Zhou ZY, Cui FZ, An YH. In vitro behavior of neural stem cells in response to different chemical functional groups. Biomaterials 30(6): 1036-44, 2009.
95. Reichardt LF, Tomaselli KJ. Extracellular matrix molecules and their receptors: functions in neural development. Annu Rev Neurosci 14: 531-70, 1991.
96. Frampton JP, Hynd MR, Shuler ML, Shain W. Fabrication and optimization of alginate hydrogel constructs for use in 3D neural cell culture. Biomed Mater 6(1): 015002-015019, 2011.
97. Suzuki M, Itoh S, Yamaguchi I, Takakuda K, Kobayashi H, Shinomiya K, Tanaka J. Tendon chitosan tubes covalently coupled with synthesized laminin peptides facilitate nerve regeneration in vivo. J Neurosci Res 72(5): 646-59, 2003.

98. Cui FZ, Tian WM, Hou SP, Xu QY, Lee IS. Hyaluronic acid hydrogel immobilized with RGD peptides for brain tissue engineering. J Mater Sci Mater Med 17(12): 1393-401, 2006.
99. Koh HS, Yong T, Chan CK, Ramakrishna S. Enhancement of neurite outgrowth using nano-structured scaffolds coupled with laminin. Biomaterials 29(26): 3574-82, 2008.
100. Dhoot NO, Tobias CA, Fischer I, Wheatley MA. Peptide-modified alginate surfaces as a growth permissive substrate for neurite outgrowth. J Biomed Mater Res A 71(2): 191-200, 2004.
101. Hashemi SM, Soudi S, Shabani I, Naderi M, Soleimani M. The promotion of stemness and pluripotency following feeder-free culture of embryonic stem cells on collagen-grafted 3-dimensional nanofibrous scaffold. Biomaterials 32(30): 7363-74, 2011.
102. Li W, Guo Y, Wang H, Shi D, Liang C, Ye Z, Qing F, Gong J. Electrospun nanofibers immobilized with collagen for neural stem cells culture. J Mater Sci Mater Med 19(2): 847-54, 2008.
103. Prabhakaran MP, Venugopal JR, Ramakrishna S. Mesenchymal stem cell differentiation to neuronal cells on electrospun nanofibrous substrates for nerve tissue engineering. Biomaterials 30(28): 4996-5003, 2009.
104. He J, Wang XM, Spector M, Cui FZ. Scaffolds for central nervous system tissue engineering Frontiers of Materials Science 6(1): 1-25, 2012.
105. Georges PC, Miller WJ, Meaney DF, Sawyer ES, Janmey PA. Matrices with compliance comparable to that of brain tissue select neuronal over glial growth in mixed cortical cultures. Biophys J 90(8): 3012-8, 2006.
106. Woerly S, Doan VD, Sosa N, de Vellis J, Espinosa-Jeffrey A. Prevention of gliotic scar formation by NeuroGel allows partial endogenous repair of transected cat spinal cord. J Neurosci Res 75(2): 262-72, 2004.
107. Oakland RJ, Hall RM, Wilcox RK, Barton DC. The biomechanical response of spinal cord tissue to uniaxial loading. Proc Inst Mech Eng H 220(4): 489-92, 2006.
108. Ozawa H, Matsumoto T, Ohashi T, Sato M, Kokubun S. Comparison of spinal cord gray matter and white matter softness: measurement by pipette aspiration method. J Neurosurg 95(2 Suppl): 221-4, 2001.
109. Straley KS, Foo CW, Heilshorn SC. Biomaterial design strategies for the treatment of spinal cord injuries. J Neurotrauma 27(1): 1-19, 2009.
110. Yao L, de Ruiter GC, Wang H, Knight AM, Spinner RJ, Yaszemski MJ, Windebank AJ, Pandit A. Controlling dispersion of axonal regeneration using a multichannel collagen nerve conduit. Biomaterials 31(22): 5789-97, 2010.
111. Gros T, Sakamoto JS, Blesch A, Havton LA, Tuszynski MH. Regeneration of long-tract axons through sites of spinal cord injury using templated agarose scaffolds. Biomaterials 31(26): 6719-29, 2010.
112. Wong DY, Leveque JC, Brumblay H, Krebsbach PH, Hollister SJ, Lamarca F. Macro-architectures in spinal cord scaffold implants influence regeneration. J Neurotrauma 25(8): 1027-37, 2008.
113. Suri S, Han LH, Zhang W, Singh A, Chen S, Schmidt CE. Solid freeform fabrication of designer scaffolds of hyaluronic acid for nerve tissue engineering. Biomed Microdevices 13(6): 983-93, 2011.

114. Kim YT, Haftel VK, Kumar S, Bellamkonda RV. The role of aligned polymer fiber-based constructs in the bridging of long peripheral nerve gaps. Biomaterials 29(21): 3117-27, 2008.
115. Bozkurt A, Brook GA, Moellers S, Lassner F, Sellhaus B, Weis J, Woeltje M, Tank J, Beckmann C, Fuchs P, Damink LO, Schugner F, Heschel I, Pallua N. In vitro assessment of axonal growth using dorsal root ganglia explants in a novel three-dimensional collagen matrix. Tissue Eng 13(12): 2971-9, 2007.
116. Bozkurt A, Deumens R, Beckmann C, Olde Damink L, Schugner F, Heschel I, Sellhaus B, Weis J, Jahnen-Dechent W, Brook GA, Pallua N. In vitro cell alignment obtained with a Schwann cell enriched microstructured nerve guide with longitudinal guidance channels. Biomaterials 30(2): 169-79, 2009.
117. Goldner JS, Bruder JM, Li G, Gazzola D, Hoffman-Kim D. Neurite bridging across micropatterned grooves. Biomaterials 27(3): 460-72, 2006.
118. Xie J, MacEwan MR, Li X, Sakiyama-Elbert SE, Xia Y. Neurite outgrowth on nanofiber scaffolds with different orders, structures, and surface properties. ACS Nano 3(5): 1151-9, 2009.
119. Corey JM, Lin DY, Mycek KB, Chen Q, Samuel S, Feldman EL, Martin DC. Aligned electrospun nanofibers specify the direction of dorsal root ganglia neurite growth. J Biomed Mater Res A 83(3): 636-45, 2007.
120. Cho YI, Choi JS, Jeong SY, Yoo HS. Nerve growth factor (NGF)-conjugated electrospun nanostructures with topographical cues for neuronal differentiation of mesenchymal stem cells. Acta Biomater 6(12): 4725-33, 2010.
121. Xie J, Willerth SM, Li X, Macewan MR, Rader A, Sakiyama-Elbert SE, Xia Y. The differentiation of embryonic stem cells seeded on electrospun nanofibers into neural lineages. Biomaterials 30(3): 354-62, 2009.
122. Wang Y, Yao M, Zhou J, Zheng W, Zhou C, Dong D, Liu Y, Teng Z, Jiang Y, Wei G, Cui X. The promotion of neural progenitor cells proliferation by aligned and randomly oriented collagen nanofibers through beta1 integrin/MAPK signaling pathway. Biomaterials 32(28): 6737-44, 2011.
123. Mironov V, Trusk T, Kasyanov V, Little S, Swaja R, Markwald R. Biofabrication: a 21st century manufacturing paradigm. Biofabrication 1(2): 022001, 2009.
124. De Laporte L, Yang Y, Zelivyanskaya ML, Cummings BJ, Anderson AJ, Shea LD. Plasmid releasing multiple channel bridges for transgene expression after spinal cord injury. Mol Ther 17(2): 318-26, 2009.
125. Teng YD, Lavik EB, Qu X, Park KI, Ourednik J, Zurakowski D, Langer R, Snyder EY. Functional recovery following traumatic spinal cord injury mediated by a unique polymer scaffold seeded with neural stem cells. Proc Natl Acad Sci U S A 99(5): 3024-9, 2002.
126. Gautier SE, Oudega M, Fragoso M, Chapon P, Plant GW, Bunge MB, Parel JM. Poly(alpha-hydroxyacids) for application in the spinal cord: resorbability and biocompatibility with adult rat Schwann cells and spinal cord. J Biomed Mater Res 42(4): 642-54, 1998.
127. Sachlos E, Czernuszka JT. Making tissue engineering scaffolds work. Review: the application of solid freeform fabrication technology to the production of tissue engineering scaffolds. Eur Cell Mater 5(29-39; discussion 39-40, 2003.

128. Malda J, Woodfield TB, van der Vloodt F, Wilson C, Martens DE, Tramper J, van Blitterswijk CA, Riesle J. The effect of PEGT/PBT scaffold architecture on the composition of tissue engineered cartilage. Biomaterials 26(1): 63-72, 2005.
129. Silva NA, Salgado AJ, Sousa RA, Oliveira JT, Pedro AJ, Leite-Almeida H, Cerqueira R, Almeida A, Mastronardi F, Mano JF, Neves NM, Sousa N, Reis RL. Development and characterization of a novel hybrid tissue engineering-based scaffold for spinal cord injury repair. Tissue Eng Part A 16(1): 45-54, 2009.
130. Woodfield TBF, Malda J, de Wijn J, Peters F, Riesle J, van Blitterswijk CA. Design of porous scaffolds for cartilage tissue engineering using a three-dimensional fiber-deposition technique. Biomaterials 25(18): 4149-4161, 2004.
131. Vozzi G, Previti A, De Rossi D, Ahluwalia A. Microsyringe-based deposition of two-dimensional and three-dimensional polymer scaffolds with a well-defined geometry for application to tissue engineering. Tissue Engineering 8(6): 1089-1098, 2002.
132. Chen XB. Modeling of rotary screw fluid dispensing processes. Journal of Electronic Packaging 129(2): 172-178, 2007.
133. Chen XB, Li MG, Ke H. Modeling of the flow rate in the dispensing-based process for fabricating tissue scaffolds. Journal of Manufacturing Science and Engineering-Transactions of the Asme 130(2): 020601.1-024503.5 2008.
134. Li MG, Tian XY, Chen XB. Modeling of Flow Rate, Pore Size, and Porosity for the Dispensing-Based Tissue Scaffolds Fabrication. Journal of Manufacturing Science and Engineering-Transactions of the Asme 131(3): 034501-5, 2009.
135. Haug A, Larsen B. Solubility of Alginate at Low Ph. Acta Chemica Scandinavica 17(6): 1653-62, 1963.
136. Danishef.I, Siskovic E. Conversion of Carboxyl Groups of Mucopolysaccharides into Amides of Amino Acid Esters. Carbohydrate Research 16(1): 199-205, 1971.
137. Leach JB, Bivens KA, Collins CN, Schmidt CE. Development of photocrosslinkable hyaluronic acid-polyethylene glycol-peptide composite hydrogels for soft tissue engineering. J Biomed Mater Res A 70(1): 74-82, 2004.
138. Mosmann T. Rapid colorimetric assay for cellular growth and survival: application to proliferation and cytotoxicity assays. J Immunol Methods 65(1-2): 55-63, 1983.
139. Estes JM, Adzick NS, Harrison MR, Longaker MT, Stern R. Hyaluronate metabolism undergoes an ontogenic transition during fetal development: implications for scar-free wound healing. J Pediatr Surg 28(10): 1227-31, 1993.
140. Wiig M, Abrahamsson SO, Lundborg G. Effects of hyaluronan on cell proliferation and collagen synthesis: a study of rabbit flexor tendons in vitro. J Hand Surg Am 21(4): 599-604, 1996.
141. Khalil S, Nam J, Sun W. Multi-nozzle deposition for construction of 3D biopolymer tissue scaffolds. Rapid Prototyping Journal 11(1): 9-17, 2005.
142. Bakshi A, Fisher O, Dagci T, Himes BT, Fischer I, Lowman A. Mechanically engineered hydrogel scaffolds for axonal growth and angiogenesis after transplantation in spinal cord injury. J Neurosurg Spine 1(3): 322-9, 2004.
143. Sparrey CJ, Keaveny TM. Compression behavior of porcine spinal cord white matter. J Biomech 44(6): 1078-82, 2011.
144. Man AJ, Davis HE, Itoh A, Leach JK, Bannerman P. Neurite outgrowth in fibrin gels is regulated by substrate stiffness. Tissue Eng Part A 17(23-24): 2931-42, 2011.

145. Scott R, Marquardt L, Willits RK. Characterization of poly(ethylene glycol) gels with added collagen for neural tissue engineering. J Biomed Mater Res A 93(3): 817-23, 2010.
146. Engler AJ, Sen S, Sweeney HL, Discher DE. Matrix elasticity directs stem cell lineage specification. Cell 126(4): 677-89, 2006.
147. Khaing ZZ, Milman BD, Vanscoy JE, Seidlits SK, Grill RJ, Schmidt CE. High molecular weight hyaluronic acid limits astrocyte activation and scar formation after spinal cord injury. J Neural Eng 8(4): 046033-44, 2011.
148. Struve J, Maher PC, Li YQ, Kinney S, Fehlings MG, Kuntz Ct, Sherman LS. Disruption of the hyaluronan-based extracellular matrix in spinal cord promotes astrocyte proliferation. Glia 52(1): 16-24, 2005.
149. Bourguignon LY, Peyrollier K, Gilad E, Brightman A. Hyaluronan-CD44 interaction with neural Wiskott-Aldrich syndrome protein (N-WASP) promotes actin polymerization and ErbB2 activation leading to beta-catenin nuclear translocation, transcriptional up-regulation, and cell migration in ovarian tumor cells. J Biol Chem 282(2): 1265-80, 2007.
150. Rowley JA, Madlambayan G, Mooney DJ. Alginate hydrogels as synthetic extracellular matrix materials. Biomaterials 20(1): 45-53, 1999.
151. Pouyani T, Prestwich GD. Functionalized derivatives of hyaluronic acid oligosaccharides: drug carriers and novel biomaterials. Bioconjug Chem 5(4): 339-47, 1994.
152. Sherman L, Skroch-Angel P, Moll J, Schwechheimer K, Ponta H, Herrlich P, Hofmann M. Schwann cell tumors express characteristic patterns of CD44 splice variants. J Neurooncol 26(3): 171-84, 1995.
153. Maharjan AS, Pilling D, Gomer RH. High and low molecular weight hyaluronic acid differentially regulate human fibrocyte differentiation. PLoS One 6(10): e26078-87, 2011.
154. Suri S, Schmidt CE. Cell-laden hydrogel constructs of hyaluronic acid, collagen, and laminin for neural tissue engineering. Tissue Eng Part A 16(5): 1703-16, 2010.
155. Shu XZ, Ghosh K, Liu Y, Palumbo FS, Luo Y, Clark RA, Prestwich GD. Attachment and spreading of fibroblasts on an RGD peptide-modified injectable hyaluronan hydrogel. J Biomed Mater Res A 68(2): 365-75, 2004.
156. Brannvall K, Bergman K, Wallenquist U, Svahn S, Bowden T, Hilborn J, Forsberg-Nilsson K. Enhanced neuronal differentiation in a three-dimensional collagen-hyaluronan matrix. J Neurosci Res 85(10): 2138-46, 2007.
157. Deister C, Aljabari S, Schmidt CE. Effects of collagen 1, fibronectin, laminin and hyaluronic acid concentration in multi-component gels on neurite extension. J Biomater Sci Polym Ed 18(8): 983-97, 2007.
158. Zhang H, Wei YT, Tsang KS, Sun CR, Li J, Huang H, Cui FZ, An YH. Implantation of neural stem cells embedded in hyaluronic acid and collagen composite conduit promotes regeneration in a rabbit facial nerve injury model. J Transl Med 6(1): 67-77, 2008.
159. Genes NG, Rowley JA, Mooney DJ, Bonassar LJ. Effect of substrate mechanics on chondrocyte adhesion to modified alginate surfaces. Arch Biochem Biophys 422(2): 161-7, 2004.
160. Lee CR, Grodzinsky AJ, Spector M. The effects of cross-linking of collagen-glycosaminoglycan scaffolds on compressive stiffness, chondrocyte-mediated contraction, proliferation and biosynthesis. Biomaterials 22(23): 3145-54, 2001.
161. Subramanian A, Lin HY. Crosslinked chitosan: its physical properties and the effects of matrix stiffness on chondrocyte cell morphology and proliferation. J Biomed Mater Res A 75(3): 742-53, 2005.

162. Cao N. Fabrication of Alginate Hydrogel Scaffolds and Cell Viability in Calcium-Crosslinked Alginate Hydrogel. Division of Biomedical Engineering, Master of Science, Saskatoon, University of Saskatchewan, 1-83, 2011.